Charles University in Prague
Faculty of Mathematics and Physics

DIPLOMA THESIS

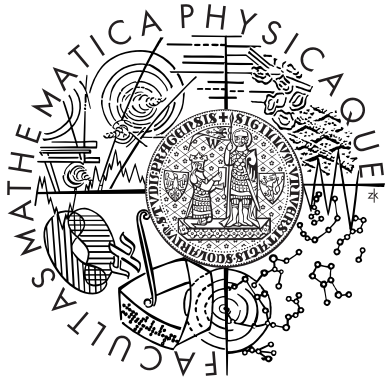

Josef Stráský

Zeeman Effect in Semiconductor Quantum Structures

Institute of Physics of Charles University

Supervisor: Assoc. Prof. Roman Grill, PhD

Study Program: Optics and optoelectronics

2011

Acknowledgement

I would like to express my gratitude to my supervisor Assoc. Prof. Roman Grill, PhD for his invaluable help and challenging consultations. Without his continuous effort and patience, this thesis would have never been finished. I would also like to thank my relatives, friends and colleagues who were affected by the never-ending story of writing this thesis.

Prohlášení

Prohlašuji, že jsem svou diplomovou práci vypracoval samostatně a použil jsem pouze podklady uvedené v přiloženém seznamu.

Nemám závažný důvod proti užití tohoto školního díla ve smyslu §60 Zákona č. 121/2000 Sb., o právu autorském, o právech souvisejících s právem autorským a o změně některých zákonů (autorský zákon).

V Praze dne 15. dubna 2011 .....Josef Stráský

Abstract

Název práce: Zeemanův jev v polovodičových kvantových strukturách
Autor: Josef Stráský
Katedra: Fyzikální ústav Univerzity Karlovy
Vedoucí diplomové práce: Doc. RNDr. Roman Grill, CSc.
E-mail vedoucího: grill@karlov.mff.cuni.cz
Abstrakt:
Tato teoretická práce prezentuje detailní studii záporně nabitých excitonů - trionů - v jednoduché potenciálové jámě a kolmém magnetickém poli. Složitý valenční pás sloučeniny GaAs/GaAlAs je popsán pomocí Luttingerova Hamiltoniánu. Po zavedení singletních a tripletních stavů záporného trionu je provedena detatilní teoretická analýza Zeemanova jevu pro různé stavy trionu. Pro popis magnetického pole je zvolena Landauova kalibrace. Vhodnost související neobvyklé báze vlnových funkcí je testována. Závislost energie základního stavu a fotoluminiscenčních spekter na magnetickém poli je vyhodnocena pro různé volby Landého g-faktorů. Dále je zkoumána prostorová distribuce pravděpodobnosti výskytu elektronu vzhledem k poloze díry a vzájemná prostorová korelační funkce elektronů.

Klíčová slova: záporný trion, Luttingerův Hamiltonián, Zeemanův jev, jednoduchá kvantová jáma, míchání stavů valenčního pásu, Landého g-faktor

---

Title: Zeeman Effect in Semiconductor Quantum Structures
Author: Josef Stráský
Supervisor: Assoc. Prof. Roman Grill, PhD
Supervisor's e-mail address: grill@karlov.mff.cuni.cz
Abstract:
This theoretical thesis presents detailed study of negatively charged excitons - trions - confined in single quantum well in presence of perpendicular magnetic field. Complex valence band of GaAs/GaAlAs compound is described within Luttinger Hamiltonian framework. Singlet and triplet states of negative trion are introduced. Advanced theoretical analysis of Zeeman effect for different states of trion is performed. Landau gauge of magnetic field and unusual wavefunctions basis is chosen and its accuracy is tested. Evolution of ground state energy and photoluminescence spectra with magnetic field is evaluated for different values of Landé g-factors. Probability of occurrence of electrons with respect to the hole position and their spatial correlation function are investigated.

Keywords: negative trion, Luttinger Hamiltonian, Zeeman effect, single quantum well, valence subband mixing, Landé g-factor

---

Contents

1 Introduction and properties of GaAlAs

1.1 Introduction

The development of advanced epitaxial techniques such as molecular beam epitaxy (MBE) or metal-organic chemical vapour deposition (MOCVD) allows growing interfaces between two semiconductors flat up to one atomic layer. Quantum heterostructures that are created by these techniques found various practical applications like light emitting diodes (LED), diode lasers, high electron mobility transistors (HEMT) etc. The most used materials are pseudo-binary compounds of GaAs and AlAs. These materials are perfectly lattice-matched and bandgap width is tunable by the Al additions.

The most simple structure is a single quantum well. Such heterostructure is considered in this thesis. Quantum heterostructures along with advanced optical and cryogenic techniques allow observation of bound states of electron and hole in semiconductors called excitons. Such bound states are well known and well described both experimentally and theoretically. However, more complicated structure of charged exciton has been also observed. Charged exciton - trion - problem is much more complicated than the excitonic one, since it is a three body problem. Whereas exciton is created by charge-charge Coulomb interaction, the trion is based on charge-dipole interaction. Positive trion consists of two holes and one electron and negative trion consists of two electrons and one hole. Both types of trions have been observed (even at one sample), however theoretically the problems are quite different. The main problem of positive trion analysis lies in the interaction between holes that is generally complicated due to complex valence band of GaAs/GaAlAs compound. The analysis of negative trion must take into account that negative trion involving two electrons is multifermionic system and thus Pauli principle must be obeyed. Symmetry considerations along with Pauli principle give rise to singlet and triplet states of the negative trion.

Main contribution of this thesis is simultaneous analysis of the negative trion using Luttinger Hamiltonian and very detailed analysis of the Zeeman effect. Luttinger Hamiltonian is popular semi-empirical method describing complex valence band. Most importantly, the Luttinger Hamiltonian mixes the heavy hole and light hole states. One trion state is thus crated by both heavy and light holed. This is extremely important in connection with the Zeeman effect. Since the heavy hole and the light hole have different projections of total angular momentum, they are affected by the Zeeman effect differently. However, due to Luttinger Hamiltonian they are both involved in one state. This has non-trivial consequences that are exploited in this thesis.

The rest of this chapter and part of the following chapter comprise wide theoretical introduction and these follow two most influential sources for theoretical part of this diploma thesis. These are Master's thesis Magnetooptical Properties of Semiconductor Quantum Structures by Štěpán Uxa [1] and basic text-book Wave Mechanics Applied to Semiconductor Heterostructures by Gerald Bastard [2].

1.2 Basic crystalline and electronic properties

GaAlAs is the most important member of III-V semiconductors group. III-V compounds crystallize in the sphalerite (zinc-blende) crystalographic structure. This structure consists of two interpenetrating face-centered cubic lattices. Each is displaced from the other by one fourth of the cube main diagonal. The reciprocal lattice of Bravais lattice corresponding to sphalerite structure is body centered cubic lattice. Finally, the first Brillouin zone of such structure is truncated octahedron 1.1. High symmetry points received specific notations, most importantly the center of the Brilloun zone (center of momentum space) - Γ point.

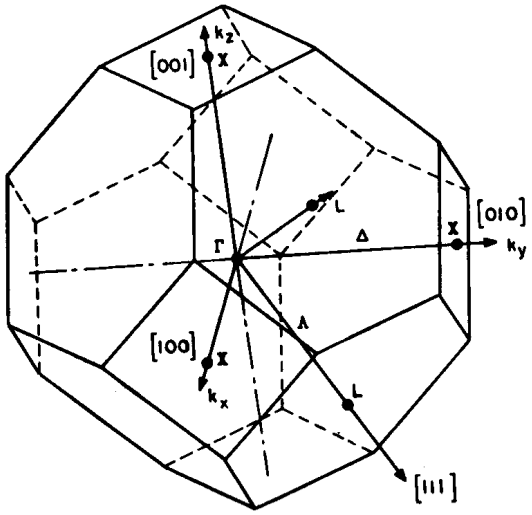

Figure 1.1: First Brillouin zone of semiconductor with sphalerite structure

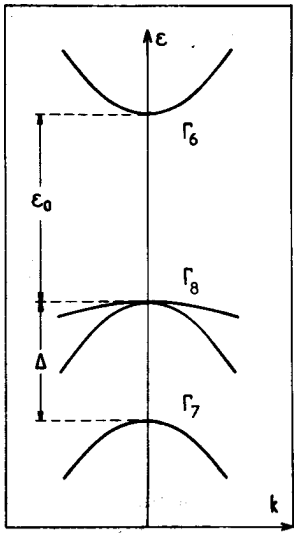

Figure 1.2: Band structure of a direct gap semiconductor in the vicinity of the Γ point

8 outter electrons per unit cell in III-V binary compounds are responsible for electrical and optical properties (in the case of GaAs - 3 electrons from Ga and 5 from As). Orbitals of every atom (e.g. Ga) hybridize with an orbital of the nearest neighbouring atoms (As) producing two levels: bonding and antibonding. Since there is a large number of unit cells, these levels broaden into bands. The bonding s-orbitals are deeply bound and always filled by two electrons. The remaining six electrons occupy three bonding p-orbitals. The lowest lying antibonding orbital (s-orbital) forms the conduction band of the material.

The top of the valence band occurs at the Γ point in all III-V semiconductors. The potential sixfold degeneracy of valence band (six electrons in the three p-orbitals) in this point is partly lifted by spin-orbit coupling. Resulting structure is depicted in Fig. 1.2. The three valence bands are split into a quadruplet (symmetry Γ_8) and doublet (symmetry Γ_7). Quadruplet refers to total angular momentum of $J = \frac{3}{2}$ whereas doublet is associated with $J = \frac{3}{2}$. Antibonding s-orbitals form the conduction band (symmetry Γ_6, $J = \frac{1}{2}$). For GaAs is the edge of the conduction band also in the center of Brillouin zone (Γ point). Thus this compound is of the direct bandgap. In the figure 1.2, the bandgap is denoted

$\mathcal{E}_0 = \mathcal{E}_{\Gamma_6} - \mathcal{E}_{\Gamma_8}$ and energetic split due to spin-orbit coupling $\Delta = \mathcal{E}_{\Gamma_8} - \mathcal{E}_{\Gamma_7}$.

Our main interest lies in AlGaAs (aluminium gallium arsenide) compound. This is ternary (or pseudo-binary) III-V semiconductor material. Since AlAs and GaAs are perfectly lattice matched, so is GaAs and AlGaAs. However, AlGaAs is of larger bandgap. Thus AlGaAs can be used as a barrier material in GaAs based heterostructres. The AlGaAs barrier confines the electrons to GaAs region.

Due to broken translational symmetry in AlGaAs (due to random distribution of Ga and Al atoms), we employ virtual crystal approximation to describe alloy electronic states. In the case of $Al_xGa_{1-x}As$ alloy we can write average potential (thus transnationally symmetric potential) as $V_{AlGaAs} = xV_{Al} + (1-x)V_{Ga} + V_{As}$, where V_{Al}, V_{Ga}, V_{As} are potentials created by different atoms separately. Once we introduce periodic potential, we can employ Bloch functions, Brillouin zone, etc.

$Al_xGa_{1-x}As$ is a direct gap semiconductor for $x < 0,45$. The bandgap is a linearly dependent on x (thus virtual crystal approximation is applicable) [1]:

$$E_g^{AlGaAs} = 1,424 + 1,247x \text{ eV}. \tag{1.1}$$

The electron effective mass m_e^{AlGaAs} at the room temperature can be computed (for $x < 0.45$) [1]:

$$m_e^{AlGaAs} = (0.063 + 0.083x)\, m_0. \tag{1.2}$$

1.3 Effective mass approximation

This section covers the basic approach how to compute electronic dispersion relations in the vicinity of the centre of Brillouin zone. The one electron Schrödinger equation in a bulk crystal can be written [2]:

$$\left[\frac{\hat{\mathbf{p}}^2}{2m_e} + V(\mathbf{r}) + \frac{\hbar}{4m_e^2c^2}(\boldsymbol{\sigma} \times \nabla V).\hat{\mathbf{p}}\right]\psi(\mathbf{r}) = \mathcal{E}\psi(\mathbf{r}), \tag{1.3}$$

where m_e is the free-electron mass, $V(r)$ is the periodic crystalline potential and σ is the vector of Pauli spin matrices. The third term refers to the spin-orbit coupling. Other relativistic corrections are ignored.

In a search for eigenfunctions of such Hamiltonian we employ Bloch theorem (due to periodicity of potential $V(r)$):

$$\psi_{n\mathbf{k}}(\mathbf{r}) = N u_{n\mathbf{k}}(\mathbf{r})\, exp(i\mathbf{k}.\mathbf{r}), \tag{1.4}$$

where N is normalization constant and $u_{n\mathbf{k}}(\mathbf{r})$ are functions with periodicity of the lattice.

For many aspects of semiconductor electronic properties (effective masses, wavefunctions...), the important knowledge is $\mathcal{E}_{n\boldsymbol{k}}$ relationship over small $\boldsymbol{k}$ range. If we insert Bloch form (Eq. 1.4) into Schrödinger equation 1.3 we get:

$$\Big[\frac{\hat{\mathbf{p}}^2}{2m_0} + V(\mathbf{r}) + \frac{\hbar}{4m_0^2c^2}(\boldsymbol{\sigma}\times\nabla V).\hat{\mathbf{p}} + \frac{\hbar^2k^2}{2m_0} + \frac{\hbar\boldsymbol{k}}{m_0}\left(\boldsymbol{p} + \frac{\hbar}{4m_0^2c^2}(\boldsymbol{\sigma}\times\nabla V)\right)\Big] u_{n\boldsymbol{k}}(\mathbf{r}) = \mathcal{E}_{n\boldsymbol{k}} u_{n\boldsymbol{k}}(\boldsymbol{r}) \tag{1.5}$$

Hamiltonian can be formally but advantageously divided into two parts:

$$H(\boldsymbol{k}=\mathbf{0}) = \frac{\hat{\mathbf{p}}^2}{2m_0} + V(\mathbf{r}) + \frac{\hbar}{4m_0^2c^2}(\boldsymbol{\sigma}\times\nabla V).\hat{\mathbf{p}} \tag{1.6}$$

$$W(\boldsymbol{k}) = \frac{\hbar^2k^2}{2m_0} + \frac{\hbar\boldsymbol{k}}{m_0}\left(\boldsymbol{p} + \frac{\hbar}{4m_0^2c^2}(\boldsymbol{\sigma}\times\nabla V)\right) \tag{1.7}$$

Eigenfunctions of $H(\boldsymbol{k}=\mathbf{0})$ are equivalently $u_{n\mathbf{0}}$ or $\psi_{n\mathbf{0}}$:

$$H(\boldsymbol{k}=\mathbf{0})\, u_{n\mathbf{0}} = \mathcal{E}_{n\mathbf{0}} u_{n\mathbf{0}} \tag{1.8}$$

Moreover, $W(\boldsymbol{k})$ commutes with operator of translational symmetry and vanish for $\boldsymbol{k}=\mathbf{0}$. Thus we can expand the solution of Eq. 1.5:

$$u_{n\boldsymbol{k}} = \sum_m c_m(\boldsymbol{k})\, u_{n\mathbf{0}} \tag{1.9}$$

We insert this expansion into Eq. 1.5, we multiply whole equation by $u^*_{n\mathbf{0}}$ and integrate over unit cell. After some manipulation we get:

$$\sum_m \Big[\left(\mathcal{E}_{n0} - \mathcal{E}_{n\boldsymbol{k}} + \frac{\hbar^2k^2}{2m_0}\right)\delta_{nm} + \frac{\hbar\boldsymbol{k}}{m_0}.\langle n\mathbf{0}|\,\boldsymbol{\pi}\,|m\mathbf{0}\rangle\Big] c_m(\boldsymbol{k}) = 0, \tag{1.10}$$

where we denoted

$$\boldsymbol{\pi} = \boldsymbol{p} + \frac{\hbar}{4m_0^2c^2}(\boldsymbol{\sigma}\times\nabla V) \tag{1.11}$$

and employ notation

$$\langle n\mathbf{0}|\,\boldsymbol{\pi}\,|m\mathbf{0}\rangle = \int u^*_{n\mathbf{0}}\boldsymbol{\pi}u_{m\mathbf{0}}d^3\boldsymbol{r} = \boldsymbol{\pi}_{nm}. \tag{1.12}$$

Somewhat tricky part follows. Some more details can be found in [2]. Equation 1.10 can be solved by perturbative approach. We need to assume that n-th band (energy $\mathcal{E}_{n0}$) is not degenerate, $\boldsymbol{k}$ is assumed to be small enough, such that $\mathcal{E}_{n\boldsymbol{k}} - \mathcal{E}_{n\mathbf{0}} << \mathcal{E}_{n\mathbf{0}} - \mathcal{E}_{m\mathbf{0}}$. Moreover, it might be found out that equation 1.10 does not contain terms proportional to $\boldsymbol{k}$ for $m=n$. As a result of these considerations, we find that $c_m(\boldsymbol{k})$ is proportional

to $\boldsymbol{k}$ and $c_n(\boldsymbol{k}) \approx 1$ (it also follows that $c_m(\boldsymbol{0}) = \delta_{mn}$ and $c_m(\boldsymbol{k}) << c_n(\boldsymbol{k})$ for $m \neq n$). Then finally it must hold that

$$c_m(\boldsymbol{k}) = \frac{\hbar \boldsymbol{k}}{m_0}.\boldsymbol{\pi}_{nm}\frac{1}{\mathcal{E}_{n\boldsymbol{0}} - \mathcal{E}_{m\boldsymbol{0}}} \tag{1.13}$$

in the first order of the perturbation theory.

This result can be inserted back to (1.10):

$$\mathcal{E}_{n0} - \mathcal{E}_{n\boldsymbol{k}} + \frac{\hbar^2 k^2}{2m_0} + \sum_{m\neq n}\left[\frac{\hbar \boldsymbol{k}}{m_0}.\pi_{mn}\frac{\hbar \boldsymbol{k}}{m_0}.\boldsymbol{\pi}_{nm}\frac{1}{\mathcal{E}_{n\boldsymbol{0}} - \mathcal{E}_{m\boldsymbol{0}}}\right] = 0 \tag{1.14}$$

and by simple manipulation we get second order correction to energy:

$$\mathcal{E}_{n\boldsymbol{k}} = \mathcal{E}_{n0} + \frac{\hbar^2 k^2}{2m_0} + \frac{\hbar^2}{m_0^2}\sum_{m\neq n}\frac{|\pi_{mn}.\boldsymbol{k}|^2}{\mathcal{E}_{n\boldsymbol{0}} - \mathcal{E}_{m\boldsymbol{0}}}. \tag{1.15}$$

This equation can be formally rewritten to get dispersion relation in the vicinity of the center of the first Brillouin zone in effective mass approximation:

$$\mathcal{E}_{n\boldsymbol{k}} = \mathcal{E}_{n0} + \frac{\hbar^2}{2}\sum_{\alpha,\beta} k_\alpha \frac{1}{\mu_n^{\alpha,\beta}} k_\beta, \tag{1.16}$$

where

$$\frac{1}{\mu_n^{\alpha,\beta}} = \frac{1}{m_0}\delta_{\alpha\beta} + \frac{2}{m_0^2}\sum_{m\neq n}\frac{\pi_{mn}^{\alpha}.\pi_{nm}^{\beta}}{\mathcal{E}_{n\boldsymbol{0}} - \mathcal{E}_{m\boldsymbol{0}}} \tag{1.17}$$

is the effective mass tensor of the n-th band edge and

$$\alpha, \beta = x, y, z.$$

Under effective mass approximation we get parabolic dispersion relations. This approximation can be generally improved by extending the perturbative treatment of $W(\boldsymbol{k})$ beyond the second order. However this is very troublesome and not particularly useful. Different approach has been taken by Kane [3].

1.4 Kane model

Although this section is not particularly useful for computations and results achieved in this work. However, the construction of new basis states is of considerable importance and framework of Kane model is further employed in crucial Luttinger approach.

Kane noticed that the three topmost valence states (previously denoted Γ_7 and Γ_8) and the lowest-lying conduction band (Γ_6) are very close to each other but fairly well separated from other bands. With this limited set of bands, $W(\boldsymbol{k})$ can be exactly diagonalized and the coupling with other states can be introduced by perturbative treatment.

It is desirable to choose such basis in that spin-orbit coupling is diagonal for $\boldsymbol{k} = \mathbf{0}$. Such basis can be achieved by forming linear combinations of 8 Bloch eigenfunctions that are associated with four bands under consideration ($|S\uparrow\rangle$, $|S\downarrow\rangle$, $|X\uparrow\rangle$, $|X\downarrow\rangle$, $|Y\uparrow\rangle$, $|Y\downarrow\rangle$, $|Z\uparrow\rangle$, $|Z\downarrow\rangle$). These new basis functions are created according to table 1.1, they are described in means of total angular momentum $\boldsymbol{J} = \boldsymbol{L} + \boldsymbol{\sigma}$ and its projection to z-axis $\boldsymbol{m_J}$ since these are diagonal in the new basis. For the S edge, $L = 0$ and $\sigma = \frac{1}{2}$, thus $J = \frac{1}{2}$ and m_J is either $\frac{1}{2}$ or $-\frac{1}{2}$. On the other hand, for P edges, adding $L = 1$ and $\sigma = \frac{1}{2}$ results in either $J = \frac{3}{2}$ and $J = \frac{1}{2}$. For $J = \frac{3}{2}$, there are four z-axis projections available ($m_J = \pm\frac{3}{2}$, $m_J = \pm\frac{1}{2}$). Thus it is associated quadruplet that is always higher energy (for III-V compounds) than the doublet $J = \frac{1}{2}$. It might be helpful to recall figure 1.2 for easier understanding. It is worth noting that that states $\left|\frac{3}{2}, \frac{3}{2}\right\rangle$ and $\left|\frac{3}{2}, -\frac{1}{2}\right\rangle$ (similarly $\left|\frac{3}{2}, -\frac{3}{2}\right\rangle$ and $\left|\frac{3}{2}, \frac{1}{2}\right\rangle$) are constructed from states with the same spins (in directions X and Y).

u_i	$\lvert J, m_J\rangle$	ψ_{J,m_J}	$\mathcal{E}_i\,(k=0)$
u_1	$\left\lvert\frac{1}{2}, \frac{1}{2}\right\rangle$	$i\lvert S\uparrow\rangle$	0
u_3	$\left\lvert\frac{3}{2}, \frac{1}{2}\right\rangle$	$\frac{1}{\sqrt{6}}\lvert(X+iY)\downarrow\rangle - \sqrt{\frac{2}{3}}\lvert Z\uparrow\rangle$	$-\mathcal{E}_0$
u_5	$\left\lvert\frac{3}{2}, \frac{3}{2}\right\rangle$	$\frac{1}{\sqrt{2}}\lvert(X+iY)\uparrow\rangle$	$-\mathcal{E}_0$
u_7	$\left\lvert\frac{1}{2}, \frac{1}{2}\right\rangle$	$\frac{1}{\sqrt{3}}\lvert(X+iY)\downarrow\rangle + \frac{1}{\sqrt{3}}\lvert Z\uparrow\rangle$	$-\mathcal{E}_0 - \Delta$
u_2	$\left\lvert\frac{1}{2}, -\frac{1}{2}\right\rangle$	$i\lvert S\downarrow\rangle$	0
u_4	$\left\lvert\frac{3}{2}, -\frac{1}{2}\right\rangle$	$-\frac{1}{\sqrt{6}}\lvert(X+iY)\uparrow\rangle - \sqrt{\frac{2}{3}}\lvert Z\downarrow\rangle$	$-\mathcal{E}_0$
u_6	$\left\lvert\frac{3}{2}, -\frac{3}{2}\right\rangle$	$\frac{1}{\sqrt{2}}\lvert(X+iY)\downarrow\rangle$	$-\mathcal{E}_0$
u_8	$\left\lvert\frac{1}{2}, -\frac{1}{2}\right\rangle$	$-\frac{1}{\sqrt{3}}\lvert(X+iY)\uparrow\rangle + \frac{1}{\sqrt{3}}\lvert Z\downarrow\rangle$	$-\mathcal{E}_0 - \Delta$

Table 1.1: Kane model - construction of new basis functions

Now we would like to construct the Hamiltonian. Matrix elements of $W(\boldsymbol{k})$ must be combined according to just constructed new basis. We further drop $\boldsymbol{k}$-dependent spin-orbit term and finally get *Kane* Hamiltonian (Table 1.2). We employ following notation:

$$k_\pm = \frac{1}{\sqrt{2}}\left(k_x \pm i k_y\right) \tag{1.18}$$

$$\mathcal{E}_0 = \mathcal{E}_{\Gamma_6} - \mathcal{E}_{\Gamma_8} \qquad \Delta = \mathcal{E}_{\Gamma_8} - \mathcal{E}_{\Gamma_7} \tag{1.19}$$

$$P = \frac{-i}{m_0}\langle S|p_x|X\rangle = \frac{-i}{m_0}\langle S|p_y|Y\rangle = \frac{-i}{m_0}\langle S|p_z|Z\rangle \tag{1.20}$$

For the sake of brevity we define new symbol $\lambda(\boldsymbol{k})$:

$$\lambda(\boldsymbol{k}) = \mathcal{E}(\boldsymbol{k}) - \frac{\hbar^2 k^2}{2m_0} \tag{1.21}$$

Solving the eigen-problem of Kane Hamiltonian we get following two equations:

$$\lambda(\boldsymbol{k}) = -\mathcal{E}_0 \tag{1.22}$$

$\frac{\hbar^2k^2}{2m_0}$	$-\sqrt{\frac{2}{3}}P\hbar k_z$	$P\hbar k_+$	$-\frac{1}{\sqrt{3}}P\hbar k_z$	0	$-\frac{1}{\sqrt{3}}P\hbar k_-$	0	$-\sqrt{\frac{2}{3}}P\hbar k_-$
$-\sqrt{\frac{2}{3}}P\hbar k_z$	$\frac{\hbar^2k^2}{2m_0}-\mathcal{E}_0$	0	0	$-\frac{1}{\sqrt{3}}P\hbar$	0	0	0
$P\hbar k_-$	0	$\frac{\hbar^2k^2}{2m_0}-\mathcal{E}_0$	0	0	0	0	0
$\frac{1}{\sqrt{3}}P\hbar k_z$	0	0	$\frac{\hbar^2k^2}{2m_0}-\mathcal{E}_0-\Delta$	$-\sqrt{\frac{2}{3}}P\hbar k_-$	0	0	0
0	$\frac{1}{\sqrt{3}}P\hbar k_+$	0	$\sqrt{\frac{2}{3}}P\hbar k_+$	$\frac{\hbar^2k^2}{2m_0}$	$-\sqrt{\frac{2}{3}}P\hbar k_z$	$P\hbar k_-$	$\frac{1}{\sqrt{3}}P\hbar k_z$
$-\frac{1}{\sqrt{3}}P\hbar k_+$	0	0	0	$-\sqrt{\frac{2}{3}}P\hbar k_z$	$\frac{\hbar^2k^2}{2m_0}-\mathcal{E}_0$	0	0
0	0	0	0	$P\hbar k_+$	0	$\frac{\hbar^2k^2}{2m_0}-\mathcal{E}_0$	0
$-\sqrt{\frac{2}{3}}P\hbar k_+$	0	0	0	$\frac{1}{\sqrt{3}}P\hbar k_z$	0	0	$\frac{\hbar^2k^2}{2m_0}-\mathcal{E}_0-\Delta$

Table 1.2: Kane model Hamiltonian

$$\lambda\left(\boldsymbol{k}\right)\left[\lambda\left(\boldsymbol{k}\right)+\mathcal{E}_0\right]\left[\lambda\left(\boldsymbol{k}\right)+\mathcal{E}_0+\Delta\right]=\hbar^2k^2P^2\left[\lambda\left(\boldsymbol{k}\right)+\mathcal{E}_0+\frac{2\Delta}{3}\right] \tag{1.23}$$

Each solution of these equations is twice degenerate (thus we have two solutions associated with the first equation and six more associated with the second one). Equation 1.22 refers to heavy holes $m_J=\pm\frac{3}{2}$ - this follows from no interaction between $\Gamma_8\left(m_J=\pm\frac{3}{2}\right)$ and Γ_6. Thus of both heavy holes and electrons have the same effective mass:

$$m^h_{\Gamma_8}=m_0 \tag{1.24}$$

The effective masses for other bands can be found by extending the equation 1.23 to the second order in $\boldsymbol{k}$:

$$\frac{1}{m_{\Gamma_6}}=\frac{1}{m_0}+\frac{4P^2}{3\mathcal{E}_0}+\frac{2P^2}{3\left(\mathcal{E}_0+\Delta\right)} \tag{1.25}$$

$$\frac{1}{m^l_{\Gamma_8}}=\frac{1}{m_0}-\frac{4P^2}{3\mathcal{E}_0} \tag{1.26}$$

$$\frac{1}{m_{\Gamma_7}}=\frac{1}{m_0}-\frac{2P^2}{3\left(\mathcal{E}_0+\Delta\right)} \tag{1.27}$$

The major shortcoming of this solution is that effective mass of heavy holes is not in accordance with experimental values. However, this can be improved by inserting the effect of other remote bands e.g. in the effective mass approximation:

$$\frac{1}{m^h_{\Gamma_8}}=\frac{1}{m_0}+\frac{2}{m_0^2}\sum_{m\neq\Gamma_6,\Gamma_7,\Gamma_8}\frac{\left|\left\langle\frac{3}{2},\pm\frac{3}{2}|p_z|u_m\right\rangle\right|}{\mathcal{E}_m-\mathcal{E}_0} \tag{1.28}$$

More details can be found in [2]. For example, it can be shown in a straightforward manner that dispersion relations are not parabolic under Kane model framework.

1.5 Heterostructures and the envelope function approximation

Heterostructure is created from two semiconductors with different bandgaps. In this work, we focus on the interface GaAs/GaAlAs. This interface has several basic advantages. It is direct bandgap semiconductor with tunable bandgap (by Al addition) from 1.4 eV up to 2 eV (to preserve direct bandgap). Both materials GaAs and AlAs are almost perfectly lattice matched which allows layers to be grown almost arbitrarily thick thanks to low induced stress. Advanced epitaxial techniques such as molecular beam epitaxy (MBE) or metal-organic chemical vapour deposition (MOCVD) made it possible to grow interfaces flat up to one atomic monolayer, which is obviously the ultimate available resolution. The possibility of fabricating a heterostructure with given parameters brought theoretical attention to the quasi-two-dimensional nature. Heterostructures shortly found various applications: laser emitting diodes (LED), diode lasers, quantum well infra-red photodetectors (QWIP), high electron mobility transistors (HEMT) and many more [13],[14],[15].

Here we assume that materials constituting the heterostructure are perfectly lattice matched and the interfaces are ideal (i.e. perfectly two-dimensionally grown). Thus, an electron in material A experiences perfect potential of bulk material A ($V_A(\boldsymbol{r})$)whereas in material B the electron feels perfect potential of bulk material B ($V_B(\boldsymbol{r})$). On the interface the potential changes step-like. In this work we deal only with single quantum well (SQW), whose potential function is schematically depicted in figure 1.3.

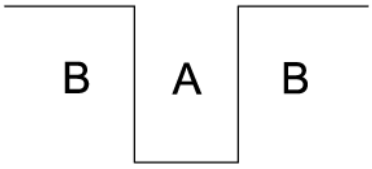

Figure 1.3: Schematic depicting of the potential of single quantum well (SQW)

Envelope function approximation is based on two crucial assumptions. The first one states that inside each layer the wave function can be expanded to the periodic parts of the Bloch functions of the states under consideration:

$$\psi(\boldsymbol{r}) = \sum_l f_l^{A,B}(\boldsymbol{r})\, u_{l,k_0}^{A,B}(\boldsymbol{r}), \tag{1.29}$$

k_0 is the point of Brillouin zone around which the heterostructure states are built, l denotes all the states that are included in calculations and $u_{l,k_0}^{(A,B)}(\boldsymbol{r})$ is a periodic part of Bloch function, that is periodic with the period of the potential $V(\boldsymbol{r})$. The truncation to finite sum over l states can be made by the assumption that the host wavevectors $\boldsymbol{k}_A$ a $\boldsymbol{k}_B$

are close to $\boldsymbol{k}_0$. This assumption is fulfilled for heterostructures consisting of materials with the same points of extreme of valence and conduction bands (e.g. both GaAs and $Al_xGa_{1-x}As$ for $x < 0,45$ are of Γ-related states).

The second assumption states that periodic parts of Bloch functions are the same in both layers:

$$u_{l,k_0}^{(A)}(\boldsymbol{r}) = u_{l,k_0}^{(B)}(\boldsymbol{r}) = u_{l,k_0}(\boldsymbol{r}). \tag{1.30}$$

Here, we in fact assume that interband matrix element $p_x = \langle S|\hat{p}_x|X\rangle$ is equal for both A and B layers. Our actual aim is to find $f_l^{(A,B)}(\boldsymbol{r})$.

We denote the growth direction of the heterostructure (quantum well) as z-axis. Since we assume ideal properties of the interface, we have translational symmetry in so-called in-plane directions (xy plane). We thus introduce two-dimensional in-plane vector $\boldsymbol{r}_\parallel$ and in-plane wave vector $\boldsymbol{k}_\parallel = (k_x, k_y)$.

We can factorize the slowly-varying envelope function

$$f_l^{(A,B)}(\boldsymbol{r}_\parallel, z) = \frac{1}{\sqrt{S}} exp\left(i\boldsymbol{k}_\parallel.\boldsymbol{r}_\parallel\right) \chi_l^{(A,B)}(z), \tag{1.31}$$

where S is the sample area.

The simplest possible Hamiltonian takes the form

$$H = \frac{\hat{\mathbf{p}}^2}{2m_0} + V_A(\boldsymbol{r})\,\theta_A(\boldsymbol{r}) + V_B(\boldsymbol{r})\,\theta_B(\boldsymbol{r}), \tag{1.32}$$

where $\theta_{(A,B)}(\boldsymbol{r})$ are step functions. θ_A and θ_B equal to one for $\boldsymbol{r}$ associated with A and B, respectively. When we act with this Hamiltonian on rapid-varying periodic part of Bloch function, we get:

$$H u_{l0}(\boldsymbol{r}) = \left(\mathcal{E}_{l0}^A \theta_A(\boldsymbol{r}) + \mathcal{E}_{l0}^A \theta_B(\boldsymbol{r})\right) u_{l0}(\boldsymbol{r}) \tag{1.33}$$

However, now we let act H on the whole $\psi(\boldsymbol{r})$, subsequently we multiply by complex conjugates: $u_{l0}^*(\boldsymbol{r})\, exp\left(-i\boldsymbol{k}_\parallel.\boldsymbol{r}_\parallel\right) \chi_l^{*(A,B)}(z)$ and integrate over the space. Moreover $p_z = -i\hbar\frac{\partial}{\partial z}$ is used. It can be found [2] that we get following equation for $\boldsymbol{\chi}$

$$\boldsymbol{D^{(0)}}\left(z, -i\hbar\frac{\partial}{\partial z}\right)\chi = \mathcal{E}\chi, \tag{1.34}$$

where

$$\begin{aligned} D_{lm}^{(0)}\left(z, -i\hbar\frac{\partial}{\partial z}\right) &= \left[\mathcal{E}_{l0}^A\theta_A(\boldsymbol{r}) + \mathcal{E}_{l0}^A\theta_B(\boldsymbol{r}) + \frac{\hbar^2 k_\parallel^2}{2m_0} - \frac{\hbar^2}{2m_0}\frac{\partial}{\partial z}\right]\delta_{lm} + \\ &+ \frac{\hbar\boldsymbol{k}_\parallel}{m_0}\langle l|\,\boldsymbol{p}_\parallel\,|m\rangle - \frac{i\hbar}{m_0}\langle l|\,\boldsymbol{p_z}\,|m\rangle\frac{\partial}{\partial z}. \end{aligned} \tag{1.35}$$

$D_{lm}^{(0)}$ might be generally $N \times N$ matrix, however calculations are restricted to bands Γ_6, Γ_8 (light and heavy holes) and Γ_7 band that is shifted due to spin-orbit coupling (recall Fig. 1.2), the matrix is then of size 8×8.

It is important to note that the in-plane terms are treated separately from the terms that affect z-direction. The effect of the remote bands can be added by perturbative approach similarly to the effective mass approximation discussed in section 1.3. At the end, the microstructural details of heterostructure are substituted by effective parameters, namely matrix elements $\langle l|\, \hat{\boldsymbol{p}_{\boldsymbol{\alpha}}}\, |\nu\rangle$ and so called band offsets $V_\nu\,(z)$, which represent the difference between energy of given band ν in the layer A and the energy of the band in the layer B. The index ν labels all states that are included into computations (including remote bands). This approach is further developed in Ben Daniel-Duke model. Even though this model is well applicable to electronic states in quantum wells, the applicability to holes is limited, due to assumption that $\boldsymbol{k}_{\parallel} = 0$ for band Γ_8. This simplification is impractical for our purpose. Detailed analysis of Ben Daniel-Duke model can be found in [2].

For our computations, it is more important to emphasize that we assume infinitely deep quantum well. The solution of this problem is fairly easy and well known. We focus only on ground states of electrons, light holes and heavy holes and further on first excited state of heavy holes. We can then simply write appropriate wave functions in z-direction:

$$\varphi_e\,(z_e) = \sqrt{\frac{2}{L}} cos\left(\frac{\pi}{L_z} z_e\right) \tag{1.36}$$

$$\varphi_{h0}\,(z_h) = \sqrt{\frac{2}{L}} cos\left(\frac{\pi}{L_z} z_h\right) \tag{1.37}$$

$$\varphi_l\,(z_h) = \sqrt{\frac{2}{L}} cos\left(\frac{\pi}{L_z} z_h\right) \tag{1.38}$$

$$\varphi_{h1}\,(z_h) = \sqrt{\frac{2}{L}} sin\left(\frac{2\pi}{L_z} z_h\right) \tag{1.39}$$

These wavefunctions are obviously defined only inside the well, more specifically $z_e, z_h \in \left(-\frac{L}{2}, \frac{L}{2}\right)$. The confinement energy of particle in infinitely deep quantum well is:

$$E_n = \frac{n^2 \hbar^2 \pi^2}{2 m L_z^2} \tag{1.40}$$

where the ground state is characterized by $n = 1$ and the first excited state is characterized by $n = 2$. The ground states confinement energy might be omitted during the computations but it contributes to the energy of optical transition and to the binding energy. The difference in confinement energies between the ground and the excited states defines the band offsets. However, the real band offset is in reality lower, because the potential well is in fact finite and thus the true wavefunctions tunnel into the barriers, which effectively means lower difference in confinement energies. (E.g. for the width of quantum well $L_z = 10$ nm we use the offset between ground and the first excited state equal to 16 nm, which would correspond to the infinitely deep quantum well with width of 13.7 nm.)

1.6 Luttinger Hamiltonian

When the in-plane wave vector $\boldsymbol{k}_{\|} \neq 0$, the heavy hole and the light hole states (denoted Γ_8^h and Γ_8^l) become coupled. This originates from the degeneracy of these two bands. In the isotropic material the Γ_8 Hamiltonian may be written as

$$H = \alpha k^2 + \beta \left(\boldsymbol{k}.\boldsymbol{J}\right)^2 \tag{1.41}$$

This Hamiltonian form was developed by Luttinger [4], [5] from somewhat abstract considerations about symmetry group theory and by precise perturbative approach.

It must be stressed that in bulk material it is always possible to rotate axes (choose $\boldsymbol{z}$ direction) such that $\boldsymbol{k}\|\boldsymbol{J}\|z$ and thus both H and J_z become diagonalized. However, in heterostructure, the direction z is given and diagonalization is not possible. The most favourable option is to quantize J along the heterostructure growth axis (z-axis) - this we have already done when dealing with Kane model. The analytical results, however, can be obtained only under very special and too restrictive conditions.

For GaAs-AlGaAs the coupling with Γ_6 band is relatively weak and can be omitted. The parabolic description of this host conduction band is also reasonable. Finally, the Luttinger Hamiltonian for the topmost valence band - Γ_8 band - of semiconductor with $\mathcal{T}_d$ symmetry in the basis composed of eigenfunctions of the total angular momentum takes the form

$$\hat{\mathbf{H}}_h = \begin{pmatrix} \hat{H}_{hh} & \hat{b} & \hat{c} & 0 \\ \hat{b}^* & \hat{H}_{lh} & 0 & \hat{c} \\ \hat{c}^* & 0 & \hat{H}_{lh} & -\hat{b} \\ 0 & \hat{c}^* & -\hat{b}^* & \hat{H}_{hh} \end{pmatrix} \begin{vmatrix} \left|\frac{3}{2}, +\frac{3}{2}\right\rangle \\ \left|\frac{3}{2}, +\frac{1}{2}\right\rangle \\ \left|\frac{3}{2}, -\frac{1}{2}\right\rangle \\ \left|\frac{3}{2}, -\frac{3}{2}\right\rangle \end{vmatrix} \tag{1.42}$$

Where we employed the notation:

$$\hat{H}_{hh} = \frac{\gamma_1 - 2\gamma_2}{2m_0}\hat{p}_z^2 + \frac{\gamma_1 + \gamma_2}{2m_0}\left(\hat{p}_x^2 + \hat{p}_y^2\right) \tag{1.43}$$

$$\hat{H}_{lh} = \frac{\gamma_1 + 2\gamma_2}{2m_0}\hat{p}_z^2 + \frac{\gamma_1 - \gamma_2}{2m_0}\left(\hat{p}_x^2 + \hat{p}_y^2\right) \tag{1.44}$$

$$\hat{b} = \frac{\sqrt{3}\gamma_3}{2m_0}\left[\left(\hat{p}_y\hat{p}_z + \hat{p}_z\hat{p}_y\right) + i\left(\hat{p}_x\hat{p}_z + \hat{p}_z\hat{p}_x\right)\right] \tag{1.45}$$

$$\hat{c} = \frac{\sqrt{3}}{2m_0}\left[\gamma_2\left(\hat{p}_x^2 - \hat{p}_y^2\right) - i\gamma_3\left(\hat{p}_x\hat{p}_y + \hat{p}_y\hat{p}_x\right)\right] \tag{1.46}$$

Parameters γ_i are so called Luttinger parameters. These empirical parameters embody the interaction between Γ_8 band and other bands including Γ_6. Luttinger parameters are considered to be position independent. It might be found from the inspection of the diagonal terms of Luttinger Hamiltonian that in-plane effective masses and effective masses in the z-direction differ and following identities hold:

$$\frac{\gamma_1+\gamma_2}{2m_0}=\frac{1}{2m_{hh\|}} \qquad \frac{\gamma_1-2\gamma_2}{2m_0}=\frac{1}{2m_{hh}^z} \tag{1.47}$$

$$\frac{\gamma_1-\gamma_2}{2m_0}=\frac{1}{2m_{lh\|}} \qquad \frac{\gamma_1+2\gamma_2}{2m_0}=\frac{1}{2m_{lh}^z} \tag{1.48}$$

Let us focus for a while on the $\hat{b}$ term. This term involves symmetrized products of $\hat{p_z}$ operator and in plane momentum operators. In our case these operators commute since we assume (and we will assume throughout this thesis) that z-component of vector potential of magnetic field is zero ($A_z = 0$) and complete vector potential $\boldsymbol{A}$ is z-independent. Moreover, the part of wavefunctions that depends on z is separated, thus we can finally write:

$$\hat{b}=\frac{\sqrt{3}\gamma_3}{2m_0}\left[\left(\hat{p}_y\hat{p}_z+\hat{p}_z\hat{p}_y\right)+i\left(\hat{p}_x\hat{p}_z+\hat{p}_z\hat{p}_x\right)\right]=\frac{\sqrt{3}\gamma_3}{m_0}\hat{p}_z\left(\hat{p}_y+i\hat{p}_x\right) \tag{1.49}$$

The operator $\hat{p}_z$ acts on z part of wavefunction so that we get the first derivative. Thus if we compute the term involving only the ground states ($\langle\varphi_l\left(z_h\right)\left|\hat{p}_z\right|\varphi_{h0}\left(z_h\right)\rangle$) we always get zero because both wavefunctions in this term are in fact cosine functions. By differentiation we get sine function that is orthogonal to the cosine one. This means that the $\hat{b}$ term may be omitted at positions of Hamiltonian matrix that combine ground state of heavy holes and light holes. But this also implies that we must include at least one excited hole state to utilize complete Luttinger framework. We include the first excited heavy hole state because of its small energy split (compared to the first excited light hole state).

To incorporate the first excited heavy hole state, the Hamiltonian matrix must be expanded by two states that correspond to the two different spin states (projections of total angular momentum). The Hamiltonian is then represented by 6 x 6 matrix. Before writing it explicitly we may inspect in a more detail Luttinger terms $\hat{b}$ and $\hat{c}$.

First, note that both terms $\hat{b}$ and $\hat{c}$ interconnect heavy hole and light hole states. Also note that $\hat{c}$ term does not act on the separated z-dependent part of the wavefunction. But these z-dependent parts are solution of confinement in the indefinitely deep quantum well and thus are orthogonal. Since the $\hat{c}$ term does not modify these functions, it is clear that all the terms involving any ground state, the $\hat{c}$ term and the excited state must be zero. $\hat{c}$ term combining these two states in Hamiltonian matrix can then be omitted. Remind that the $\hat{b}$ term can on the other hand be omitted when combining two ground states. We can thus finally write (with some reordering) extended 6 x 6 Hamiltonian.

$$\hat{\mathbf{H}}_h=\begin{pmatrix} \hat{H}_{hh0} & 0 & 0 & 0 & 0 & \hat{c} \\ 0 & \hat{H}_{hh1} & 0 & 0 & 0 & \hat{b} \\ 0 & 0 & \hat{H}_{lh} & \hat{c} & -\hat{b} & 0 \\ 0 & 0 & \hat{c}^* & \hat{H}_{hh0} & 0 & 0 \\ 0 & 0 & \text{-}\hat{b}^* & 0 & \hat{H}_{hh1} & 0 \\ \hat{c}^* & \hat{b}^* & 0 & 0 & 0 & \hat{H}_{lh} \end{pmatrix} \begin{vmatrix} \left|\frac{3}{2},+\frac{3}{2}\right\rangle\left|hh_0\right\rangle \\ \left|\frac{3}{2},+\frac{3}{2}\right\rangle\left|hh_1\right\rangle \\ \left|\frac{3}{2},+\frac{1}{2}\right\rangle\left|lh\right\rangle \\ \left|\frac{3}{2},-\frac{3}{2}\right\rangle\left|hh_0\right\rangle \\ \left|\frac{3}{2},-\frac{3}{2}\right\rangle\left|hh_1\right\rangle \\ \left|\frac{3}{2},-\frac{1}{2}\right\rangle\left|lh\right\rangle \end{vmatrix} \tag{1.50}$$

The minus sign in front of some of the $\hat{b}$ terms appears due to reverse order of the z-dependent parts of the wavefunctions in these terms, which is responsible for the sign reversal.

It is of extreme importance that this Hamiltonian can be divided into two independent matrices that can be diagonalized separately. These 3x3 Hamiltonian matrices are following:

$$\hat{\mathbf{H}}_h = \begin{pmatrix} \hat{H}_{hh0} & 0 & \hat{c} \\ 0 & \hat{H}_{hh1} & \hat{b} \\ \hat{c}^* & \hat{b}^* & \hat{H}_{lh} \end{pmatrix} \begin{matrix} \left|\frac{3}{2}, +\frac{3}{2}\right\rangle |hh_0\rangle \\ \left|\frac{3}{2}, +\frac{3}{2}\right\rangle |hh_1\rangle \\ \left|\frac{3}{2}, -\frac{1}{2}\right\rangle |lh\rangle \end{matrix} \tag{1.51}$$

$$\hat{\mathbf{H}}_h = \begin{pmatrix} \hat{H}_{hh0} & 0 & \hat{c} \\ 0 & \hat{H}_{hh1} & \hat{b} \\ \hat{c}^* & \hat{b}^* & \hat{H}_{lh} \end{pmatrix} \begin{matrix} \left|\frac{3}{2}, -\frac{3}{2}\right\rangle |hh_0\rangle \\ \left|\frac{3}{2}, -\frac{3}{2}\right\rangle |hh_1\rangle \\ \left|\frac{3}{2}, +\frac{1}{2}\right\rangle |lh\rangle \end{matrix} \tag{1.52}$$

The Hamiltonians differ only by projection of total angular momentum (actually spin). In our computations these two Hamiltonians will differ only by signs of Zeeman terms and can be treated separately throughout the work. With no magnetic field included, the dispersion relations can be easily computed and depicted. Figure 1.4 (taken from [1]) shows the in-plane dispersion relations of a hole in a single quantum well with parameters

- $\gamma_1 = 6.85,\ \gamma_2 = 2.10,\ \gamma_3 = 2.90,\ L_z = 10\,\mathrm{nm}$
- a) $E^{(0)}_{HH1} = 0\,\mathrm{meV},\ E^{(0)}_{LH1} = -10\,\mathrm{meV},\ E^{(0)}_{HH2} = -16\,\mathrm{meV}$
- b) $E^{(0)}_{HH1} = 0\,\mathrm{meV},\ E^{(0)}_{LH1} = -20\,\mathrm{meV},\ E^{(0)}_{HH2} = -40\,\mathrm{meV}$

$HH1$ refers to the heavy hole state on lowest energy level in quantum well. $LH1$ is the lowest light hole state and $HH2$ is the first excited heavy hole state. $E^{(0)}_{LH1}$ and $E^{(0)}_{HH2}$ are appropriate energy splits at $\boldsymbol{k}_{\|} = 0$. Dashed lines represent dispersion relations for diagonal approximation (omitting of Luttinger terms $\hat{b}$ and $\hat{c}$ - parabolic dispersion). Note the mass reversal (the mass of the heavy hole is lower then the mass of the light hole) which results in crossing of the bands. On the other hand, solid lines represent computed dispersion relations for full Luttinger Hamiltonian. The mixing of light hole and heavy hole states leads to anticrossing of the bands and even to negative effective mass of the light hole in the vicinity of the origin (actually, notation of the bands as heavy hole or light hole states loses its physical significance due to mutual mixing).

It is useful now to introduce the simple electronic Hamiltonian:

$$H_e = \frac{\boldsymbol{p}^2}{2m_e} = \frac{p_x^2 + p_y^2}{2m_e} + \frac{p_z^2}{2m_e} \tag{1.53}$$

This simple Hamiltonian is diagonal in the basis of Luttinger Hamiltonian, thus it must be added to all diagonal elements of the Hamiltonian matrix in the case if we want to investigate system of hole and electron (exciton - see further).

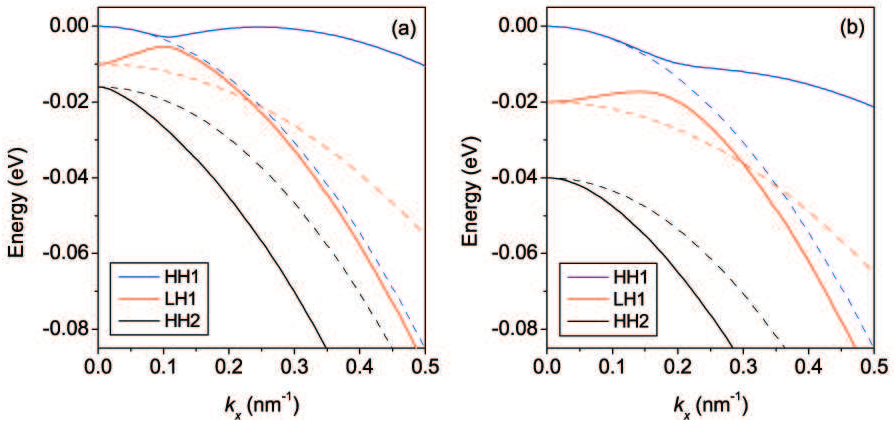

Figure 1.4: Dispersion relations for two different sets of parameters. Dashed lines represent parabolic dispersion whereas solid lines represent the dispersion according to complete Luttinger Hamiltonian.

1.7 Inclusion of Magnetic Field

Magnetic field is included in fundamental and straightforward way. The momentum operator $\hat{\boldsymbol{p}}$ is substituted by $\hat{\boldsymbol{p}} - e\boldsymbol{A}$, where A is vector potential.

In this work, we assume magnetic field only perpendicular to the quantum well: $\boldsymbol{B} = (0, 0, B_z)$. It is well known that the vector potential is not uniquely determined. The calibration must be chosen in accordance with chosen wave function basis. In this respect, an important example is an approach utilized by Whittaker and Shields [6]. They chose symmetric calibration which is seemingly the most appropriate considering the cylindrical symmetry of the problem. However, this calibration inevitably leads to computation in polar coordinates and to wave functions involving complicated Laguerre polynomials.

Our approach is based on the Landau calibration in a form: $\boldsymbol{A} = (0, B_z x, 0)$ or in compact form $A_y = B_z x$. From now on we write only B, implicitly assuming that it is in z-direction. The Hamiltonian in x-direction takes the form of the linear harmonic oscillator. In this instructive approach, the x-dependent part of the eigenfunction is the eigenfunction of linear harmonic oscillator problem, whereas y-dependent part is a simple plane wave. It is useful to introduce magnetic length

$$\lambda = \sqrt{\frac{\hbar}{eB}} = \frac{25.66}{\sqrt{B[T]}}\mathtt{nm} \tag{1.54}$$

which depends only on B and thus it is a measure of magnetic field, that is in fact measured in metres, in our case usually more conveniently in nanometres. We can derive the in-plane parts of diagonal terms of Luttinger Hamiltonian (the term is the same for both heavy and light holes - just differs in the effective masses) and also in-plane parts of electronic Hamiltonian. Note that after the inclusion of magnetic field we write the remaining

momentum operators without hat and these operators now represents only $p_j = -i\hbar\frac{\partial}{\partial j}$ $j = x, y, z$ and all these operators commute.

$$H_h = \frac{p_{x_h}^2}{2m_h} + \frac{1}{2m_h}\left(p_{y_h} - eBx_h\right)^2 = \frac{1}{2m_h}\left(p_{x_h}^2 + p_{y_h}^2 - 2\frac{\hbar}{\lambda^2}x_h p_{y_h} + \frac{\hbar^2}{\lambda^4}x_h^2\right) \tag{1.55}$$

$$H_e = \frac{p_{x_e}^2}{2m_e} + \frac{1}{2m_e}\left(p_{y_e} + eBx_e\right)^2 = \frac{1}{2m_e}\left(p_{x_e}^2 + p_{y_e}^2 + 2\frac{\hbar}{\lambda^2}x_e p_{y_e} + \frac{\hbar^2}{\lambda^4}x_1^2\right) \tag{1.56}$$

Note that e refers to absolute value of elementary charge. We derive further the Luttinger terms in the presence of the magnetic field

$$\hat{b} = \frac{\sqrt{3}\gamma_3}{2m_0}p_z\left(p_x - ip_y + ieBx\right) = \frac{\sqrt{3}\gamma_3}{2m_0}p_z\left(p_x - ip_y + i\frac{\hbar x}{\lambda^2}\right) \tag{1.57}$$

$$\hat{c} = \frac{\sqrt{3}}{2m_0}\left[\gamma_2\left(p_x^2 - p_y^2 + 2p_y eBx - e^2B^2x^2\right) - i\gamma_3\left(2p_x p_y - p_x eBx - eBxp_x\right)\right] \tag{1.58}$$

$$= \frac{\sqrt{3}}{2m_0}\left[\gamma_2\left(p_x^2 - p_y^2 + 2p_y\frac{\hbar x}{\lambda^2} - \frac{\hbar^2x^2}{\lambda^4}\right) - i\gamma_3\left(2p_x p_y - p_x\frac{\hbar x}{\lambda^2} - \frac{\hbar x}{\lambda^2}p_x\right)\right] \tag{1.59}$$

It is illustrative to exploit these terms further. Let us focus only on the terms affecting the x-component and let us omit some constants

$$\hat{b}_x \sim \left(p_x + i\frac{\hbar x}{\lambda^2}\right) \sim \left(\frac{d}{dx} - \frac{x}{\lambda^2}\right) \tag{1.60}$$

This representation of $\hat{b}_x$ immediately reminds of a creation operator of linear harmonic oscillator problem. The eigenfunctions in the Landau quantization considering only x-direction can be written as follows (quantum number n actually labels the Landau levels):

$$\Psi_n = \frac{1}{\sqrt{\lambda\sqrt{\pi}}}\sqrt{\frac{1}{2^n n!}}H_n\left(\frac{x}{\lambda}\right)e^{-\frac{x^2}{2\lambda^2}} \tag{1.61}$$

where H_n are Hermitian polynomials. It might be easily found that the operator $\hat{b}_x$ acts on Ψ_n as a creation operator. Due to the orthogonality of the linear harmonic oscillator eigenfunctions the term $\left\langle \Psi_m|\hat{b}|\Psi_n \right\rangle$ is non-zero only for $m = n+1$. Similarly, the complex conjugate $\hat{b}_x^* \sim \left(p_x - i\frac{\hbar x}{\lambda^2}\right) \sim \left(\frac{d}{dx} + \frac{x}{\lambda^2}\right)$ acts as an annihilation operator on Landau levels. Interestingly enough, similar analysis can be done for $\hat{c}$ term (under the assumption $\gamma_2 = \gamma_3$)

$$\hat{c}_x \sim \left(p_x^2 - \frac{\hbar^2 x^2}{\lambda^4} + i p_x \frac{\hbar x}{\lambda^2} + i \frac{\hbar x}{\lambda^2} p_x \right) \tag{1.62}$$

$$\hat{c}_x \sim \left(\frac{d^2}{dx^2} + \frac{x^2}{\lambda^4} - \frac{d}{dx}\frac{x}{\lambda^2} - \frac{x}{\lambda^2}\frac{d}{dx} \right) \sim \left(\frac{d}{dx} - \frac{x}{\lambda^2} \right) \left(\frac{d}{dx} - \frac{x}{\lambda^2} \right) \tag{1.63}$$

The operator $\hat{c}_x$ acts twice as a creation operator. Similarly the complex conjugate $\hat{c}^*$ acts as two annihilation operators. We can finally conclude that minimum of two Landau levels must be included in the analysis for both Luttinger terms to take effect.

1.8 Zeeman terms

The shift and splitting of the energy spectra due to the presence of external magnetic field are called *Zeeman effect*. The study of such Zeeman splitting of bound complexes such as excitons or trions give us information about the binding energies, coupling of states, etc. Moreover some bound complexes are only stable in the presence of the external magnetic field inducing corresponding Zeeman energy shift. Basic theory of Zeeman splitting in atoms is given in many textbooks (e.g. [7]). The most important concepts that are obviously relevant for these thesis are the introduction of Bohr magneton $\mu_B = \frac{\hbar e}{2m_0}$ and the introduction of Landé g-factor, which can be exactly computed for simple systems. The energy splitting for spinless particles is referred to as *normal Zeeman effects* with the split of adjacent energies

$$\Delta E = \mu_B B \tag{1.64}$$

whereas for systems with spin there is additional coefficient - Lande g-factor - and the energy splitting of so called anomalous Zeeman effect is given as

$$\Delta E = g \mu_B B \tag{1.65}$$

The Zeeman term for electrons and holes in semiconductors has been derived by Luttinger purely from symmetric consideration. Actually, very careful handling with wavevectors (or momentum operators) that do not commute is the most important. The derivation can be found in a very detail in [4], however, very schematically, the Zeeman term evolves from the commutation relations of momentum operators in the presence of magnetic field. In the Luttinger analysis, there appears following term that leads to Zeeman the term

$$\frac{i}{2m_0} [\hat{p_x}, \hat{p_y}] = \frac{i}{2m_0} \left(p_x \left(p_y - eBx \right) - \left(p_y - eBx \right) p_x \right) \tag{1.66}$$

$$= \frac{i}{2m_0} \left(-i\hbar \frac{\partial}{\partial x} eBx \right) \tag{1.67}$$

$$= \frac{\hbar e B}{2m_0} = \mu_B B \tag{1.68}$$

The theory of Zeeman splitting in systems related to this thesis will be further developed in the next section after introduction of exciton and trion concepts. Some experimental results of g-factor measurements are presented in the Literature review section.

2 Excitons and Trions

2.1 Exciton

Exciton is an electrically neutral quasiparticle that represents bound state of an electron and hole that are attracted to each other by the Coulomb force. This attractive force ensures that exciton has lower energy than unbound electron and hole thus new excitonic energy level inside the forbidden gap is created. When dealing computationally with the excitonic problem, the fundamental step is always the decomposition of centre-of-motion movement and the relative coordinate that describes just the distance between the hole and the electron. Let us now outline the solution for three gradually more complicated cases. The first describes excitons in a bulk semiconductor, the second takes into account quantum heterostructure and the third includes the magnetic field.

2.1.1 Excitons in an idealized bulk semiconductor

Let us consider simple semiconductor that can be characterized by single conduction band and single valence band that are both described by parabolic dispersion relations:

$$\mathcal{E}_c(\boldsymbol{k}) = E_g + \frac{\hbar^2 k^2}{2m_c} \tag{2.1}$$

$$\mathcal{E}_v(\boldsymbol{k}) = -\frac{\hbar^2 k^2}{2m_v} \tag{2.2}$$

m_c and m_v are corresponding effective masses. The ground state is a state with completely filled valence band and empty conduction band. However, if an electron is excited into the conduction band, one place in the valence band is left unoccupied. It is useful then to introduce the concept of *hole*. The valence band with one unoccupied state can be considered as the filled band plus a *hole*. The hole is characterized by wavevector $\boldsymbol{k}_h = -\boldsymbol{k}_v$, effective mass $m_h = -m_v$ and positive charge $+e$. For unbound state, the energy of the first excited state would be E_g, but for the excitonic bound state, the particles are attracted by Coulombic force and the energy is modified and it can be determined by the solution of Schrödinger equation:

$$\left[\frac{\hat{\boldsymbol{p}}_e^2}{2m_e} + \frac{\hat{\boldsymbol{p}}_h^2}{2m_h} - \frac{e^2}{4\pi\varepsilon\left|\boldsymbol{r}_e - \boldsymbol{r}_h\right|}\right]\psi(\boldsymbol{r}_e, \boldsymbol{r}_h) = (E - E_g)\,\psi(\boldsymbol{r}_e, \boldsymbol{r}_h) \tag{2.3}$$

Electronic effective mass can be identified as $m_e \equiv m_c$ and ε is the static dielectric constant of the semiconductor. The structure of this Schrödinger equation is equivalent to that describing the hydrogen atom and can be treated in the same way. The first and crucial step is defining of new coordinate system, in other words, the introduction of

centre-of-mass.

$$\boldsymbol{r} = \boldsymbol{r}_e - \boldsymbol{r}_h \tag{2.4}$$

$$\boldsymbol{R} = \frac{m_e \boldsymbol{r}_e + m_h \boldsymbol{r}_h}{m_e + m_h} \tag{2.5}$$

$$\hat{\boldsymbol{p}} = -i\hbar \frac{\partial}{\partial \boldsymbol{r}} \tag{2.6}$$

$$\hat{\boldsymbol{P}} = -i\hbar \frac{\partial}{\partial \boldsymbol{R}} \tag{2.7}$$

$$\hat{\boldsymbol{P}} = \hat{\boldsymbol{p_e}} + \hat{\boldsymbol{p_h}} \tag{2.8}$$

$$\hat{\boldsymbol{p}} = \frac{m_h \hat{\boldsymbol{p_e}} - m_e \hat{\boldsymbol{p_h}}}{m_e + m_h} \tag{2.9}$$

$$M = m_e + m_h \tag{2.10}$$

$$\mu = \frac{m_e m_h}{m_e + m_h} \tag{2.11}$$

By this set of substitutions we obtain following equation:

$$\left[\frac{\hat{\boldsymbol{P}}^2}{2M} + \frac{\hat{\boldsymbol{p}}^2}{2\mu} - \frac{e^2}{4\pi\varepsilon r} \right] \psi(\boldsymbol{r}, \boldsymbol{R}) = (E - E_g)\, \psi(\boldsymbol{r}, \boldsymbol{R}) \tag{2.12}$$

The main importance of this substitution is that the Hamiltonian terms acting on $\boldsymbol{r}$ and $\boldsymbol{R}$ are well separated. The Hamiltonian structure thus enables to separate the wave function into parts that depend on $\boldsymbol{r}$ and $\boldsymbol{R}$, respectively. Moreover, the centre-of-mass moves like the free particle since Hamiltonian acting on $\boldsymbol{R}$ is a free particle Hamiltonian. In other words $\hat{\boldsymbol{P}} = \hbar \boldsymbol{K}$ is a good quantum number, thus we can decompose the wavefunction as:

$$\psi(\boldsymbol{r}, \boldsymbol{R}) = \frac{1}{\sqrt{W}} exp(i\boldsymbol{K}.\boldsymbol{R})\, \phi(\boldsymbol{r}) \tag{2.13}$$

The constant W just normalizes the wavefunctions. In order to solve the Schrödinger equation for relative coordinate $\boldsymbol{r}$ only, it is necessary to rescale the energy:

$$E = E_g + \frac{\hbar K^2}{2M} + \mathcal{E} \tag{2.14}$$

We thus finally obtained following equation, that is formally equivalent to the hydrogen atom problem:

$$\left[\frac{\hat{\boldsymbol{p}}^2}{2\mu} - \frac{e^2}{4\pi\varepsilon r} \right] \phi(\boldsymbol{r}) = \mathcal{E} \phi(\boldsymbol{r}) \tag{2.15}$$

The solutions to this equation are the hydrogen like wavefunctions (e.g. [7]). Most

importantly, for the ground state holds:

$$\phi(\boldsymbol{r}) = \frac{1}{\sqrt{\pi a_B^3}} exp\left(\frac{-r}{a_B}\right) \tag{2.16}$$

$$\mathcal{E} = -\frac{\mu e^4}{32\pi^2\varepsilon^2\hbar^2} \tag{2.17}$$

$$a_B = \frac{4\pi\varepsilon\hbar^2}{\mu e^2} \tag{2.18}$$

a_B is the effective excitonic Bohr radius. Exciton can be thus considered as quasi particle with the mass of $M = m_e + m_h$ and the ground energy $E < E_g$.

2.1.2 Excitons in an idealized heterostructure

Now, let us consider single quantum well that is created by a layer of material A in between of material B. We need to assume that both materials A and B have the same dielectric constant ε and that effective masses m_h and m_e are equal in both A and B. We also assume now that dispersion relations of both electrons and holes are simple parabolic. Under these assumptions we can write Schrödinger equation as follows:

$$\left[\frac{\hat{\boldsymbol{p}}_e^2}{2m_e} + \frac{\hat{\boldsymbol{p}}_h^2}{2m_h} - \frac{e^2}{4\pi\varepsilon\left|\boldsymbol{r}_e - \boldsymbol{r}_h\right|} + U_e(z_e) + U_h(z_h)\right]\psi(\boldsymbol{r}_e, \boldsymbol{r}_h) = \\ = (E - E_g)\,\psi(\boldsymbol{r}_e, \boldsymbol{r}_h) \tag{2.19}$$

$U_e(z_e)$ and $U_h(z_h)$ are step-like quantum well potentials for electrons and holes. Under the assumption of infinitely deep quantum well, these potentials effectively confine the excitons inside the quantum well. Anyway, due to the confining potentials, it is not possible to carry out the centre-of-mass transformation in the z-direction. It is only possible to define new coordinate system for the in-plane components x and y.

$$\boldsymbol{r}_\parallel = \boldsymbol{r}_{e\parallel} - \boldsymbol{r}_{h\parallel} \tag{2.20}$$

$$\boldsymbol{R}_\parallel = \frac{m_e\boldsymbol{r}_{e\parallel} + m_h\boldsymbol{r}_{h\parallel}}{m_e + m_h} \tag{2.21}$$

$$\hat{\boldsymbol{p}}_\parallel = -i\hbar\frac{\partial}{\partial\boldsymbol{r}_\parallel} \tag{2.22}$$

$$\hat{\boldsymbol{P}}_\parallel = -i\hbar\frac{\partial}{\partial\boldsymbol{R}_\parallel} \tag{2.23}$$

$$\hat{\boldsymbol{P}}_\parallel = \hat{\boldsymbol{p_e}}_\parallel + \hat{\boldsymbol{p_h}}_\parallel \tag{2.24}$$

$$\hat{\boldsymbol{p}}_\parallel = \frac{m_h\hat{\boldsymbol{p_e}}_\parallel - m_e\hat{\boldsymbol{p_h}}_\parallel}{m_e + m_h} \tag{2.25}$$

Resulting Schrödinger equation can be written as follows using already defined M and μ:

$$\left[\frac{\hat{\boldsymbol{P}}^2}{2M}+\frac{\hat{\boldsymbol{p}}^2}{2\mu}+\frac{\hat{\boldsymbol{p}}_{z_e}^2}{m_e}+\frac{\hat{\boldsymbol{p}}_{z_h}^2}{2m_h}-\frac{e^2}{4\pi\varepsilon\sqrt{\boldsymbol{r}_\parallel^2+(z_e-z_h)^2}}+U_e(z_e)+U_h(z_h)\right]\times$$
$$\times\psi\left(\boldsymbol{r}_\parallel,\boldsymbol{R}_\parallel,z_e,z_h\right)=(E-E_g)\,\psi\left(\boldsymbol{r}_\parallel,\boldsymbol{R}_\parallel,z_e,z_h\right) \tag{2.26}$$

We can again factorize the wavefunction $\psi\left(\boldsymbol{r}_\parallel,\boldsymbol{R}_\parallel,z_e,z_h\right)$. Moreover the '$xy$-centre-of-mass' moves in the xy-plane like the free particle thus we can write

$$\psi\left(\boldsymbol{r}_\parallel,\boldsymbol{R}_\parallel,z_e,z_h\right)=\frac{1}{\sqrt{W}}exp\left(i\boldsymbol{K}_\parallel.\boldsymbol{R}_\parallel\right)\phi\left(\boldsymbol{r}_\parallel,z_e,z_h\right) \tag{2.27}$$

The solution of Eq.2.26 for $\phi\left(\boldsymbol{r}_\parallel,z_e,z_h\right)$ is still uneasy, but the decomposition of movement into relative coordinates is perfectly feasible as it has been shown. The solution of this problem is out of sight of this thesis since the formulation of the problem does not involve the real valence-band structure.

2.1.3 Excitons in an idealized heterostructure with inclusion of magnetic field

Let us first remind that we assume only magnetic field perpendicular to the quantum well $\boldsymbol{B}=(0,0,B_z)$ and Landau calibration in the form: $\boldsymbol{A}=(0,B_zx,0)$. Hamiltonian can thus be written as:

$$\Big[\frac{p_{xe}^2+(p_{ye}+eBx_e)^2}{2m_e}+\frac{p_{xh}^2+(p_{yh}-eBx_h)^2}{2m_h}+\frac{p_{ze}^2}{2m_e}+\frac{p_{zh}^2}{2m_h}$$
$$-\frac{e^2}{4\pi\varepsilon\left|\boldsymbol{r}_e-\boldsymbol{r}_h\right|}+U_e(z_e)+U_h(z_h)\Big]\psi\left(\boldsymbol{r}_e,\boldsymbol{r}_h\right)=$$
$$=(E-E_g)\,\psi\left(\boldsymbol{r}_e,\boldsymbol{r}_h\right) \tag{2.28}$$

Showing that even this Hamiltonian is well decomposed by centre-of-mass transform is still straightforward but it needs some computational effort. We use the same set of identities to defining the new coordinate system as in the previous part. That transform does not affect the z-components and the Coulombic potential term includes apart of the z-components only the relative coordinate $\boldsymbol{r}_\parallel$. This means that we need to deal only with the first two fractions. To be very explicit we write the exact substitutions that must be made

$$\boldsymbol{r}_{h\parallel}=\boldsymbol{R}_\parallel-\frac{m_e}{m_e+m_h}\boldsymbol{r}_\parallel \tag{2.29}$$

$$\boldsymbol{r}_{e\parallel}=\boldsymbol{R}_\parallel+\frac{m_h}{m_e+m_h}\boldsymbol{r}_\parallel \tag{2.30}$$

$$\boldsymbol{p}_{h\parallel}=-\boldsymbol{p}_\parallel+\frac{m_h}{m_e+m_h}\boldsymbol{P}_\parallel \tag{2.31}$$

$$\boldsymbol{p}_{e\parallel}=\boldsymbol{p}_\parallel+\frac{m_e}{m_e+m_h}\boldsymbol{P}_\parallel \tag{2.32}$$

and the used notation

$$\begin{aligned} \boldsymbol{r}_{h\parallel} &= (x_h, y_h) & \boldsymbol{r}_{e\parallel} &= (x_e, y_e) & \boldsymbol{r}_{\parallel} &= (x, y) & \boldsymbol{R}_{\parallel} &= (X, Y) \\ \boldsymbol{p}_{h\parallel} &= (p_{xh}, p_{yh}) & \boldsymbol{p}_{e\parallel} &= (p_{xe}, p_{ye}) & \boldsymbol{p}_{\parallel} &= (p_x, p_y) & \boldsymbol{P}_{\parallel} &= (P_x, P_y) \end{aligned}$$

After straightforward but lengthy computation we get following formula describing the first two fractions in the Hamiltonian 2.28:

$$\begin{aligned} \frac{\hat{\boldsymbol{P}}^2}{2M} + \frac{\hat{\boldsymbol{p}}^2}{2\mu} + eB\left(\frac{p_y X}{\mu} + \frac{Pyx}{M} + p_y x(m_e^{-1} - m_h^{-1})\right) + \\ + e^2B^2\left(\frac{X^2}{2\mu} + \frac{m_h^2 + m_e^2 - m_e m_h}{2m_e m_h(m_e + m_h)}x^2 + Xx(m_e^{-1} - m_h^{-1})\right) \end{aligned} \tag{2.33}$$

This part of the Hamiltonian does not seem to be decomposed at all. However, it is possible to choose following wavefunctions that leads to intended decomposition:

$$\Psi = \psi(X, Y, y)\phi(x, y, z_e, z_h) = exp\left[i\left(K_x - \frac{eBy}{\hbar}\right)X + iK_y Y\right]\phi(x, y, z_e, z_h) \tag{2.34}$$

Let us now act with the important part of Hamiltonian on such wavefunction. We need to avoid all the terms that include X or Y, thus we write only those problematic terms (extreme caution must be paid when dealing with the first following term since double differentiation of product results in three terms altogether):

$$\frac{\hat{\boldsymbol{p}}^2}{2\mu}\Psi = \frac{e^2B^2X^2}{2\mu}\Psi + \frac{i\hbar eBX}{\mu}\psi\frac{\partial\phi}{\partial y} + ... \tag{2.35}$$

$$eB\frac{p_y X}{\mu}\Psi = -\frac{e^2B^2X^2}{\mu}\Psi - \frac{i\hbar eBX}{\mu}\psi\frac{\partial\phi}{\partial y} \tag{2.36}$$

$$eBp_y x(m_e^{-1} - m_h^{-1})\Psi = -e^2B^2Xx(m_e^{-1} - m_h^{-1})\Psi \tag{2.37}$$

$$e^2B^2\left(\frac{X^2}{2\mu} + Xx(m_e^{-1} - m_h^{-1})\right)\Psi = \frac{e^2B^2X^2}{2\mu}\Psi + e^2B^2Xx(m_e^{-1} - m_h^{-1})\Psi \tag{2.38}$$

It is now obvious that if we sum the right hand sides we get zero. Thus no term involving the centre-of-mass coordinates is left and the problem is reduced to find eignefunctions $\phi(x, y, z_e, z_h)$ that are independent of the centre-of-mass motion.

2.1.4 Excitons and Luttinger Hamiltonian

In the previous chapter, we used Luttinger Hamiltonian framework to describe the valence band. Now, we would like to describe whole exciton in this framework. However, this is rather simple. The electronic Hamiltonian is diagonal in the basis of Luttinger Hamiltonian, as well as confining potentials and Coulombic term. The excitonic Hamiltonian can thus be shortly written as:

$$\hat{\mathbf{H}} = \hat{\mathbf{H}}_h + \left(\hat{H}_e + U_e + U_h - V_{e-h}\right)\mathbf{1} = \hat{\mathbf{H}}_h + \hat{\mathcal{H}}\mathbf{1} \tag{2.39}$$

where **1** means 4×4 identity matrix. We can write the Hamiltonian in a more detail:

$$\hat{\mathbf{H}}\,|\psi\rangle = \begin{pmatrix} \hat{\mathbf{H}}_{hh} + \hat{\mathcal{H}} & \hat{b} & \hat{c} & 0 \\ \hat{b}^* & \hat{\mathbf{H}}_{lh} + \hat{\mathcal{H}} & 0 & \hat{c} \\ \hat{c}^* & 0 & \hat{\mathbf{H}}_{lh} + \hat{\mathcal{H}} & -\hat{b} \\ 0 & \hat{c}^* & -\hat{b}^* & \hat{\mathbf{H}}_{hh} + \hat{\mathcal{H}} \end{pmatrix} \begin{vmatrix} \frac{3}{2}, +\frac{3}{2} \rangle \\ \frac{3}{2}, +\frac{1}{2} \rangle \\ \frac{3}{2}, -\frac{1}{2} \rangle \\ \frac{3}{2}, -\frac{3}{2} \rangle \end{vmatrix} \tag{2.40}$$

Note that if we assume infinitely deep quantum well, the confining potentials U_e and U_h can be omitted since exciton is completely confined inside the well. Luttinger Hamiltonian effectively mixes the light and heavy hole states. As a result, the exciton can consist of both heavy and light holes at once. Due to energetic shift of light holes, the exciton involves heavy hole with much higher probability, thus the light hole exciton is often omitted.

Let us remind the simple electronic Hamiltonian:

$$\hat{H}_e = \frac{\hat{\boldsymbol{p}}_e^2}{2m_e} = \frac{\hat{p}_{z_e}^2}{2m_e} + \frac{\hat{p}_{x_e}^2 + \hat{p}_{y_e}^2}{2m_e} \tag{2.41}$$

It is notable that we assume the same electron effective mass m_e in both $\boldsymbol{z}$ and $\boldsymbol{r}_{\parallel}$ directions. The magnetic field can be formally included through momentum operators, however Zeeman term has not been explicitly mentioned since it is the topic of following section.

2.1.5 Excitons and Zeeman effect

The literature considering Zeeman splitting of the excitons in different systems is completely inconclusive. Moreover, even the basic description differs among the authors which makes brief overview almost impossible. In the most cases, authors consider only such exciton that includes the heavy hole. Such exciton contains an electron that has spin either $-\frac{1}{2}$ or $\frac{1}{2}$ and heavy hole that can possess two different values of total angular momentum $\pm\frac{3}{2}$. This is the case of excitonic spectrum shown in Fig. 2.1. In the presence of magnetic field the degenerate excitonic energy level splits into four levels due to Zeeman effect. The exciton can annihilate and corresponding energy is emitted, but this is the case only for optically active - allowed transitions. These allowed transitions always involve the change of total spin by ± 1. This means that we can observe two allowed photoluminiscence (PL) optical transitions from heavy hole exciton annihilation. Actually, the transition during which the spin changes by $+1$ can be observed in right-handed circularly polarized PL light (σ^+) and the transition associated with the spin change by -1 in left-handed circularly polarized PL light (σ^-). However, there is no complete agreement about which transition belongs to which polarization. Moreover some authors possibly just confuse σ^+ and σ^- polarizations. Under this simplified framework we can observe two transitions whose energetic splitting can be written as:

$$\Delta E = g_{eff}\mu_B B. \tag{2.42}$$

g_{eff} denotes the effective excitonic g-factor. In experimental works, the energy difference is usually taken positive and thus the effective g-factor is also assumed to be positive

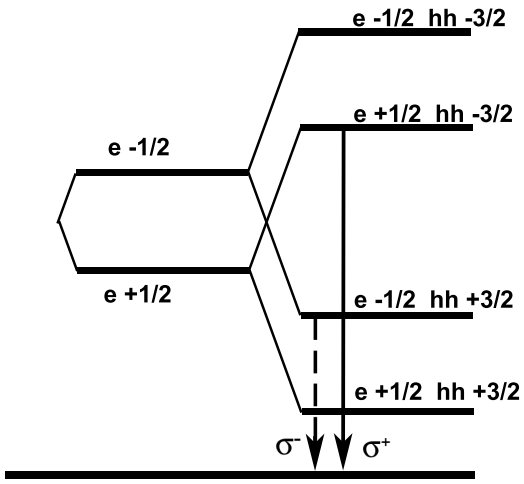

Figure 2.1: Zeeman splitting - heavy hole exciton

according to this definition, which sometimes appear to be quite impractical. Setting the value of such effective g-factor is an important experimental result, however, we want now to establish some theoretical underpinning.

The spin Hamiltonian of the exciton has been derived by Van Kesteren et al. [8] from symmetric considerations. Here we point out only parts that are important for this thesis (mainly focusing on magnetic field perpendicular to quantum well - in z-direction). Spin Hamiltonian of electron can be written as:

$$H_S^{e_z} = \mu_B g_e S_{ez} B_z \tag{2.43}$$

where g_e is an electronic g-factor and S_{ez} takes the values $\pm\frac{1}{2}$. For the hole we can write:

$$H_S^{h_z} = -2\mu_B \kappa J_{hz} B_z \tag{2.44}$$

where κ is another Luttinger parameter (see [4]). For the heavy hole J_{hz} takes the values $\pm\frac{3}{2}$. In this simple analysis we omitted (apart of anything that may happen in x and y directions) cubic term ($\sim J_{hi}^3$) and the spin-spin coupling of the electron and the hole forming the exciton. Putting these terms together we may write:

$$H_S^{exciton_z} = g_e S_{ez} \mu_B B_z - g_h J_{hz} \mu_B B_z \tag{2.45}$$

Here we introduce also the hole g-factor g_h. By this definition the g_e and g_h respect the energetic shift (e.g. in case that g_h is positive and the spin of the actual hole is also positive, the energy level is shifted down). First thing to note is that g_e is negative in both GaAs and AlAs($g_e = -0.44$, [11]) thus the negative electron spin in fact raises the energy level. The concept of g_h is the source of the most confusions. We assume that g_h

must always multiplied by the total angular momentum of the hole, the effective g-factor is for the heavy hole exciton $g_{eff} = |g_e - 3g_h|$. On the other hand - some authors, who assume only heavy holes, incorporate the triple total angular moment already into g_h, which makes the effective g-factor $g_{eff}^{alternative} = |g_e - g_h|$ only. In order to draw the energy schemes for Zeeman splitting we need to choose the sign of g_h. According to the scheme in Fig. 2.1 we choose g_h to be positive. The topmost energy level thus consists of negative spins of both electron and hole. Moreover we assume that $3\,|g_h| > |g_e|$. It must be stressed that the scheme might be inappropriate in the case that either g_h or g_e have different sign than assumed or the assumption of the mutual relationship is not fulfilled.

The important conceptual step is to allow for the existence of light-hole exciton. Fig. 2.2 shows the Zeeman splitting for exciton involving the light hole with the assumptions: $g_e < 0$, $g_h > 0$ and $|g_e| > |g_h|$. In the case that $|g_e| < |g_h|$, the two middle energy levels interchange their position, what actually does not have qualitative impact on the observed spectra.

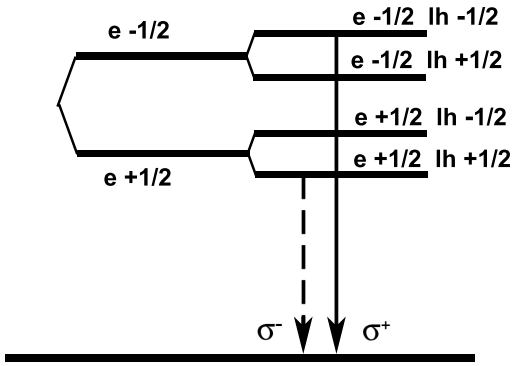

Figure 2.2: Zeeman splitting - light hole exciton

The optical properties of both heavy and light hole excitons are qualitatively given by the allowed optical transitions. The allowed transitions are those transitions for that total angular momentum changes exactly by $+1$ or -1. The transition associated with the change of momentum by $+1$ is visible in the right handed circularly polarized light (σ^+),whereas the transition associated with the change of momentum by -1 is visible in the left handed circularly polarized light (σ^-). For each heavy and light hole exciton we thus have two allowed optical transition, each of those visible in one polarization.

Our approach is, however, based on the Luttinger Hamiltonian that mixes both light hole and heavy hole excitons into one quantum state. The Zeeman terms in the Luttinger Hamiltonian framework have been instructively developed by Winkler et al. [12]. The

Zeeman terms of the holes can be written as (under assumption of only perpendicular magnetic field):

$$\hat{\mathbf{H}}_s \left|\psi\right\rangle = -g_h \mu_B \begin{pmatrix} \frac{3}{2}B_z & 0 & 0 & 0 \\ 0 & \frac{1}{2}B_z & 0 & 0 \\ 0 & 0 & -\frac{1}{2}B_z & 0 \\ 0 & 0 & 0 & -\frac{3}{2}B_z \end{pmatrix} \begin{vmatrix} \frac{3}{2}, +\frac{3}{2} \rangle \\ \frac{3}{2}, +\frac{1}{2} \rangle \\ \frac{3}{2}, -\frac{1}{2} \rangle \\ \frac{3}{2}, -\frac{3}{2} \rangle \end{vmatrix} \tag{2.46}$$

This form is instructive in a way how to add the Zeeman terms into the Hamiltonian. The resulting Zeeman splitting does not follow any of the depicted schemes, since heavy and light holes are mixed. The mixed state thus does not possess any well defined spin, because the spin operator is not the eigenoperator of the problem. The optical activity of given mixed state depends on the relative weights of heavy hole and light hole, thus any suitable excitonic state might be visible in both σ^+ and σ^- polarizations. Evolution of the Zeeman splitting with magnetic field and quantum well width of such complicated structures like exciton (or even trion) can be rather complex and it is an active field of current research.

Whole this section about excitons provided an introduction to the most important concepts and serves for instant comparison with the features of more complicated structures of charged excitons - trions.

2.2 Trion

Neutral exciton (X^0) can be bound with one additional electron or one additional hole and form charged exciton denoted as **trion**. Obviously, two fundamental types of trions exist. Positive trion (X^+) consists of one electron and two holes and negative trion consists of two electrons and one hole (X^-). Exciton can be considered as a solid state analogue of hydrogen atom. Similarly, the trion is an analogical problem to either H^- or He^+. However, the computational treatment is quite different since in the case of both excitons and trions all the charge carriers are of comparable masses.

The creation of an exciton results from the interaction between two charges, whereas trion results from the interaction between dipole and charge. This means that the binding energy of trion is much lower. However, the precise definition of binding energy, mainly in the presence of magnetic field is ambiguous and differs substantially among various authors. That is why we postpone the discussion about binding energy and the energy of transition to the foregoing section.

In this thesis we want to use the Luttinger Hamiltonian framework that describes the hole states in a very detail. Positive trion consists of two such holes and in the Luttinger framework the two hole system would substantially complicate the computations (mainly it would increase the size of the Hamiltonian matrix at least by the factor of two). It should be possible to analyse the positive trion in the Luttinger framework, however it is beyond the scope of this thesis, which focuses solely on the **negative trion**.

2.2.1 Trion in an idealized heterostructure

In this part we discuss the possibility of centre-of-mass transform for the trion. This transform has been already derived for the exciton, so we will focus on the important differences.

The Hamiltonian of the negative trion in the effective mass approximation with no external field can be written as:

$$\Big[\frac{\hat{\boldsymbol{p}}_{e1}^2}{2m_e}+\frac{\hat{\boldsymbol{p}}_{e2}^2}{2m_e}+\frac{\hat{\boldsymbol{p}}_{h}^2}{2m_h}-\frac{e^2}{4\pi\varepsilon\left|\boldsymbol{r}_{e1}-\boldsymbol{r}_h\right|}-\frac{e^2}{4\pi\varepsilon\left|\boldsymbol{r}_{e2}-\boldsymbol{r}_h\right|}+\frac{e^2}{4\pi\varepsilon\left|\boldsymbol{r}_{e1}-\boldsymbol{r}_{e2}\right|}$$
$$+U_{e1}(z_{e1})+U_{e2}(z_{e2})+U_h(z_h)\Big]\psi\left(\boldsymbol{r}_{e1},\boldsymbol{r}_{e2},\boldsymbol{r}_h\right)=\left(E-E_g\right)\psi\left(\boldsymbol{r}_{e1},\boldsymbol{r}_{e2},\boldsymbol{r}_h\right) \tag{2.47}$$

Subscripts $e1$ and $e2$ obviously refer to first and second electron, respectively. Note that Hamiltonian involves additionally the kinetic energy term for the second electron and mainly two new Coulombic terms. Hamiltonian eigenfunctions depend on three spatial variables, that consist of nine parameters altogether. The centre-of-mass transformation can be carried out similarly to the exciton in in-plane components only.

$$\boldsymbol{r}_{1\parallel}=\boldsymbol{r}_{e1\parallel}-\boldsymbol{r}_{h\parallel} \tag{2.48}$$
$$\boldsymbol{r}_{2\parallel}=\boldsymbol{r}_{e2\parallel}-\boldsymbol{r}_{h\parallel} \tag{2.49}$$
$$\boldsymbol{R}_{\parallel}=\frac{m_e\boldsymbol{r}_{e1\parallel}+m_e\boldsymbol{r}_{e2\parallel}+m_h\boldsymbol{r}_{h\parallel}}{2m_e+m_h} \tag{2.50}$$
$$\hat{\boldsymbol{P}}_{\parallel}=\boldsymbol{p}_{\hat{\boldsymbol{e}}\boldsymbol{1}\parallel}+\boldsymbol{p}_{\hat{\boldsymbol{e}}\boldsymbol{2}\parallel}+\boldsymbol{p}_{\hat{\boldsymbol{h}}\parallel} \tag{2.51}$$
$$\hat{\boldsymbol{p}_{1\parallel}}=\frac{(m_e+m_h)\boldsymbol{p}_{\hat{\boldsymbol{e}}\boldsymbol{1}\parallel}-m_e\boldsymbol{p}_{\hat{\boldsymbol{e}}\boldsymbol{2}\parallel}-m_e\boldsymbol{p}_{\hat{\boldsymbol{h}}\parallel}}{2m_e+m_h} \tag{2.52}$$
$$\hat{\boldsymbol{p}_{2\parallel}}=\frac{(m_e+m_h)\boldsymbol{p}_{\hat{\boldsymbol{e}}\boldsymbol{2}\parallel}-m_e\boldsymbol{p}_{\hat{\boldsymbol{e}}\boldsymbol{1}\parallel}-m_e\boldsymbol{p}_{\hat{\boldsymbol{h}}\parallel}}{2m_e+m_h} \tag{2.53}$$

Resulting Schrödinger equation can be written as follows:

$$\Big[\frac{\hat{\boldsymbol{P}}^2}{2M'}+\frac{\left(\hat{\boldsymbol{p}}_1+\hat{\boldsymbol{p}}_2\right)^2}{2\mu'}+\frac{m_h}{m_e}\frac{\hat{\boldsymbol{p}}_1{}^2+\hat{\boldsymbol{p}}_2{}^2}{2\mu'}+\frac{\hat{\boldsymbol{p}}_{z_{e1}}^2}{m_e}+\frac{\hat{\boldsymbol{p}}_{z_{e2}}^2}{m_e}+\frac{\hat{\boldsymbol{p}}_{z_h}^2}{2m_h}$$
$$-\frac{e^2}{4\pi\varepsilon\sqrt{\boldsymbol{r}_{1\parallel}^2+\left(z_{e1}-z_h\right)^2}}-\frac{e^2}{4\pi\varepsilon\sqrt{\boldsymbol{r}_{2\parallel}^2+\left(z_{e2}-z_h\right)^2}}+\frac{e^2}{4\pi\varepsilon\sqrt{\left(\boldsymbol{r}_{1\parallel}-\boldsymbol{r}_{2\parallel}\right)+\left(z_{e1}-z_{e2}\right)^2}}$$
$$+U_{e1}(z_{e1})+U_{e2}(z_{e2})+U_h(z_h)\Big]\psi\left(\boldsymbol{r}_{e1},\boldsymbol{r}_{e2},\boldsymbol{r}_h\right)=\left(E-E_g\right)\psi\left(\boldsymbol{r}_{e1},\boldsymbol{r}_{e2},\boldsymbol{r}_h\right) \tag{2.54}$$

We employed new notation $M'=2m_e+m_h$ and $\mu'=\frac{m_hM'^2}{(m_e+m_h)^2}$. Note that the movement of the centre-of-mass is well separated from the evolution of relative coordinates. We can thus factorize the wavefunction $\psi\left(\boldsymbol{r}_{1\parallel},\boldsymbol{r}_{2\parallel},\boldsymbol{R}_{\parallel},z_{e1},z_{e2},z_h\right)$. Moreover the '$xy$-centre-of-mass' moves in the xy-plane like the free particle thus we can write

$$\psi\left(\boldsymbol{r}_{1\parallel},\boldsymbol{r}_{2\parallel},\boldsymbol{R}_{\parallel},z_{e1},z_{e2},z_h\right)=\frac{1}{\sqrt{W}}exp\left(i\boldsymbol{K}_{\parallel}.\boldsymbol{R}_{\parallel}\right)\phi\left(\boldsymbol{r}_{1\parallel},\boldsymbol{r}_{2\parallel},z_{e1},z_{e2},z_h\right) \tag{2.55}$$

The situation becomes incomparably more complicated in the case of non-zero magnetic field. The Hamiltonian in the effective mass approximation can be written as:

$$\Big[\frac{p_{xe1}^2+\left(p_{ye1}+eBx_{e1}\right)^2}{2m_e}+\frac{p_{xe12}^2+\left(p_{ye2}+eBx_{e2}\right)^2}{2m_e}+\frac{p_{xh}^2+\left(p_{yh}-eBx_h\right)^2}{2m_h}+$$
$$+\frac{p_{ze1}^2}{2m_e}+\frac{p_{ze2}^2}{2m_e}-\frac{e^2}{4\pi\varepsilon\left|\boldsymbol{r}_{e1}-\boldsymbol{r}_h\right|}-\frac{e^2}{4\pi\varepsilon\left|\boldsymbol{r}_{e2}-\boldsymbol{r}_h\right|}+\frac{e^2}{4\pi\varepsilon\left|\boldsymbol{r}_{e1}-\boldsymbol{r}_{e2}\right|}$$
$$+U_{e1}(z_{e1})+U_{e2}(z_{e2})+U_h(z_h)\Big]\psi\left(\boldsymbol{r}_{e1},\boldsymbol{r}_{e2},\boldsymbol{r}_h\right)=\left(E-E_g\right)\psi\left(\boldsymbol{r}_{e1},\boldsymbol{r}_{e2},\boldsymbol{r}_h\right) \tag{2.56}$$

It is lengthy, though straightforward, to develop the Hamiltonian in the transformed coordinates and new momentum operators and the result is not shown here. Similarly as in the case of exciton, there appear terms (actually much more such terms than in the case of exciton) that combine the movement of the centre-of-mass and the relative coordinates. The Hamiltonian itself is thus not well decomposed. In the excitonic case we were able to choose such function that effectively allows for the Hamiltonian decomposition. However, in the case of trion, the situation is much more complicated. The main reason is that the trion has non-zero charge. Thus in the magnetic field its centre-of-mass does not propagate as free particle and cannot be described as a plane wave. Actually, due to Landau calibration, in the Y direction, the centre-of-mass moves freely and can be described as a plane wave. But this does not hold in the X direction, in which the centre-of-mass movement should be described by eigenfunctions of Landau level quantization. The ground state eigenfunction can be written in a form:

$$\Psi(X,Y,x_1,y_1,x_2,y_2,z_{e1},z_{e2},z_h)=exp\left[-\frac{\left(X-K_y\lambda^2\right)^2}{\lambda^2}+iK_yY\right]\phi(x_1,y_1,x_2,y_2,z_{e1},z_{e2},z_h) \tag{2.57}$$

It is of extreme importance that if the Hamiltonian act on this wavefunction, the X and Y coordinates and the relative coordinates will not separate and this centre-of-mass transform does not lead to the desired decomposition. This is in accordance with Whittaker and Shields [6] who claim that Hamiltonian involves terms coupling the relative and center-of-mass parts. The problem may lay in the fact that the centre-of-mass does not coincide with the centre-of-charge, which becomes important due to Lorentz force in the magnetic field. On the other hand, Redlinski and Kossut used center-of-mass transform. They used functions with separated relative and centre-of-mass parts for their variational treatment, but more details about the transform and its consequences are not provided.

The impossibility (or at least extreme complications) of center-of-mass transform is caused by fundamental difference between exciton and trion computational treatment. The centre-of-mass transform is not used in this thesis.

2.2.2 Singlet and triplet

Negative trion contains two electrons. It is thus multi-fermionic system that must obey the Pauli principle. This means that the total wavefunction (including the spin part)

must be antisymmetric. This allows for two situations, either the spin wavefunction is antisymmetric and the orbital function is symmetric or the other way round.

There is only one possibility how to construct antisymmetric spin wavefunction for the two fermions:

$$\psi_{Se}^{singlet} = \frac{1}{\sqrt{2}}\left(\left|-\frac{1}{2}\right\rangle\left|\frac{1}{2}\right\rangle - \left|\frac{1}{2}\right\rangle\left|-\frac{1}{2}\right\rangle\right) \tag{2.58}$$

This sole spin function thus define so called **singlet**. The orbital function of the singlet must be symmetric with respect to the exchange of electrons.

On the other hand, there are three possibilities how to construct symmetric wave function.

$$\psi_{Se}^{triplet_1} = \left|-\frac{1}{2}\right\rangle\left|-\frac{1}{2}\right\rangle \tag{2.59}$$

$$\psi_{Se}^{triplet_2} = \frac{1}{\sqrt{2}}\left(\left|-\frac{1}{2}\right\rangle\left|\frac{1}{2}\right\rangle + \left|\frac{1}{2}\right\rangle\left|-\frac{1}{2}\right\rangle\right) \tag{2.60}$$

$$\psi_{Se}^{triplet_3} = \left|\frac{1}{2}\right\rangle\left|\frac{1}{2}\right\rangle \tag{2.61}$$

The states consisting of these functions are denoted as **triplet**. The orbital function of the tripet state must be antisymmetric with respect to the exchange of electrons. The binding energies for the triplet and singlet state may differ. Note that two triplet states have a non-zero total electron spin, which contributes to the Zeeman splitting.

2.2.3 Binding energy and energy of transition

Binding energy $E(X)_{binding}$ of the exciton is the difference between the energy of the electron that creates the exciton and the free electron in the conduction band. Note that the centr-of-mass of any optically active exciton must not move, otherwise the particles cannot annihilate. Thus the energy of the excitonic state $E(X)$ can be associated to the binding energy $E(X)_{binding}$. We assume that we measure the energy of exciton in negative values (the higher is the absolute value of the energy the stronger is the binding). The energy of the transition that is observable in the optical spectra can be written as $E(X)_{transition} = E_g + E(X)$. It is clear, that this energy is smaller for the bound electrons than the energy of the forbidden gap. Note that for now we omit the confinement energy of the exciton that is set in the quantum well.

Binding energy of the negative trion $E(X^-)_{binding}$ is verbally defined as the energy drop when the exciton becomes bounded with an additional electron. If we thus measure the energy of the trion $E(X^-)$ we need to know the energy of the corresponding exciton to establish the binding energy $E(X^-)_{binding} = E(X^-) - E(X)$. The optical transition in the negative trion involves the annihilation of one electron and one hole which leaves one electron remaining. The own energy of such electron must not be forgotten in the definition of the transition energy and we may write: $E(X^-)_{transition} = E_g + E(X^-) - E_e$. In the experimental works, the binding energy of the trion is usually established as $E(X^-)_{binding} = E(X^-)_{transition} - E(X)_{transition}$, which agrees with the definition of the binding energy only in the special case when $E_e = 0$.

Serious problems arise with the definition of the trion binding energy if we allow for the magnetic field. The Zeeman effect splits the energies for both exciton and trion and moreover since the effective g-factors for exciton and trion differ, the splitting may also be different. This problem occurs even if we assume only the singlet state of the trion. Such situation is depicted in Fig. 2.3 [10]. Due to different effective g-factors of exciton and trion, the binding energy under scheme I depends on the magnetic field. On the other hand, the scheme II refers only to the binding energy of trion in zero magnetic field. However, this is quite inappropriate since some trion states are not bounded without presence of the magnetic field and these states become bounded thanks to the Zeeman effect. Scheme I is thus more useful, however it must be considered that the binding energy depends on the magnetic field, the g-factor of the trion and moreover on the g-factor of the corresponding exciton.

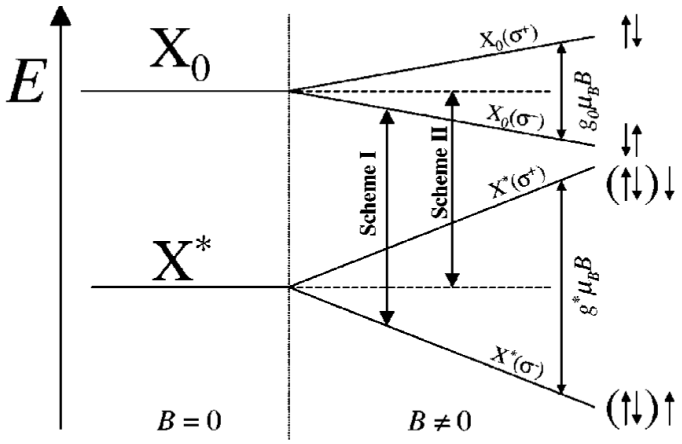

Figure 2.3: Possible definitions of trion binding energy; X_0 - exciton; X^* - singlet state of the trion [10]

2.2.4 Negative trion under Luttinger Hamitlonian framework

The treatment of the negative trion under Luttinger Hamiltonian framework is a straightforward extension to the excitonic case. Note that the Luttinger Hamiltonian for positive trion would be much more complicated. In the case of negative trion, both electronic Hamiltonians are diagonal and so are three Coulombic terms. We can thus write shortly:

$$\hat{\mathbf{H}} = \hat{\mathbf{H}}_h + \left(\hat{H_{e1}} + \hat{H_{e2}} + U_{e1} + U_{e2} + U_h - V_{e1-h} - V_{e2-h} + V_{e1-e2}\right)\mathbf{1} = \hat{\mathbf{H}}_h + \hat{\mathcal{H}}\mathbf{1} \quad (2.62)$$

where $\mathbf{1}$ means 4×4 unity matrix. The meaning of other terms is obvious. $\hat{H_{e1}}$ and $\hat{H_{e2}}$ are Hamiltonians corresponding to the two electrons. U_{e1}, U_{e2}, and U_h are quantum well

confining potentials - may be omitted in the case of infinitely deep QW. V_{e1-h}, V_{e2-h}, and V_{e1-e2} are Coloumbic potentials describing mutual interactions of three particles involved. Compare this Hamiltonian to the excitonic one defined by Eq. 2.39. This trion Hamiltonian might be rewritten in a detail as 4×4 matrix, but such equation would be equivalent to Eq. 2.40 just with different meaning of $\hat{\mathcal{H}}$. It is also notable that even though three Coulombic terms do not involve anything conceptually new, it represents substantial complication for computations since these terms are usually treated numerically.

2.2.5 Negative trion and Zeeman effect

Similarly to the Eq. 2.45 we can derive the z-direction spin Hamiltonian for the negative trion:

$$H_S^{trion_z} = g_e \left(S_{e1z} + S_{e2z}\right) \mu_B B_z - g_h J_{hz} \mu_B B_z \tag{2.63}$$

The effective g-factor for trion remains the same (i.e. $g_{eff} = |g_e - 3g_h|$ for the heavy hole trion and $g_{eff} = |g_e - g_h|$ for the light hole one). The energy levels structure is more complicated for the case of trion and so are the optical spectra due to higher amount of allowed optical transitions. We assume the relationships following relationship between g-factors: $g_e < 0$; $g_h > 0$; $3\,|g_h| > 2\,|g_e|$; and $2\,|g_e| > |g_h|$). We can thus draw the Zeeman splitting for the heavy hole negative trion in the triplet state Fig 2.4 and the light hole negative trion in the triplet state Fig 2.5. The total spin of the electrons is always zero for the singlet state and this leads to the simple Zeeman splitting for the heavy hole negative trion in the singlet state Fig 2.6 and the light hole negative trion in the singlet state Fig 2.7.

The spins of two electrons give rise to three different energy levels for the triplet and that is why this state may be found in any of the three spin states of the electron pair. Each of the three energy levels is further split to the two levels due to total angular momentum of the hole. Thus the Zeeman effect causes the energy split to the six energy levels. The annihilation of trion means that one of the electrons recombine with the hole, whereas the other remains unbounded in the conduction band. Thus even the final state of the trion annihilation is split into two levels due to Zeeman splitting of single electron. The allowed optical transitions involve the change of total angular momentum by $+1$ or -1. For heavy-hole trion triplet we thus have four allowed transitions, whereas for light-hole trion all six energy levels transitions may contribute to the optical spectra.

As in the case of excitons, the heavy-hole negative trion state is much more probable than the light-hole one. Thus only the heavy-hole trions are observed in the experiments and usually only those are considered in the theoretical works. Let us thus consider only the heavy-hole trion triplet scheme (Fig 2.4) for now. No allowed optical transition exists for the lowest energetic state, which is actually triplet state. That is why it is called *dark triplet*. Although it is not explicitly mentioned in the literature, it must be noted that in the case that $g_e > 0$ and g_h remaining positive the order of electronic levels flips. The ground state would then be described by $S_e = -1$ and the total angular momentum of heavy hole $+3/2$, which would mean that the ground state is not *dark* anymore. Moreover,

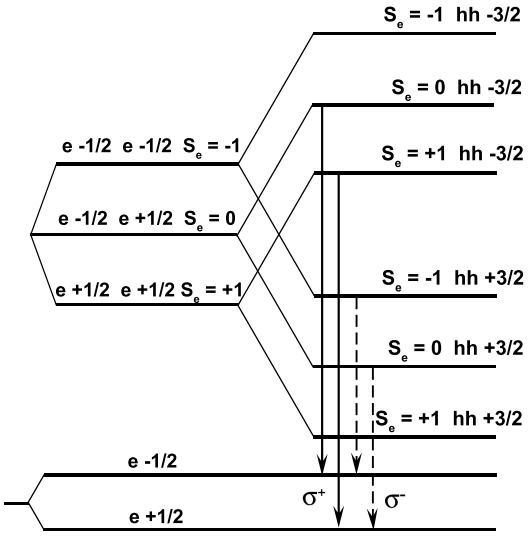

Figure 2.4: Zeeman splitting - heavy hole negative trion in triplet state

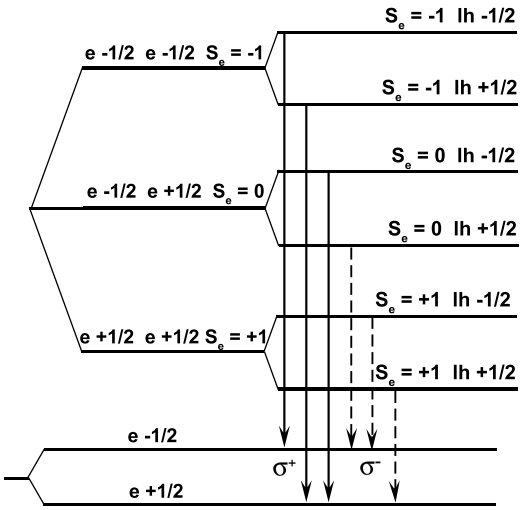

Figure 2.5: Zeeman splitting - light hole negative trion in triplet state

as argued by Volkov [16], the triplet is often localized near the impurity in the potential barrier and due to break of symmetry even the dark triplet state might be visible. Under our original assumptions on g-factors, it is the topmost energy level that is also *dark*.

The other four states in triplet schemes are referred to as *bright triplet* states. Note that both *bright triplet* states associated with heavy hole trion that are visible in σ^- light have the same transition energy and thus are optically indistinguishable (see Fig 2.4). The

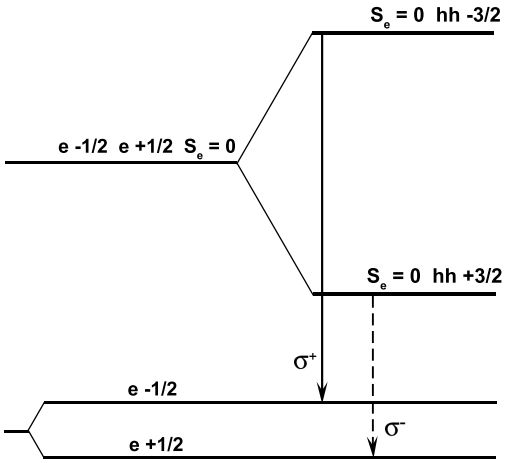

Figure 2.6: Zeeman splitting - heavy hole negative trion in singlet state

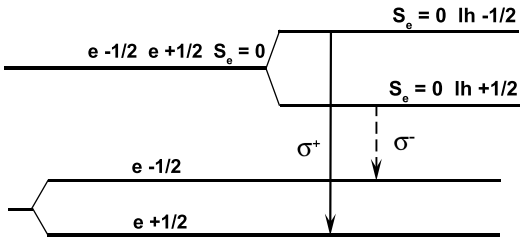

Figure 2.7: Zeeman splitting - light hole negative trion in singlet state

same holds for the two states that are visible in the σ^+ light.

Both heavy-hole singlet states are visible and are often denoted as *bright singlet*. Some of these states are usually visible trion states in the photo-luminescence experiments. In the case of light-hole trion, there are no *dark* states since for each level there exists an allowed optical transition.

The real situation is, however, more complicated. It has already been mentioned in the case of excitons that the light and heavy holes states become coupled under Luttinger Hamiltonian framework. The Zeeman terms of the holes are the same in the case of negative trion as they were for the exciton and so they are defined by equation 2.46. The new point is that we have three different spin levels for the pair of electrons. Moreover, the orbital wavefunctions differ for the singlet and triplet states of trion. We thus have four different states of the two electrons in the negative trion and the corresponding Zeeman Hamiltonian can be written as:

$$\hat{\mathbf{H}}_{s_e}|\psi\rangle = g_e\mu_b \begin{pmatrix} 0 & 0 & 0 & 0 \\ 0 & -1.B_\perp & 0 & 0 \\ 0 & 0 & 1.B_\perp & 0 \\ 0 & 0 & 0 & 0 \end{pmatrix} \begin{matrix} |\psi\rangle_{singlet}\,\frac{1}{\sqrt{2}}\left(\left|-\frac{1}{2}\right\rangle\left|\frac{1}{2}\right\rangle - \left|\frac{1}{2}\right\rangle\left|-\frac{1}{2}\right\rangle\right) \\ |\psi\rangle_{triplet}\left|-\frac{1}{2}\right\rangle\left|-\frac{1}{2}\right\rangle \\ |\psi\rangle_{triplet}\left|\frac{1}{2}\right\rangle\left|+\frac{1}{2}\right\rangle \\ |\psi\rangle_{triplet}\,\frac{1}{\sqrt{2}}\left(\left|-\frac{1}{2}\right\rangle\left|\frac{1}{2}\right\rangle + \left|\frac{1}{2}\right\rangle\left|-\frac{1}{2}\right\rangle\right) \end{matrix} \tag{2.64}$$

where $|\psi\rangle_{singlet}$ is symmetric with respect to the exchange of the electrons whereas $|\psi\rangle_{triplet}$ is antisymmetric. The complete wavefunction of two electrons is thus antisymmetric as it is required for fermions. The singlet and triplet thus differ in the symmetry of orbital function and moreover, for triplet there are three allowed values of spin projection of electron pair: $S_e = -1, 0, 1$, whereas for singlet we have only $S_e = 0$. Altogether this gives rise to four different electronic states of negative trion. Note that we must combine all four electronic states as defined by this Hamiltonian and four hole states defined by Luttinger Hamiltonian. Thus putting these two Hamiltonians together results in the 16×16 Hamiltonian, which may be divided into four blocks of size 4×4. Let us recall the discussion about the involvement of one excited heavy hole state, which leads to the 6×6 Luttinger Hamitonian. Thus the Hamiltonian under considerations that describes the negative trion under Luttinger framework is of the size 24×24. However, this Hamiltonian can also be divided into four blocks, and moreover each of these blocks can be further decomposed into two separate Hamiltonians (recall Eqs. 1.51 and 1.52). Thus we need to solve 8 separate Schrödinger's equations each involving Hamiltonian of the size 3×3. The exact form of the Hamiltonian is further developed in the 'Own computations' chapter after detailed explanation of the chosen wavefunction basis.

2.3 Literature review

This section should serve as a brief overview of the state-of-the-art in the research relevant to the charged excitons. This survey is not comprehensive but presents the most important experimental results and theoretical approaches that were the most influential for this thesis. Although the research papers usually include theoretical part, we present the experimental results separately.

2.3.1 Experimental results

For the purpose of this thesis, two types of experimental results are of extreme importance. Firstly, these are optical spectra of excitons and trions from photo-luminescence and absorption experiments, because this thesis attempts to explain such results theoretically. Secondly experimentally evaluated values of g-factors of Zeeman splitting are of fundamental importance, since the holes and electrons g-factors are exogenous parameters of our theoretical model and thus must be inserted according to suitable experimental results.

Optical spectra

Optical properties of thin GaAl-AlGaAs quantum wells in the presence of perpendicular magnetic field were studied by Schmitt-Rink et al. (1991) [17]. Authors investigated optical properties of 8.5 nm wide GaAs/AlGaAs quantum well sample. The absorption optical spectra (σ^- light) for magnetic field up to 12 T are depicted in Figs 2.8 and 2.9 in two different graphical representations. The absorption spectrum for B = 12 T is also depicted separately in Fig 2.10 for both light polarizations. Authors also attempt to explain experimental results theoretically. Their sophisticated approach takes into account even biexcitons or triexcitons, but the concept of charged exciton is not introduced.

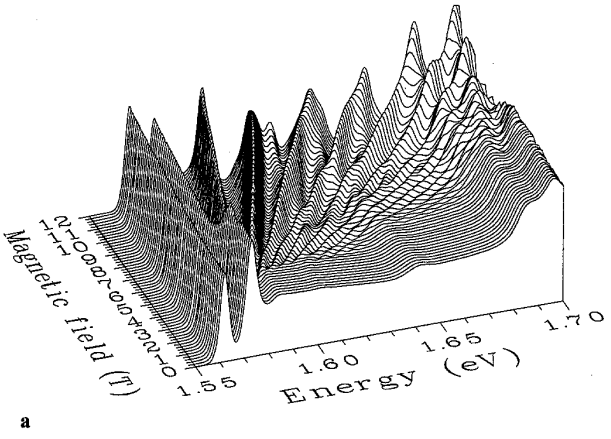

Figure 2.8: Linear absorption spectra vs. magnetic field for σ^- circularly polarized light [17]

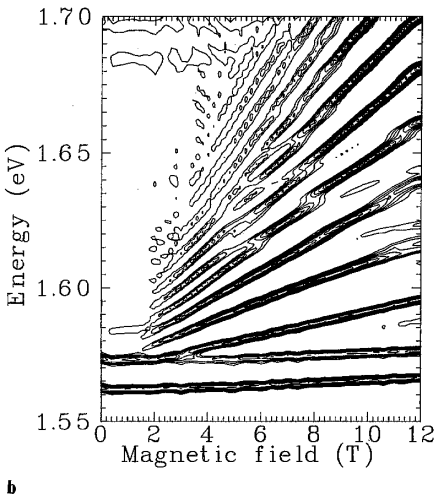

Figure 2.9: Mean absorption curvature vs. magnetic field for σ^- circularly polarized light [17]

The charged exciton has been observed for the first time by Kheng et al. (1993) [20] in the absorption spectra of CdTe - CdZnTe multiple quantum wells. Finkelstein et al. (1995) [21] observed the charge excitons on the GaAs-AlGaAs interface for the first time. The excess electrons enable negative trion to be observable. The binding energy of the negative trion is established to be 1.2 meV without presence of magnetic field.

An influential article by Shields et al. (1998) [31] reports observation of negative trion on n-type structure with quantum well width of 30 nm and also of positive trion on p-type structure with QW width od 20 nm. Singlet and triplet states of negative trion are observed and dependence of their binding energies on electric field is investigated. Authors also claim that high sensitivity of resonance of both neutral and charged trions can be used in electro-absorption modulators and other optical devices. Experimental results are supported by theoretical model in effective-mass approximation and wavefunctions constructed from a finite set of Landau level states. Singlet wave function is found to be relatively compact compared to the triplet wavefunction.

More comprehensive view on both negatively and positively charged excitons is given by

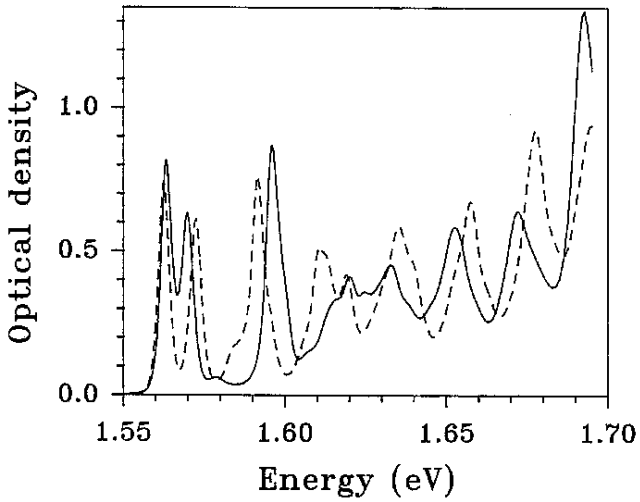

Figure 2.10: Linear absorption spectra at 12 T for σ^- (dashed line) and σ^+ (solid line) circularly polarized light [17]

Glasberg et al. (1999) [22]. Authors could tune the experiment via illumination intensity so that they were able to observe both positive and negative trion on one sample. The resulting spectra were measured for 20 nm wide quantum well and are shown in the Fig 2.11. In addition to the visible peaks in this spectrum, authors claim that weak satellite peaks that are observed in the lower energies may result from shakeup process, in which a recombination of one of the electrons in the X^- with the hole is accompanied by an ejection of the remaining electron to a higher Landau level (i.e. an effect analogous to Auger recombination). The paper also examines the evolution of transition energies with magnetic field up to 7 T. Fig 2.12 shows transition energies for exciton (X), negative trion in singlet state (X_s^-) and negative trion in triplet state (X_t^-).

One of the most influential experimental article for this thesis is by Vanhoucke (2001) [9]. After invaluable introduction to negative trions, authors present the evolution of transition energies for both exciton and negative trion and for both light polarizations. Moreover, Zeeman splittings for exciton and trion are separately depicted. The experiment was repeated for three different widths of quantum well (10 nm, 12 nm, 15 nm). Authors do not define, which negative trion state is actually observed.

Teran et al. observed both positive and negative trions in a 9 nm GaAs quantum well. Authors identified the negative trion peak at the energy of 1.5597 eV and established its binding energy as $E(X^-)_{binding} = 2.1meV$ in zero magnetic field.

Finally, brief and consistent article by Yusa et al. [32] must be mentioned. Authors studied photo-luminescence of 20 nm GaAs quantum well under very low temperature (20 mK) and dilute 2DEG with low density ($5 \times 10^9 cm^{-2}$). The dark triplet state, being the ground one, is well observable, which might be attributed to fluctuating potential of remote donors that may scatter the dark triplet and transfer its excess angular momentum so that

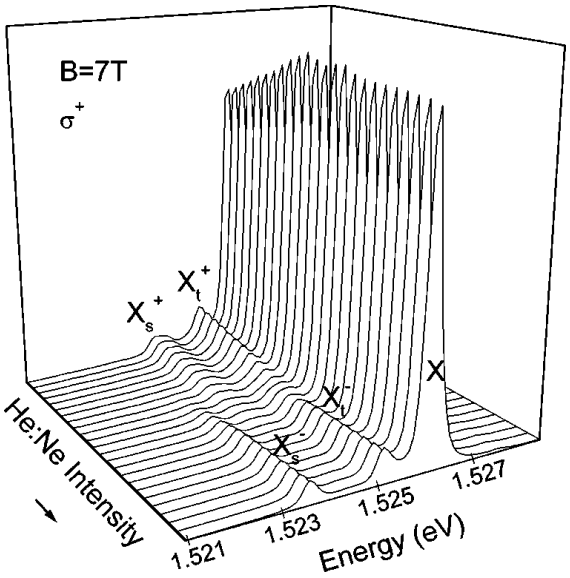

Figure 2.11: Evolution of σ^+ polarized PL spectra at 7 T from X^+ to X^- spectrum through a neutral exciton [22]

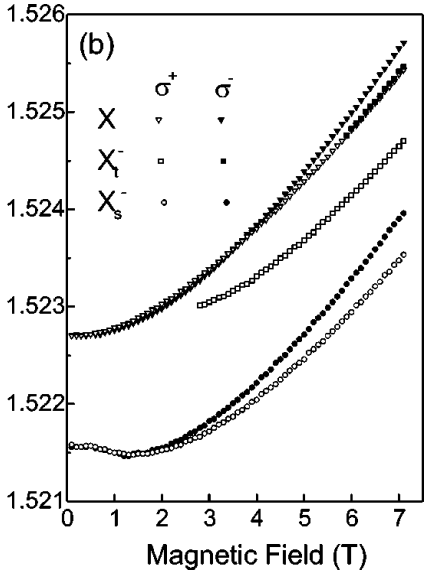

Figure 2.12: The energy dispersion of the X^- PL peaks as function of magnetic field [22]

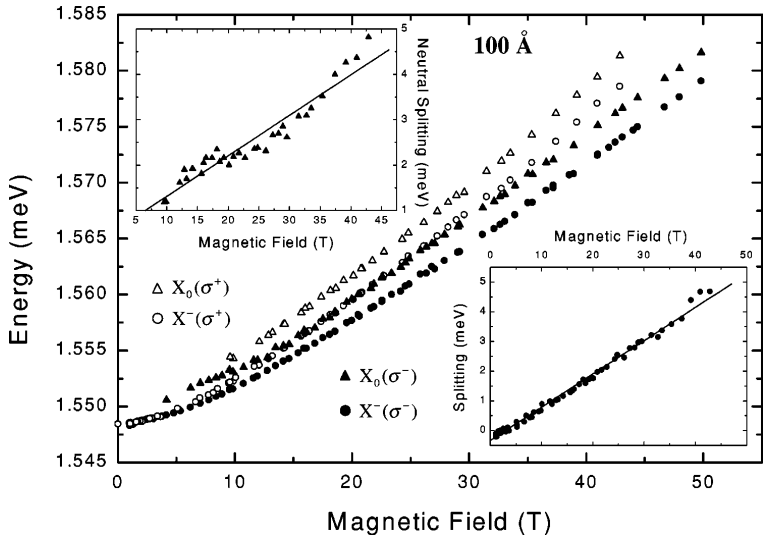

Figure 2.13: Field dependence of the PL energy. Upper inset shows the Zeeman splitting of the neutral exciton (X_0), whereas the lower inset refers to the splitting of the states of negative trion.

dark triplet undergoes radiative recombination. The PL spectrum and its dependence on temperature is shown in Fig 2.14 and the dependence of binding energies of singlet, bright triplet and dark triplet is shown in Fig 2.15. The connection between charged exciton

states and fractional quantum Hall effect is discussed in the paper.

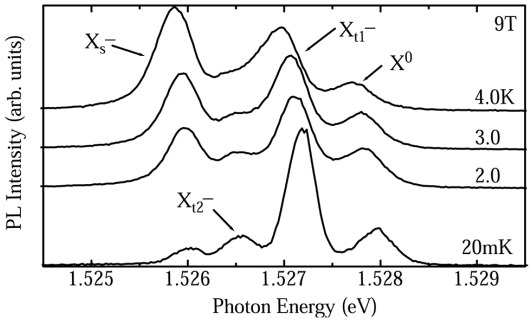

Figure 2.14: PL spectrum as a function of temperature. X^0 - exciton; X_s^- - singlet; X_{t1}^- - bright triplet; X_{t2}^- - dark triplet [32]

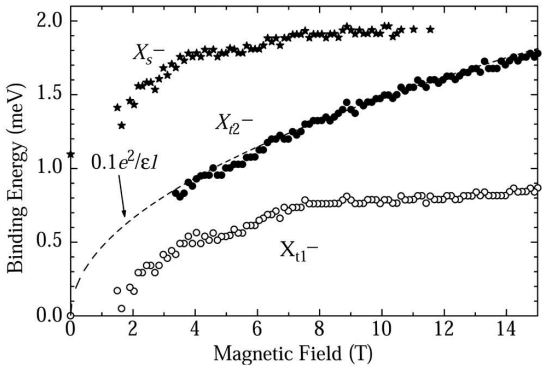

Figure 2.15: The binding energies as a function of B. X^0 - exciton; X_s^- - singlet; X_{t1}^- - bright triplet; X_{t2}^- - dark triplet [32]

Landé g-factors

The determination of g-factors experimentally is an uneasy task. The current literature is inconclusive in this respect. Some authors believe that the g-factors do not change with the quantum well size and the magnetic field, while others claim that g-factor depends on magnetic field and/or the well width. Experimentally determined values of g-factors are rarely in mutual accordance.

Following list of important experimental results is based on rather comprehensive summary by Groholová (2006) [23]. However, all original research papers have been checked and few more experimental results added.

Van Kesteren et al. (1990) studied the excitons in narrow (up to 2.5 nm) typeII GaAs/AlAs quantum wells employing optically detected magnetic resonance. Landé g-factor for electrons has been found independent on quantum well width and has value of $g_e = 1.9$. The hole g-factor is found to be the lowest for the widest examined QW, $g_h = 2.3$, whereas for QW width of 1.7 nm it is $g_h = 2.9$. Snelling et al. [24] studied the magnitude and the sign of the g-factor for electrons as a function of width of type I GaAs/AlGaAs quantum well. For $L < 5$ nm the electron spend most of time in the $Al_{0.3}Ga_{0.7}As$ barrier and thus the g-factor attains the bulk value for $Al_{0.3}Ga_{0.7}As$ being $\sim +0.4$. With increasing well width the g-value approaches the GaAs bulk value of -0.44. g_e therefore must reverse its sign and it is reported to cross zero for $L = 5$ nm. For the width that is relevant for this thesis ($L = 10$ nm) the reported value of electron g-factor is roughly $g_e = -0.2$. Hole and exciton g-factors have been studied in another paper by Snelling et al. (1992) [25]. The PL spectra have been studied in type I GaAs/AlGaAs quantum well with barrier content of 0.36. Substantial increase of g-factor of holes has been reported for growing width of QW. For $L < 8$ nm, the holes g-factor is negative and for wider wells it becomes positive. Due to bigger absolute values of g_h and its stronger dependence on the well width when compared to electron g-factor (g_e), the complete exciton g-factor (g_{exc}) is driven by the

hole one. For narrow wells, the value of g_{exc} might reach -2 and it also reverses sign for the $L \sim 10$ nm reaching the values of $g_{exc} = 0.5$ for $L = 20$ nm. The authors also inspected the dependence of Zeeman spitting on the magnetic field. For relevant QW width ($L = 11.2$ nm) the Zeeman splitting reverses its sign at around 2 Tesla.

Two already cited papers by Glasberg et al.[22] and Vanhoucke et al.[9] also report g-factors values for excitons and moreover for trions. Glasberg used 20 nm QW and relatively low magnetic field up to 7 T. The dependence of effective g-factor g_{eff} on the magnetic field is shown in Fig 2.16. On the other hand, Vanhoucke used high magnetic field (23 - 50 T) and found g_{eff} to be independent on the magnetic field. The dependence of g_{eff} on quantum well width is shown in Tab 2.1.

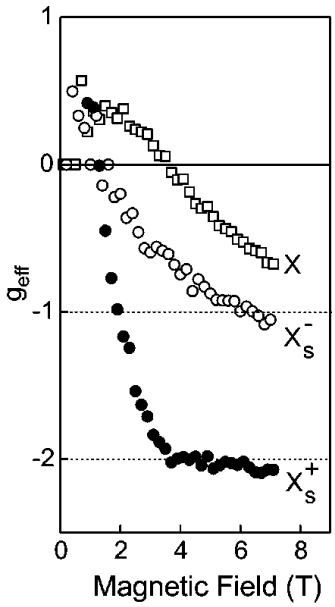

Figure 2.16: g_{eff} for exciton X, negative trion in singlet state X_s^- and positive trion X_s^+ [22]

QW	Singlet	Triplet	Exciton
10nm	$g_{eff} = 1.9$	$g_{eff} = 1.9$	$g_{eff} = 1.5$
12nm	$g_{eff} = 1.9$	$g_{eff} = 2.1$	
15nm	$g_{eff} = 1.3$	$g_{eff} = 1.4$	

Table 2.1: Experimental values for g_{eff} for negative trion in singlet and triplet state and for exciton for three different QW widths. [9]

Two influential papers brought the attention to the dependence of g-factor on the density of the charge carriers. Tutuc et al. (2002) [26] focused on the dependence of electron g-factor on the total density of the two-dimensional dilute electron gas (2DEG) using Shubnikov-de-Haas oscillations and in-plane magnetoresistance. The g_e is reported to

vary from 1.3 up to 2.6. However, the g-factor elicitation is in-direct and the g-factor is defined by the field that achieve full polarization.

Similarly, Proskuryakov et al. (2002) [27] studied two-dimensional dilute hole gas (2DHG). Hole g-factor is again defined through field that corresponds to the full spin polarization. A linear growth of the g_h has been found with values varying from 0.4 up to 1.45.

It must be, unfortunately, concluded, that experimental determination g-factors values is indistinct. This might be attributed to prevailing uncertainty which parameters affect the g-factors, and moreover often some parameters of substantial importance are not reported. It is thus problematic to use some g-factor value as an input of the model presented in this thesis. Another option is to tune the g-factor so that the theoretical results fit measured optical spectra of exciton - negative trion system.

2.3.2 Theoretical works

Several important theoretical research works have already been mentioned when deriving the important concepts for this thesis. In this survey, we summarize the most important research results dealing with charged excitons. Many of the theoretical approaches were very influential for this thesis.

The first article to mention is Bauer and Ando (1988) [11], although dealing with neutral excitons only. Conceptually important is that authors used the Luttinger Hamiltonian framework that implies the mixing of light hole and heavy hole states. Moreover, authors described the complex energy splitting due to the lack of symmetry caused by quantum well confinement and moreover due to Zeeman splitting in the mixed heavy hole and light hole states of exciton. Authors performed exact diagonalization of the Hamiltonian in the radial basis involving Laguerre polynomials. Energy dispersion as well as dependence of binding energies on well width and applied magnetic field are comprehensively presented.

The most influential theoretical article for this thesis is written by Whittaker and Shields [6], which deals comprehensively with negative trion. Some concepts and notes from this source are recalled in the 'Own computations' section. Authors do not use any centre-of-mass transform, however they use wavefunction basis that respects the symmetry (antisymmetry) for singlet (triplet) state and also involves Laguerre polynomials. There are three independent quantum numbers for each particle, however, only eight independent quantum numbers altogether, because total angular momentum is a constant of motion. The whole trion is treated as quantized to Landau levels and symmetric gauge is chosen for the vector potential of magnetic field. The most complicated task represents the computation of Coulomb term for particles in the finite potential well. The most important result is the binding energy of X^- for 10 nm quantum well Fig (2.17) and also for 30 nm quantum well. Some results are compared to the previously reported experimental results and they are in good agreement. Moreover, radial probabilities of two electrons with respect to the hole are shown along with electron-electron radial correlation functions. Authors also claim that they carried out some calculations using Luttinger Hamiltonian. However, no details are provided and authors only claim that this approach does not lead to better theoretical description of experimental data.

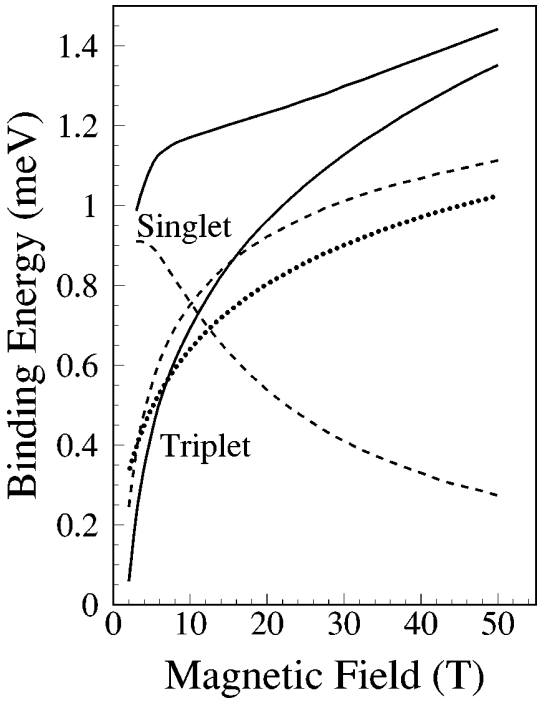

Figure 2.17: Binding energies of the singlet and triplet state of X^- relative to the neutral exciton. Dotted lines - lowest Landau level approximation; dashed lines - lowest subband approximation; solid lines - full results

Riva, Peeters and Varga studied trions in quantum wells in the series of research articles: [28], [29] and [30]. Authors use the effective-mass approximation and stochastic variational method with 'deformed' correlated Gaussian functions (DCG) as trial functions. The results of the calculations are compared to different experimental results by other authors e.g. Glasberg et al. [22] and Yusa et al. [32], see Fig 2.18. The binding energies evolution with magnetic field is also compared to other theoretical results, e.g. by Whittaker and Shields [6] for 10 nm quantum well, see Fig 2.19.

Redliński and Kossut [33] performed centre-of-mass transformation and employing trial envelope wavefunctions they computed transition and binding energies of negative trion in CdTe quantum wells. The authors claim that the singlet state is an example of an entangled state (opposite to the triplet state). By application of magnetic field, it is then possible to entangle or disentangle the ground state, which opens opportunities for the physics of quantum computers and quantum cryptography.

Elaborated and comprehensive article by Wójs and Quinn (2007) [34] exploit the dependence of binding energies of trion with respect to quantum well width, magnetic field and electron concentration. The computation accounts for finite depth and width of quantum well and the asymmetry caused by one-side doping, moreover several accuracy and convergence tests are undertaken. Anyway it is beyond the scope of this thesis to explain complete theoretical approach. The resulting computed binding energies are shown

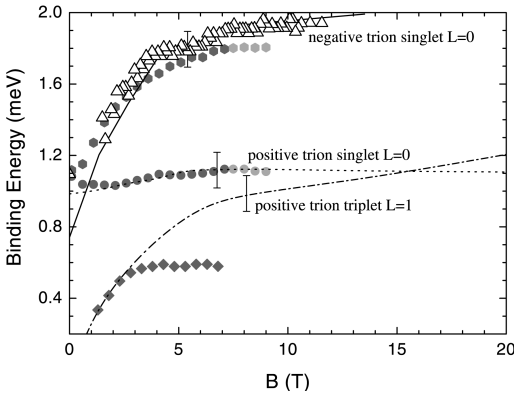

Figure 2.18: Theoretical results (curves) compared to experimental results from Refs. [22] (full symbols) and [32] (open triangles)for a QW of width 20 nm [30]

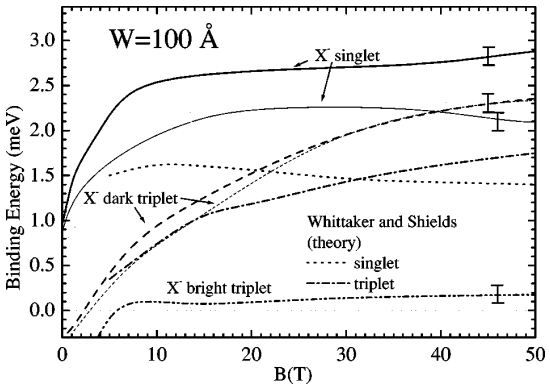

Figure 2.19: The binding energies of charged excitons from Ref [28] (solid and dashed lines, different approximations) as a function of B. Compared with results from by Whittaker and Shields [6]. Taken from [28]

in Fig 2.20. The appropriate Zeeman terms must be added to determine absolute ground state or splitting in the PL spectra. These terms of course shift the magnetic field for that occurs crossing of the singlet and triplet states. The computations also allow for so-called dark singlet that may become weakly bound for very high fields. The effect of remote donors is also discussed and it is established that the effect on the singlet is relatively weak, whereas the trion may be essentially unbind. Despite indisputable complexity of the paper, the off-diagonal terms of Luttinger Hamiltonian have been neglected.

During last years, there have been several attempts to describe the negative trion system in the GaAs quantum wells. However, only few works used the Luttinger Hamiltonian framework and moreover none of those works provided necessary details of computation that would allow for replication of the procedure. This thesis aims to fill this gap in the literature. Moreover, the Zeeman splitting of negative trion system is elaborated in a more detail than it is common in the research papers. At the expense of this improvements, some substantial simplifications (e.g. infinite depth of a quantum well) are made and some effects that might be of physical importance are omitted. Nevertheless, it is the literature review section that should warn about possible shortcomings of our approach and may inspire future readers for improvements of our model and calculations.

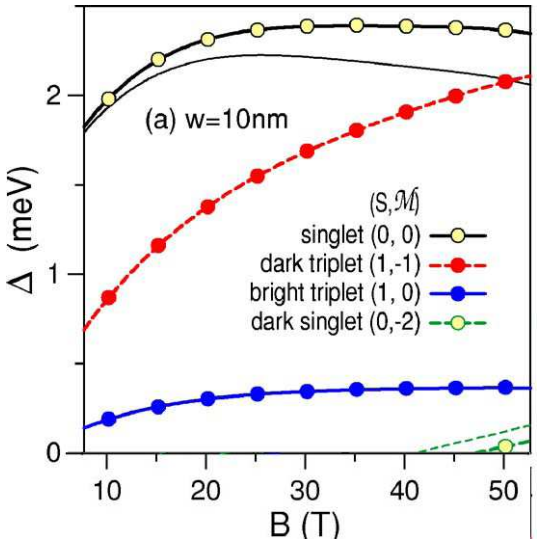

Figure 2.20: Dependence of the trion binding energies Δ on magnetic field B for undoped or symmetric GaAs quantum well. The thick lines correspond to results after inclusion of two subbands confined in quantum well, whereas thin lines correspond only two lowest subband calculations. [34]

3 Own Computations

3.1 Wavefunction basis

In this section, we construct the novel asymmetric wavefunction basis for the trion problem. The total wavefunction basis consists of three blocks according to the structure of 3×3 Hamiltonian given by (1.51) and (1.52). Each block then consists of the wavefunctions that correspond to the Landau theory of charged particles in magnetic field. The functions respect the Landau gauge $\boldsymbol{A} = (0, B_z x, 0)$. Note that these functions are not symmetric in xy-plane. This unusual choice does not respect the symmetry of the physical problem. However, it will be later shown that the basis functions are almost symmetric for sufficient size of the basis. The main advantage is that the basis wavefunctions involve relatively simple Hermite polynomials. The construction of the wavefunction basis is now exploited in detail.

The basis functions depend altogether on nine spatial variables. However, in the z-direction the particles are confined in the infinitely deep quantum well. Thus the total wavefunction can be decomposed as:

$$\Psi_{total}(x_1, x_2, x_h, y_1, y_2, y_h, z_1, z_2, z_h) = \Psi_{in-plane}(x_1, x_2, x_h, y_1, y_2, y_h).\Phi(z_1, z_2, z_h) \quad (3.1)$$

The subscripts 1 and 2 refers to the electrons of the negative trion, whereas subscript h naturally denotes the hole. The wavefunction in the z-direction can be further decomposed

as:

$$\Phi(z_1, z_2, z_h) = \phi(z_1)\phi(z_2)\phi(z_h) \tag{3.2}$$

The electron functions $\phi(z_1)$ and $\phi(z_2)$ are defined by equation (1.36), whereas the hole function $\phi(z_h)$ is defined by one of the equations (1.37) - (1.39) depending whether the hole state is the ground state of the heavy hole, the first excited state of the heavy hole or the ground state of the light hole. This difference in the hole wavefunction in the z-direction is the only difference between the three groups of wavefunction basis functions that are associated with the three blocks of the Hamiltonian defined by (1.51) and (1.52). Thus further derived in-plane wavefunction basis is valid for each of the three blocks.

The in-plane wavefuncitons can be decomposed into the single-particle wavefunctions:

$$\Psi_{in-plane}(x_1, x_2, x_h, y_1, y_2, y_h) = \psi^{e1}(x_1, y_1)\psi^{e2}(x_2, y_2)\psi^{h}(x_h, y_h) \tag{3.3}$$

Each of this wavefunctions is eigenfunction of the problem of one charged particle in the magnetic field under Landau calibration. Let us remind that we chose vector potential $\boldsymbol{A} = (0, B_z x, 0)$. It implies that in the y-direction the particle is described as the plane wave with wave vector k. On the other hand in the x-direction the eigenfunctions are the harmonic oscillator eigenstates shifted by $x_0 = \frac{\hbar k}{m\omega_c} = \lambda^2 k$. The one particle eigenfunction can thus be, according to Landau quantization theory written as:

$$\Psi_n(x, y) = \frac{1}{\sqrt{L_y}} \frac{1}{\sqrt{\lambda\sqrt{\pi}}} \sqrt{\frac{1}{2^n n!}} H_n\left(\frac{x - \lambda^2 k}{\lambda}\right) e^{-\frac{(x-\lambda^2 k)^2}{2\lambda^2}} e^{iky} \tag{3.4}$$

The function involves two quantum numbers. Quantum number n defines the Landau level. Throughout this thesis, we restrict ourselves to $n = 0, 1, 2$ due to computation burden. The other quantum number is the wave-vector k, nevertheless wave vector is represented by single number only, since we assume plane wave in y-direction only. Note also that change in k efficiently shifts the wave function along the x-axis due to shift $\lambda^2 k$.

The trion is assumed to be enclosed in the y-direction in the box of the size L_y. The periodic boundaries are assumed and the values of the wave-vector are quantized as $k = \frac{2\pi n_k}{Ly}$, where n_k is an integer and $-N \leq n_k \leq N$. According to the Landau quantization, it is further assumed that the center of the oscillator must physically lie within $-\frac{L_x}{2} < x_0 < \frac{L_x}{2}$. It immediately follows that the upper limit $N = \frac{L_x L_y}{4\pi\lambda^2}$. Following table illustrates the values of magnetic length λ and values of N for different magnetic fields under assumption $L_x = L_y = 100$ nm

The maximum range of the wave vectors is usually not utilized, since the set of the wave vectors is usually truncated due to the computational burden.

B [T]	λ[nm]	N
1	25.6554	1
5	11.4734	6
10	8.1130	12
15	6.6242	18
20	5.7367	24
50	3.6282	60
100	2.5655	120

Table 3.1: Dependence of magnetic length λ and wavevector value bounds N on magnetic field B

The three one-particle wavefunctions can be described as:

$$\psi^h_{n_h}(x_h, y_h) = \frac{1}{\sqrt{L_y}} \sqrt{\frac{1}{2^{n_h} n_h!}} \frac{1}{\sqrt{\lambda\sqrt{\pi}}} H_{n_h}\left(\frac{x_h + \lambda^2 k_h}{\lambda}\right) e^{-\frac{(x_h+\lambda^2 k_h)^2}{2\lambda^2} - i k_h y_h} \tag{3.5}$$

$$\psi^{e1}_{n_1}(x_1, y_1) = \frac{1}{\sqrt{L_y}} \sqrt{\frac{1}{2^{n_1} n_1!}} \frac{1}{\sqrt{\lambda\sqrt{\pi}}} H_{n_1}\left(\frac{x_1 - \lambda^2 k_1}{\lambda}\right) e^{-\frac{(x_1-\lambda^2 k_1)^2}{2\lambda^2} + i k_1 y_1} \tag{3.6}$$

$$\psi^{e2}_{n_2}(x_2, y_2) = \frac{1}{\sqrt{L_y}} \sqrt{\frac{1}{2^{n_2} n_2!}} \frac{1}{\sqrt{\lambda\sqrt{\pi}}} H_{n_2}\left(\frac{x_2 - \lambda^2 k_2}{\lambda}\right) e^{-\frac{(x_2-\lambda^2 k_2)^2}{2\lambda^2} + i k_2 y_2} \tag{3.7}$$

The in-plane wavefunction $\Psi_{in-plane}(x_1, x_2, x_h, y_1, y_2, y_h)$ is thus characterized by six quantum numbers n_1, n_2, n_h, k_1, k_2 and k_h. However, the total momentum $K = k_1 + k_2 - k_h$ is constant of motion and thus it is conserved. Note that minus sing for k_h term is due to convention in chosen wavefunction $\psi^h_{n_h}(x_h, y_h)$. The both signs might be reversed with equivalent result. We set $K = 0$ and thus only such in-plane trion functions for that holds $k_1 + k_2 - k_h = 0$ are included in the wavefunction basis.

The size of the wave basis grows rapidly with growing upper bound for the wave vectors N. It can be found out that the size of the basis (for one Landau level and one type of hole states) can be computed as $Size_n = 3N^2 + 3N + 1$. For $N = 5$ it makes the size 76×76. We also consider three Landau levels for each particle, which makes 27 different combinations. Moreover, three different hole states are involved. The basis size is then altogether 6156×6156. The value of N thus imply the total size of the wavefunction basis. The appropriate value of N is chosen according to the numerical analysis that is undertaken after the evaluation of Coulomb terms (see below).

3.2 Diagonal terms of the Hamiltonian

The only non-diagonal terms are Coulomb and Luttinger terms that will be discussed separately. The diagonal terms consist of the energies of the Landau levels and of the offsets of the light holes and the excited heavy holes state. The Landau levels energies are defined by:

$$E^{h}_{Landau} = \frac{\hbar^2(n_h+1)}{2\lambda^2 m_h}, \tag{3.8}$$

$$E^{e1}_{Landau} = \frac{\hbar^2(n_1+1)}{2\lambda^2 m_e}, \tag{3.9}$$

$$E^{e2}_{Landau} = \frac{\hbar^2(n_2+1)}{2\lambda^2 m_e}, \tag{3.10}$$

$$E^{trion}_{Landau} = E^{h}_{Landau} + E^{e1}_{Landau} + E^{e2}_{Landau}. \tag{3.11}$$

The Landau energy of the trion ground state is thus:

$$E^{trion}_{ground} = \frac{\hbar^2}{2\lambda^2 m_h} + 2\frac{\hbar^2}{2\lambda^2 m_e} \tag{3.12}$$

We consider $n = 0, 1, 2$ for each particle. We thus have 27 combinations of Landau levels for three particles involved.

Let us now evaluate the effective masses of each particle. The mass of the free electron can be expressed as $m_0 = 511$ keV. All the effective masses are then related to this value. We recall the values of the Luttinger parameters $\gamma_1 = 6.85$ $\gamma_2 = 2.10$ $\gamma_3 = 2.90$. The effective masses are then defined by equations (1.47) and (1.48).

$$m_{hh\|} = 0.112m_0 \qquad m^z_{hh} = 0.377m_0 \tag{3.13}$$

$$m_{lh\|} = 0.211m_0 \qquad m^z_{lh} = 0.090m_0 \tag{3.14}$$

Note the mass reversal in the in-plane coordinates in that the light holes are heavier than the heavy holes. For illustration we can establish ground Landau energy for magnetic field of 15 T $E^{trion}_{ground}(15T) = 33.7$ meV.

Confinement energy of the particles in the hole ground state is set to zero. However, the confinement energy of the excited heavy hole must be added as the offset of ground state and excited state heavy holes. The correct value for the infinite quantum well of the width $L_z = 10$ nm is according to (1.40):

$$E_{offset} = \frac{4\hbar^2\pi^2}{2mL_z^2} - \frac{\hbar^2\pi^2}{2mL_z^2} = 30meV \tag{3.15}$$

However, this value substantially overestimates the real value. The quantum well is not infinitely deep in reality. Thus the particles' wavefunctions tend to tunnel into the barrier. As the result the effective width of the quantum well increases. Throughout the computations, we use the offset of 16 meV that corresponds to the effective quantum well width of 13.7 nm.

We also need to use the offset parameter that is associated with the light holes. We assume light holes' states to be shifted from ground state heavy hole states by 10 meV [18].

To sum up, the diagonal terms (except of Coulomb terms) consist of the appropriate energies of the Landau levels of each particle, the offset for the light hole states and the confinement offset for the first excited heavy hole states.

3.3 Coulomb terms

The evaluation of all Coulomb terms lies in the center of computations. Due to competition between spherical symmetry of Coulomb interaction, cylindrical symmetry of magnetic field and quantum well confinement, it is impossible to diagonalize the Coulomb terms [28]. Coulomb interaction involves two particles and so in Cartesian coordinate system it depends on six coordinates. Using simplified notation we may write Coulomb potential between two particles as:

$$V_{12}(\vec{r}) = V_{12}(x_1, y_1, z_1, x_2, y_2, z_2) = \frac{q_1 q_2}{4\pi\varepsilon} \frac{1}{\sqrt{(x_2 - x_1)^2 + (y_2 - y_1)^2 + (z_2 - z_1)^2}}. \quad (3.16)$$

Coulomb interaction is (except of sign reversion) equal between hole and electron and between two electrons thus we use indices 1 and 2 irrespective whether the particle is an electron or a hole. If we multiply Coulomb potential from both sides with wavefunctions of both particles involved and generally integrating over all space, we get the Coulomb term of Hamiltonian (we skip the constant prefactor):

$$V = \int \Psi^*(x_1, y_1, z_1)\Psi^*(x_2, y_2, z_2)V_{12}(|x_2 - x_1|, |y_2 - y_1|, |z_2 - z_1|)\times \\ \times\Psi'(x_1, y_1, z_1)\Psi'(x_2, y_2, z_2)dx_1dx_2dy_1dy_2dz_1dz_2 \quad (3.17)$$

The strategy of evaluating such Coulomb term is of course based on the chosen wave function basis. We know that in the x-direction the particles are localized (the integration over all space is finite) thanks to the Gaussian type wave function (though modified by Hermite polynomials for higher Landau levels). Similarly, in the z-direction the particles are localized in the quantum well. Since we assume indefinitely deep QW, the particles cannot appear outside the well and thus are localized in the interval $\left(-\frac{L_z}{2}, \frac{L_z}{2}\right)$. In the y-direction, there is no such confinement, however,trion is assumed to be localized in a 'box' of side L_y in the y-direction (since trion is either confined or localized in both other directions we can really consider the situation as if trion is closed in a 'box'). Coulomb potential affects the trion both within our assumed 'box' but also between these 'boxes'. Each 'box' contains one elementary charge (negative charge in the case of negative trion), but the system as a whole must be neutral. Thus we need to assume (positive) charge that is uniformly distributed in each 'box' and so the overall charge is zero. This construct can be efficiently used when dealing with Coulomb term and it is a variant of so called Ewald summation [19].

We need to deal with following integration:

$$\frac{1}{L_y^2}\int_{-\frac{L_z}{2}}^{\frac{L_z}{2}} dz_1 \int_{-\frac{L_z}{2}}^{\frac{L_z}{2}} dz_2 \int_{-\infty}^{\infty} dx_1 \int_{-\infty}^{\infty} dx_2 \int_{-\frac{L_y}{2}}^{\frac{L_y}{2}} dy_2 \int_{y_2-\frac{L_y}{2}}^{y_2+\frac{L_y}{2}} dy_1 \tag{3.18}$$

$$V_{12}(|x_2-x_1|,|y_2-y_1|,|z_2-z_1|)e^{i(k_2'-k_2)y_2}e^{i(k_1'-k_1)y_1}\times \tag{3.19}$$

$$\times\,\psi_{n_1',k_1'}(x_1)\psi_{n_1,k_1}(x_1)\psi_{n_2',k_2'}(x_2)\psi_{n_2,k_2}(x_2)\varphi_1^2(z_1)\varphi_2^2(z_2). \tag{3.20}$$

We define $\psi_{n,k}(x)$ in accordance with Eqs. (3.5) - (3.6):

$$\psi_{n,k}(x)=\sqrt{\frac{1}{2^n n!}}\frac{1}{\sqrt{\lambda\sqrt{\pi}}}H_n\left(\frac{x-\lambda^2 k}{\lambda}\right)e^{-\frac{(x-\lambda^2 k)^2}{2\lambda^2}} \tag{3.21}$$

Let us first focus on the most complicated integrating over y_1 and y_2. For the sake of brevity we denote: $a^2=(x_1-x_2)^2+(z_1-z_2)^2$, $a\geq 0$:

$$\frac{1}{L_y^2}\int_{-\frac{L_y}{2}}^{\frac{L_y}{2}} dy_2 \int_{y_2-\frac{L_y}{2}}^{y_2+\frac{L_y}{2}} dy_1 V_{12}(a,|y_2-y_1|)e^{i(k_2'-k_2)y_2}e^{i(k_1'-k_1)y_1} \tag{3.22}$$

We use following substitution:

$$y=y_1-y_2 \tag{3.23}$$

$$y_1=y+y_2 \tag{3.24}$$

$$\frac{1}{L_y^2}\int_{-\frac{L_y}{2}}^{\frac{L_y}{2}} dy_2 \int_{-\frac{L_y}{2}}^{\frac{L_y}{2}} dy \frac{1}{\sqrt{a^2+y^2}}e^{i(k_2'-k_2+k_1'-k_1)y_2}e^{i(k_1'-k_1)y} \tag{3.25}$$

This integral is non-zero only if $k_2'-k_2+k_1'-k_1=0$ holds and we deal with the integration:

$$\frac{1}{L_y}\int_{-\frac{L_y}{2}}^{\frac{L_y}{2}} dy \frac{1}{\sqrt{a^2+y^2}}e^{i(k_1'-k_1)y} \tag{3.26}$$

Now, let us employ the Ewald summation. The main trick is that we integrate inverse Fourier transform of Fourier transform (instead of direct integration). Following previous computations, Coulomb potential can be written as:

$$V(y)=\frac{1}{\sqrt{a^2+y^2}} \tag{3.27}$$

However, this potential acts between charges separately in each 'box' in y direction. Thus it is periodic function in y with period L_y and total potential can be written as:

$$\tilde{V}(y)=\sum_{j=-\infty}^{\infty}\frac{1}{\sqrt{a^2+(y+jL_y)^2}}, \tag{3.28}$$

where j is integer. Now, let us formally write the Coulomb potential as a one dimensional Fourier expansion:

$$\tilde{V}(y) = \sum_{n=-\infty}^{\infty} V_q e^{-iq_n y}, \tag{3.29}$$

where $q_n = \frac{2\pi}{Ly} n$ and n is integer.

It clearly follows from the periodicity of $\tilde{V}(y)$ that:

$$\int_{-\frac{L_y}{2}}^{\frac{L_y}{2}} dy \tilde{V}(y) e^{iq_n y} = L_y V_q \tag{3.30}$$

This identity gives us a hint how to compute the Fourier transform V_q:

$$V_q = \frac{1}{L_y} \int_{-\frac{L_y}{2}}^{\frac{L_y}{2}} dy \tilde{V}(y) e^{iq_n y} = \frac{1}{L_y} \int_{-\frac{L_y}{2}}^{\frac{L_y}{2}} dy \sum_{j=-\infty}^{\infty} \sum_{n=-\infty}^{\infty} \frac{e^{iq_n y}}{\sqrt{a^2 + (y + jL_y)^2}} \tag{3.31}$$

$$= \sum_{j=-\infty}^{\infty} \sum_{n=-\infty}^{\infty} \frac{1}{L_y} \int_{-\frac{L_y}{2}}^{\frac{L_y}{2}} dy \frac{e^{iq_n y}}{\sqrt{a^2 + (y + jL_y)^2}} \tag{3.32}$$

Let us now focus on the sum over j and evaluation of the integrals. If we substitute in integral for each j in a manner: $y' = y + jL_y$ we must add a term jL_y to the integration limits. Each of these integrals is thus performed in 'its own box'. The sum over j can thus be written as one integral but over all y.

$$V_q = \sum_{n=-\infty}^{\infty} \frac{1}{L_y} \int_{-\infty}^{\infty} dy \frac{e^{iq_n y}}{\sqrt{a^2 + z^2}}, \tag{3.33}$$

This formula can be evaluated analytically:

$$V_q = \frac{2}{L_y} K_0 (|q_n| |a|), \tag{3.34}$$

where K_0 is Bessel K-function of zeroth order. Now we finally perform integration over y as defined by Eq. (3.40) of inverse Fourier transform:

$$\frac{2}{L_y^2} \int_{-\frac{L_y}{2}}^{\frac{L_y}{2}} dy \sum_{n=-\infty}^{\infty} K_0 (|q_n| |a|) e^{i(k_1' - k_1)y} e^{-iq_n y} \tag{3.35}$$

From exponentials we get following condition: $q_n = k_1' - k_1$ (note that $|k_1' - k_1| = |k_2' - k_2|$). By this we got rid of integration over y and summation over n. The result is following formula:

$$\frac{2}{L_y} K_0 \left(\left| k_1' - k_1 \right| |a| \right) \tag{3.36}$$

We have thus simplified the original integral to the following form:

$$\frac{2}{L_y}\int_{-\frac{L_z}{2}}^{\frac{L_z}{2}} dz_1 \int_{-\frac{L_z}{2}}^{\frac{L_z}{2}} dz_2 \int_{-\infty}^{\infty} dx_1 \int_{-\infty}^{\infty} dx_2 K_0\left(\left|k_1' - k_1\right| \sqrt{(x_1-x_2)^2+(z_1-z_2)^2}\right) \quad (3.37)$$

$$\psi_{n_1,k_1'}(x_1)\psi_{n_1,k_1}(x_1)\psi_{n_2,k_2'}(x_2)\psi_{n_2,k_2}(x_2)\varphi_1^2(z_1)\varphi_2^2(z_2). \quad (3.38)$$

We thus reduced the problem to integration over four variables z_1, z_2, x_1, x_2. However, it is possible to get rid of one of the z and one of the x variables analytically. The derivation is straightforward but not simple at all and is shown in Appendix A.

Using the results from Appendix A, we finally get the integral:

$$V_{12} = \int_0^{L_z} dz \int_{-\infty}^{\infty} dx \frac{2}{L_y} K_0\left(\left|k_1' - k_1\right| \sqrt{(x^2+z^2}\right) f(x)g(z), \quad (3.39)$$

where functions $f(x)$ and $g(z)$ are appropriate functions resulting from partial analytical integration. This integral can be solved numerically for $|k_1' - k_1| \neq 0$.

For $|k_1' - k_1| = 0$, this integral diverges to infinity. However, such infinite potential is compensated by assumed uniformly distributed positive charge (note that Fourier transform of uniform distribution is delta function).

We, therefore, need to treat Coulomb terms for that $k_1' - k_1 = 0$ holds in a different manner (note that this condition is for non-zero Coulomb terms equivalent to $k_2' - k_2 = 0$). The singularity is of Coulombic term is weakened by integrating only over the assumed 'box'. Recall Eq. (3.26):

$$\frac{1}{L_y}\int_{-\frac{L_y}{2}}^{\frac{L_y}{2}} dy \frac{1}{\sqrt{a^2+y^2}} e^{i(k_1'-k_1)y} = \frac{1}{L_y}\int_{-\frac{L_y}{2}}^{\frac{L_y}{2}} dy \frac{1}{\sqrt{a^2+y^2}} \quad (3.40)$$

Using results form Appendix A we can write final formula for Coulomb terms $V_{k_1=k_1'}$:

$$V_{k_1=k_1'} = \int_0^{L_z} dz \int_{-\infty}^{\infty} dx \int_{-\frac{L_y}{2}}^{\frac{L_y}{2}} dy \frac{1}{L_y} \frac{1}{\sqrt{x^2+y^2+z^2}} f(x)g(z) \quad (3.41)$$

This triple integral must then be evaluated numerically.

3.4 Luttinger terms

In this section, we compute the Luttinger terms given by (1.57) and (1.58) for chosen wavefunctions basis. The computation is rather simple and straightforward, however deserves some comments. Luttinger terms couple the hole wavefunctions. Let us recall the definition of Luttinger $\hat{b}$ term under Landau calibration of magnetic field

$$\hat{b} = \frac{\sqrt{3}\gamma_3}{2m_0} p_z \left(p_x - ip_y + i\frac{\hbar x}{\lambda^2}\right) = g\left(p_x - ip_y + i\frac{\hbar x}{\lambda^2}\right) \quad (3.42)$$

where $g = \frac{\sqrt{3}\gamma_3}{2m_0} p_z$. Observe that g is non-zero only when mixing the ground state and the first excited state of the heavy hole. Let us first act by g on the excited state.

$$\langle \varphi_{h0}(z)|g_{01}|\varphi_{h1}(z)\rangle = \frac{\sqrt{3}\gamma_3}{2m_0}\frac{2}{L_z}\int_{-\frac{L_z}{2}}^{\frac{L_z}{2}} dz cos\left(\frac{\pi}{L_z}z\right)(-i\hbar)\frac{\partial}{\partial z} sin\left(\frac{2\pi}{L_z}z\right) \tag{3.43}$$

$$= -\frac{8i\gamma_3\hbar}{\sqrt{3}L_z m_0} \tag{3.44}$$

Now let g act on the ground state:

$$\langle \varphi_{h1}(z)|g_{10}|\varphi_{h0}(z)\rangle = \frac{\sqrt{3}\gamma_3}{2m_0}\frac{2}{L_z}\int_{-\frac{L_z}{2}}^{\frac{L_z}{2}} dz sin\left(\frac{2\pi}{L_z}z\right)(-i\hbar)\frac{\partial}{\partial z} cos\left(\frac{\pi}{L_z}z\right) \tag{3.45}$$

$$= \frac{8i\gamma_3\hbar}{\sqrt{3}L_z m_0} \tag{3.46}$$

The acting by g on the ground state leads only to the sign reversal when compared to the previous case. Note that the changing of the order of the wavefunctions is equivalent to the complex conjugation of g. We thus have four different possibilities (g_{01}, g_{10},g^*_{01}, g^*_{10}) with two possible outcomes.

It has been already discussed that $\hat{b}$ terms act like the creation operators, thus they mix only states on the ground Landau level with the first excited and the states on the first excited level with those on the second excited level. Let us first act on the ground state.

$$\left\langle \psi_1^h(x,y)\right| \hat{b} \left|\psi_0^h(x,y)\right\rangle = g\int_{-\frac{L_y}{2}}^{\frac{L_y}{2}} dy \int_{-\infty}^{\infty} dx \psi_1^{h*}(x,y)\left(-i\hbar\frac{\partial}{\partial x} + \hbar\frac{\partial}{\partial y} + i\frac{\hbar x}{\lambda^2}\right)\psi_0^h(x,y) \tag{3.47}$$

$$= g\frac{i\hbar\sqrt{2}}{\lambda} \tag{3.48}$$

Note that $\langle\ \psi_0^h(x,y)|\ \hat{b}\ |\psi_1^h(x,y)\rangle = 0$. We can now compute the complex conjugated term $\hat{b}^*$ that behaves like an annihilation operator.

$$\left\langle \psi_0^h(x,y)\right| \hat{b^*} \left|\psi_1^h(x,y)\right\rangle = g\int_{-\frac{L_y}{2}}^{\frac{L_y}{2}} dy \int_{-\infty}^{\infty} dx \psi_0^{h*}(x,y)\left(-i\hbar\frac{\partial}{\partial x} + \hbar\frac{\partial}{\partial y} + i\frac{\hbar x}{\lambda^2}\right)\psi_1^h(x,y) \tag{3.49}$$

$$= -g^*\frac{i\hbar\sqrt{2}}{\lambda} \tag{3.50}$$

Under assumption that the order of $\varphi_{h0}(z)$ and $\varphi_{h1}(z)$ remains unchanged, the numerical value of $\langle\ \Psi_1|\ \hat{b}\ |\Psi_0\rangle$ is equal to $\langle\ \Psi_0|\ \hat{b}\ |\Psi_1\rangle$.

Similarly we can compute terms that mix the first and the second excited Landau levels.

$$\left\langle \psi_2^h(x,y)\right| \hat{b} \left|\psi_1^h(x,y)\right\rangle = g\int_{-\frac{L_y}{2}}^{\frac{L_y}{2}} dy \int_{-\infty}^{\infty} dx \psi_2^{h*}(x,y)\left(-i\hbar\frac{\partial}{\partial x} + \hbar\frac{\partial}{\partial y} + i\frac{\hbar x}{\lambda^2}\right)\psi_1^h(x,y) \tag{3.51}$$

$$= g\frac{2i\hbar}{\lambda} \tag{3.52}$$

$$\left\langle \psi_1^h(x,y)\right| \hat{b^*} \left|\psi_2^h(x,y)\right\rangle = g\int_{-\frac{L_y}{2}}^{\frac{L_y}{2}} dy \int_{-\infty}^{\infty} dx \psi_1^{h*}(x,y)\left(-i\hbar\frac{\partial}{\partial x} + \hbar\frac{\partial}{\partial y} + i\frac{\hbar x}{\lambda^2}\right)\psi_2^h(x,y) \tag{3.53}$$

$$= -g^*\frac{2i\hbar}{\lambda} \tag{3.54}$$

Now, we treat the $\hat{c}$ terms. It has been shown that $\hat{c}$ mixes only states on the ground Landau level with the the states on the second excited level.

$$\hat{c} = \frac{\sqrt{3}}{2m_0}\left[\gamma_2\left(p_x^2 - p_y^2 + 2p_y\frac{\hbar x}{\lambda^2} - \frac{\hbar^2x^2}{\lambda^4}\right) - i\gamma_3\left(2p_xp_y - p_x\frac{\hbar x}{\lambda^2} - \frac{\hbar x}{\lambda^2}p_x\right)\right] \tag{3.55}$$

$$\left\langle \psi_0^h(x,y)\right| \hat{c} \left|\psi_2^h(x,y)\right\rangle = \tag{3.56}$$

$$\frac{\sqrt{3}}{2m_0}\int_{-\frac{L_y}{2}}^{\frac{L_y}{2}} dy \int_{-\infty}^{\infty} dx \psi_0^{h*}\Big[\gamma_2\left(-\hbar^2\frac{\partial^2}{\partial x^2} + \hbar^2\frac{\partial^2}{\partial y^2} - 2i\hbar\frac{\partial}{\partial y}\frac{\hbar x}{\lambda^2} - \frac{\hbar^2x^2}{\lambda^4}\right) \tag{3.57}$$

$$- i\gamma_3\left(-2\hbar^2\frac{\partial^2}{\partial x\partial y} + i\hbar\frac{\partial}{\partial x}\frac{\hbar x}{\lambda^2} + i\hbar\frac{\hbar x}{\lambda^2}\frac{\partial}{\partial x}\right)\Big]\psi_2^h(x,y) \tag{3.58}$$

$$\left\langle \psi_0^h(x,y)\right| \hat{c} \left|\psi_2^h(x,y)\right\rangle = \frac{\hbar^2\sqrt{6}(-\gamma_2 + 2\gamma_3}{2\lambda^2 m_0} \tag{3.59}$$

$$\tag{3.60}$$

It can be easily found and that $\left\langle \psi_2^h(x,y)\right| \hat{c} \left|\psi_0^h(x,y)\right\rangle = 0$, however the complex conjugate $\hat{c}^*$ acts like two annihilation operators:

$$\left\langle \psi_0^h(x,y)\right| \hat{c}^* \left|\psi_2^h(x,y)\right\rangle = \tag{3.61}$$

$$\frac{\sqrt{3}}{2m_0}\int_{-\frac{L_y}{2}}^{\frac{L_y}{2}} dy \int_{-\infty}^{\infty} dx \psi_0^{h*}\Big[\gamma_2\left(-\hbar^2\frac{\partial^2}{\partial x^2} + \hbar^2\frac{\partial^2}{\partial y^2} - 2i\hbar\frac{\partial}{\partial y}\frac{\hbar x}{\lambda^2} - \frac{\hbar^2x^2}{\lambda^4}\right) \tag{3.62}$$

$$+ i\gamma_3\left(-2\hbar^2\frac{\partial^2}{\partial x\partial y} + i\hbar\frac{\partial}{\partial x}\frac{\hbar x}{\lambda^2} + i\hbar\frac{\hbar x}{\lambda^2}\frac{\partial}{\partial x}\right)\Big]\psi_2^h(x,y) \tag{3.63}$$

$$\left\langle \psi_0^h(x,y) \right| \hat{c}^* \left| \psi_2^h(x,y) \right\rangle = \frac{\hbar^2\sqrt{6}(-\gamma_2 - 2\gamma_3)}{2\lambda^2 m_0} \tag{3.64}$$

$$\tag{3.65}$$

The value of Luttinger terms thus depends, apart of physical constants, only on the magnetic field. Appropriate pre-calculated Luttinger terms are simply added to the correct positions in the Hamiltonian matrix.

3.5 Numerical analysis of the basis size

Apart of theoretical and conceptual progress that has been derived in the last few sections, this thesis aims also in quantitative computations and reliable results. The choice of the size of the wavebasis is then crucial. The most time-consuming procedure is the numerical computation of Coulomb terms. Even for big matrices, the evaluation of all Coulomb terms takes longer time than the matrix diagonalization. Since the procedures takes substantial computing time, the size of the Hamiltonian matrix must be restricted by appropriate choice of the wavefunctions basis size.

It has been already pointed out that, we restrict the computations to the ground and the two excited Landau levels. This is not only due to substantial computational effort when dealing with numerical integration, but also because of substantial amount of analytical integrations over variable x that have to be performed for all combinations of Landau levels independently.

The other parameter determining the size of the basis is the number of the wave vectors k_1, k_2 and k_h that are taken to account. We consider the same number of the wave vectors for each particle, thus the key parameter of the size of the Hamiltonian matrix is $N = N_1 = N_2 = N_h$.

The final size of the basis has been chosen according to three criteria:

- Convergence of the Coulomb terms
- Symmetry of the ground wavefunction
- Computational time

3.5.1 Convergence of the Coulomb terms

The Coulomb terms are real physical quantities that should not depend on the choice of the basis size. We thus need sufficiently large basis so that the Coulomb terms are not affected by too restrictive choice. In the testing procedure, we construct the small block of Hamiltonian matrix that involves only particles in the ground Landau level and the hole wavefunctions describe only the heavy hole ground state. Generalization to complete matrix (involving 3 Landau levels for each particle and 3 different hole states) would make

the complete analysis extremely time-demanding, however we confirmed for some that analysis of this small block is sufficient.

Such small block may involve only the Coulomb terms, since other terms would shift all eigen-energies. Simplified Hamiltonians for different choices or parameters are diagonalized and the convergence of the smallest eigenvalue (ground energy) is investigated. Note that the Coulomb terms depend on parameter N, on the size of the box in the y-direction L_y and the magnetic length λ associated with given magnetic field B. It can be found out that the smaller is the L_y, the faster is the convergence of Coulomb terms with increasing N. However, the parameter L_y has no real physical significance and occurs due to construction of the basis. Thus the Coulomb terms need to converge also with growing L_y. It is thus necessary to find sufficient values of N and L_y so that Coulomb terms do not change with increasing values of those parameters.

B [T]	15	15	15	15	B [T]	5	5	30	30	50	50
λ[nm]	6.62	6.62	6.62	6.62	λ[nm]	11.47	11.47	4.68	4.68	3.63	3.63
L_y	10	50	100	200	L_y	100	200	50	100	50	100
N = 1	-21.7	-14.7	-12.0	-8.4	N = 1	-8.9	-6.9	-18.2	-13.7	-20.6	-15.2
N = 2	-21.7	-15.1	-14.2	-11.0	N = 2	-9.4	-8.5	-19.8	-17.1	-24.1	-19.6
N = 3	-21.7	-15.1	-15.0	-12.8	N = 3	-9.4	-9.1	-20.1	-18.9	-24.9	-21.9
N = 4		-15.1	-15.2	-13.9	N = 4	-9.4	-9.4	-20.1	-19.7	-25.1	-23.4
N = 5		-15.1	-15.3	-14.6	N = 5		-9.5	-20.1	-20.1	-25.1	-24.2
N = 6			-15.3	-15.0	N = 6		-9.5		-20.2	-25.1	-24.6
N = 7			-15.3	-15.2	N = 7						-24.8
N = 8				-15.3	N = 8						-24.9
N = 9				-15.3	N = 9						

Table 3.2: Dependence of the lowest eigenvalue of the Hamiltonian matrix containing Coulomb terms only on the size of 'box' in y-direction (L_y), magnetic field (B, λ) and size of the basis N (lowest Landau level approximation).

The left panel of Table 3.5.1 shows the dependence of the lowest energy on the size of the box L_y and on the size of the basis for magnetic field $B = 15$ T. For large L_y there is a need for large basis to attain the convergence. However, the value of the eigen-energy is more reliable. We can thus inspect the convergence for smaller L_y. It might be observed that for $L_y = 50$ nm the final value is unreliable (consider resolution ± 0.1 meV. Optimal choice is thus $L_y = 100$ nm and convergence is attained for $N = 5$.

The right panel of Table 3.5.1 shows the same analysis but for different magnetic fields. For low magnetic field of $B = 5$ T the convergence is faster, however it is found to be more reliable for larger L_y. This is not surprising result since lower magnetic field allows larger movement of particles and therefore L_y is more restrictive. On the other hand, for higher magnetic fields the convergence is slower but reliable for lower values of L_y. Throughout this thesis we consider $L_y = 100$ nm for magnetic fields $B \leq 30$ T and $L_y = 50$ nm for $B = 50$ T.

3.5.2 Symmetry of the ground wavefunction

The special feature of the chosen wavefunction basis is that the basis is not *a priori* radially symmetrical. This choice allows relatively easier manipulations but does not reflect the physical reality. However, it might be shown that for sufficiently big basis the wavefunctions become fairly symmetric.

We undertook simple symmetry analysis. Hamiltonian matrix under lowest Landau level approximation has been constructed and diagonalized. The wavefunction associated with the lowest energetic state has been depicted. Two different graphical representation are chosen. The first is attractive 3D representation, whereas the second is more synoptical depiction by contour plots. Both series of graphs (3.1) - (3.4) and (3.5) - (3.8) show the dependence of the wavefunction over xy-plane on the basis size. It is clear that the circularity of the wavefunction improves with rising N. For $N \geq 5$, the wavefunction is already fairly symmetrical. The laceration of the graph for $N = 7$ is unresolved, however it may be associated with change of the sign of wavefunction or with some numerical imperfections.

More exact analysis of the wavefunction symmetry is carried out by evaluation of eccentricity. We treat the contour that labels the half of the maximum of the wavefunction as if it is an ellipse. Such ellipse obviously has its major semi-axis a in the y-direction and minor semi-axis b in the x-direction. We may now construct some non-symmetry parameter $e = \frac{a-b}{a}$. (Note that this construction is similar to the definition of eccentricity, however the eccentricity is based on the deviation in squares.) $e = 0$ represents perfectly symmetric wavefunction, where as $e \to 1$ reflects very elongated wavefunction in y-direction. We state that $e \leq 0.5$ describes sufficiently symmetric wavefunction.

B [T]	5	15	30
N = 1	0.72	0.88	0.92
N = 2	0.62	0.80	0.86
N = 3	0.45	0.71	0.80
N = 4	0.29	0.61	0.73
N = 5	0.17	0.52	0.67
N = 6	0.12	0.42	0.61
N = 7	0.11	0.33	0.54

Table 3.3: Dependence of the basis wavefunction non-symmetry on magnetic field and the size of the basis (only the lowest Landau level included)

Table 3.5.2 contains the values of e for different magnetic fields and different sizes of basis. It is obvious and not surprising that for lower magnetic fields sufficient symmetry is attained already by smaller basis. Larger magnetic fields have adverse effect on the chosen wavefunctions basis due to non-symmetric Landau gauge. Depending on its size, the wavefunctions basis might be inappropriate for very high magnetic fields. The wavefunction symmetry is also illustrated by figures (3.9) - (3.12) for different magnetic fields.

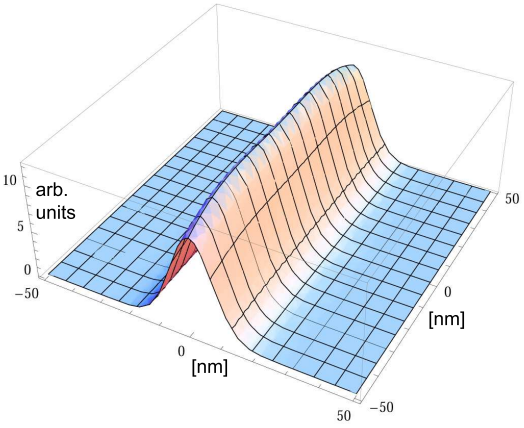

Figure 3.1: 3D plot of probability density of electron with respect to the position of the hole; B = 15 T; N = 1

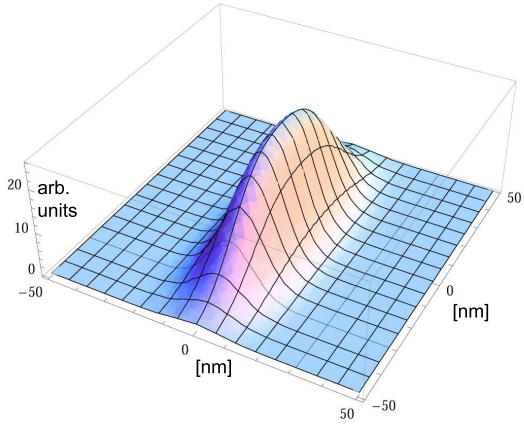

Figure 3.3: 3D plot of probability density of electron with respect to the position of the hole; B = 15 T; N = 3

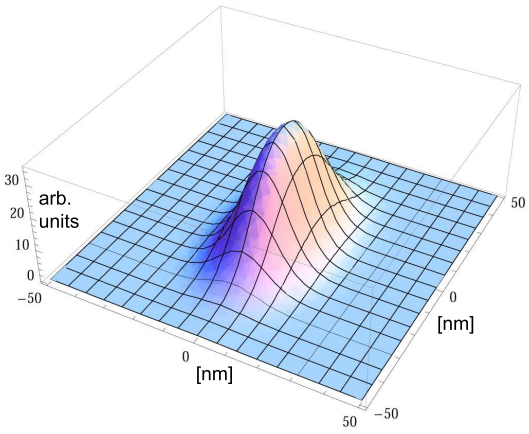

Figure 3.2: 3D plot of probability density of electron with respect to the position of the hole; B = 15 T; N = 5

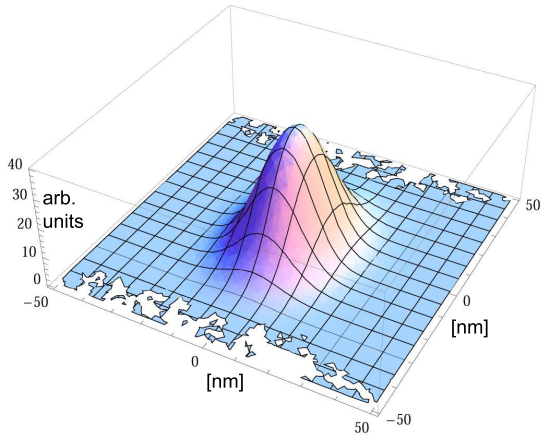

Figure 3.4: 3D plot of probability density of electron with respect to the position of the hole; B = 15 T; N = 7

3.5.3 Computational issues

All computations have been carried out in Mathematica, version 6.0, 64 bit version. Mathematica proved its superior ability to deal with presented problems. Well-arranged graphical interface allows easier development of programming procedures in particular it allows immediate modifications to functions, what is extremely favourable for quick testing computations. Well-established documentation, block arrangement of programs and functions that do not require any compiling is appreciated mainly for programming beginners. Important developed functions are described in Appendix B.

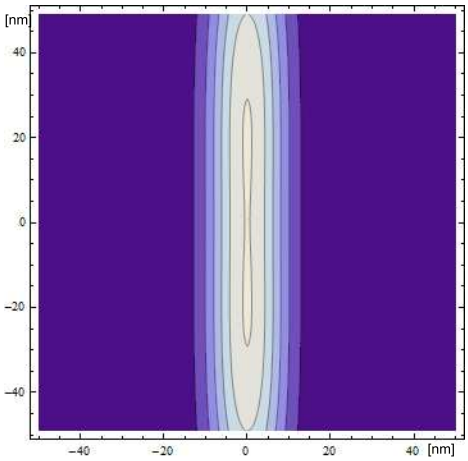

Figure 3.5: Contour plot of probability density of electron with respect to the position of the hole; B = 15 T; N = 1

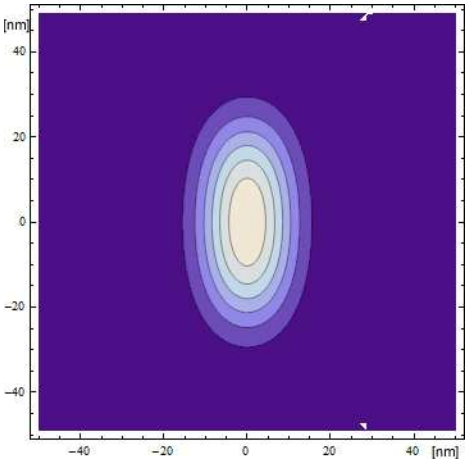

Figure 3.6: Contour plot of probability density of electron with respect to the position of the hole; B = 15 T; N = 5

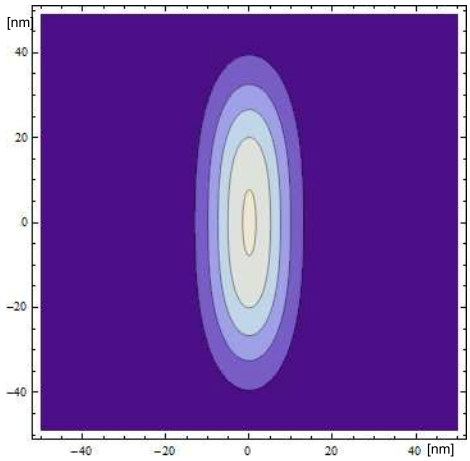

Figure 3.7: Contour plot of probability density of electron with respect to the position of the hole; B = 15 T; N = 3

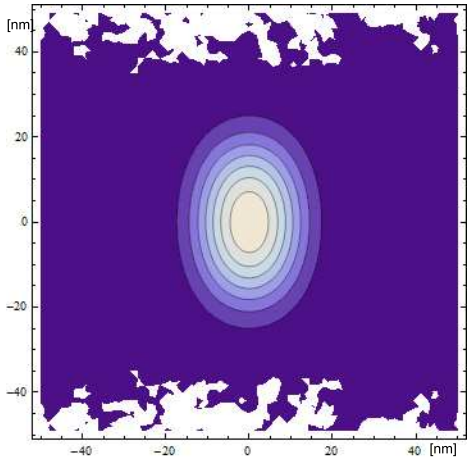

Figure 3.8: Contour plot of probability density of electron with respect to the position of the hole; B = 15 T; N = 7

The computations were carried only on ordinary PC with four core 3 GHz processor and 4 GB RAM memory. The size of the basis has been set to $N = 5$ for all computations. Recall that this might be inappropriate for higher magnetic fields ($B > 30$ T). Note also that restriction to three Landau levels only may be inappropriate for low magnetic fields for that Landau levels are close to each other. Our approach is thus well suited for middle fields around $B = 15$ T.

The most time-demanding procedure is computation of all Coulomb terms and their arrangement into Hamiltonian matrix. For full setting (3 Landau levels and three types

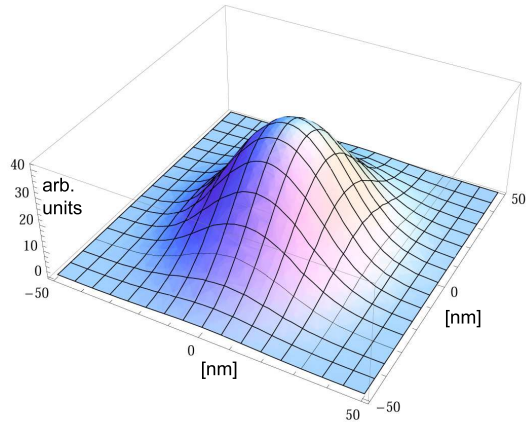

Figure 3.9: 3D plot of probability density of electron with respect to the position of the hole; B = 5 T; N = 5

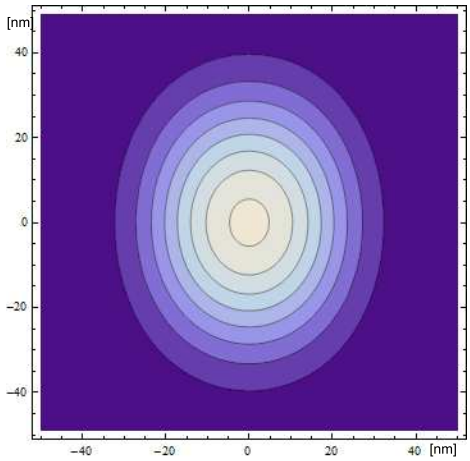

Figure 3.11: Contour plot of probability density of electron with respect to the position of the hole; B = 5 T; N = 5

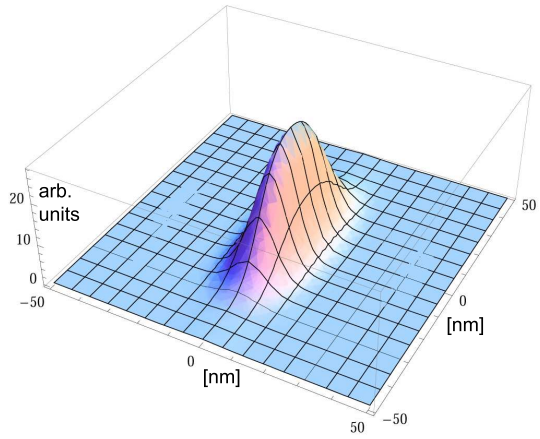

Figure 3.10: 3D plot of probability density of electron with respect to the position of the hole; B = 30 T; N = 5

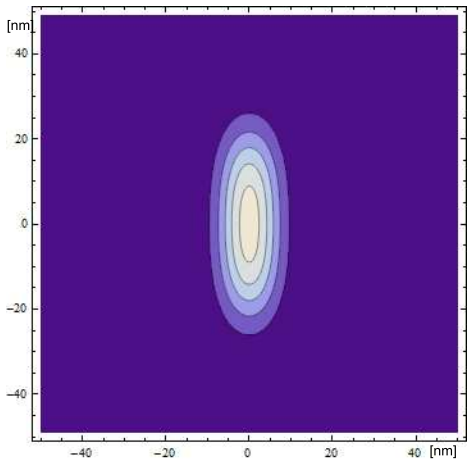

Figure 3.12: Contour plot of probability density of electron with respect to the position of the hole; B = 30 T; N = 5

of hole states) this procedure takes around 4-5 hours (running on one processor core) even after optimization described in the following subsection. Diagonalization then takes less then one hour. Mathematica automatically chooses appropriate diagonalization method. For the numeric input it uses so-called LAPACK method and takes into account that the matrix is symmetric. Other manipulations are generally fast apart of construction of singlet and triplet Hamiltonian matrices as described in following section, which may take over an hour. Allowing more time for computations or using more powerful machine may allow for larger basis and thus more accurate results. This is an open issue for future

work.

3.6 Symmetry considerations

This section covers two related problems. The first part describes optimized computation of Coulomb terms by considering their symmetry. The second one then explains extremely important creation of two Hamiltonian matrices that are related to the singlet and to the triplet states.

3.6.1 Coulomb terms

We have already pointed out that computation of Coulomb terms is hurtful. It is quite clear that the Coulomb terms does not have to be computed for each and every position in the Hailtonian matrix. Not only that majority of the terms are zero but also many terms are equal and thus should be computed only once. The procedure that computes independently all the distinct Coulomb terms has been developed. The procedure is based on inspection of Coulomb terms computation and considering their symmetry with respect to the wavevectors k_1 and k_2 and Landau levels n_1 and n_2 of the two particles involved. The list that contains all distinct Coulomb terms that appears in the Hamiltonian matrix for given settings is computed first. The Hamiltonian matrix of Coulomb terms is subsequently compiled. The addition of diagonal terms and Luttinger terms is then straightforward and fast.

3.6.2 Construction of singlet and triplet Hamiltonian

It has been explained in the theory that the orbital wavefunction must be either perfectly symmetric or perfectly antisymmetric with respect to the interchange of the electrons. The symmetric wavefunctions belong to the singlet, whereas the antisymmetric are triplet. The total antisymmetry that is required by Pauli principle is then attained by spin part. Note that spin part does not enter the Hamiltonian in any way (except of Zeeman terms that are somewhat associated with spin).

Once we construct and diagonalize developed Hamiltonian and inspect the eigenvectors, we find that each eigenvector is either perfectly symmetric or perfectly antisymmetric with respect to electrons interchange. Each eigenvector and its eigen-energy thus belong to either singlet or triplet. In other words, our basis contains both singlet and triplet states since no special symmetry issues have been considered until now.

We now reconstruct the basis so that we introduce new singlet and triplet basis states. As a result, we get the basis of the same size but the singlet and triplet states will be separated. This allows for separate diagonalization of singlet and triplet Hamiltonian and more importantly correct addition of Zeeman terms is then possible. The construction of new states is related to the Slater determinant and is rather straightforward. Each of the basis functions is defined by nine quantum numbers - n_h, k_h, n_1, k_1, n_2, k_2. Note that one

of the wave-vectors is not independent. The construction of symmetric and antisymmetric states for singlet and triplet is following:

$$|n_h, k_h, n_1, k_1, n_2, k_2\rangle_S = \frac{1}{\sqrt{2}} \left(|n_h, k_h, n_1, k_1, n_2, k_2\rangle + |n_h, k_h, n_2, k_2, n_1, k_1\rangle\right) \tag{3.66}$$

$$|n_h, k_h, n_1, k_1, n_2, k_2\rangle_T = \frac{1}{\sqrt{2}} \left(|n_h, k_h, n_1, k_1, n_2, k_2\rangle - |n_h, k_h, n_2, k_2, n_1, k_1\rangle\right) \tag{3.67}$$

Note in particular that state for that holds $n_h = k_h = n_1 = k_1 = n_2 = k_2 = 0$ is included in the singlet states only. The Hamiltonian matrix must be rearranged (two Hamiltonians are created) so that it corresponds to those new states. The eigen-energies are retained and eigenvectors (when reconstructed for the original basis states) are retained as well. This rearranging procedure is one of the most complicated procedures that have been newly developed.

3.7 Zeeman terms

Provided the two Hamiltoinians for singlet and triplet respecitvely, the addition of Zeeman terms is simple. These terms appear on the diagonal. We have two Zeeman effects, one for electrons and one for holes.

Considering the hole effect we recall that the Luttinger Hamiltonian is split into two parts defined by (1.51) and (1.52). The first one mixes heavy hole with total angular momentum projection $+\frac{3}{2}$ and light hole $-\frac{1}{2}$ and the second one mixes $+\frac{3}{2}$ with $-\frac{1}{2}$. For the sake of brevity we denote the first case as $+3/2$ and the second one $-3/2$. The appropriate added hole Zeeman term in the case of $+3/2$ Hamiltonian is $+\frac{3}{2}g_h\mu_b B$ for the heavy hole states and $-\frac{1}{2}g_h\mu_b B$. In the case of $-3/2$ Hamiltonian the signs of Zeeman terms are just switched. Assuming $g_h \neq 0$, these two Hamiltonians have clearly different eigen-energies and eigenstates.

Now let us consider the electron Zeeman effect. The splitting due to electron Zeeman effect is best described by the Schrödinnger equation (2.64). Singlet Hamiltonian is unaffected by electronic splitting due to its antisymmetric spin part of wavefunction. On the other hand, triplet splits into three levels according to the sum of the spins of the two electrons involved. These three states can be naturally labelled as -1, 0 and $+1$. The associated Zeeman terms are then $-g_e\mu_b B$, 0 and $+g_e\mu_b B$.

Since we have two different settings due to hole Zeeman splitting and four settings (singlet + 3 triplets) due to electron Zeeman splitting, we need to construct eight Hamiltonians with Zeeman terms that are summarized in following table:

Note that hole Zeeman terms must be added before diagonalization because of mixing between light and heavy holes. On the other hand, electron Zeeman terms only shift all eigen-energies and such shift might be added after diagonalization.

Symmetry	El. split	Hole split	Heavy h. Zeeman	Light h. Zeeman	El. Zeeman
Singlet	0	+3/2	$+\frac{3}{2}g_h\mu_b B$	$-\frac{1}{2}g_h\mu_b B$	0
Singlet	0	-3/2	$-\frac{3}{2}g_h\mu_b B$	$+\frac{1}{2}g_h\mu_b B$	0
Triplet	0	+3/2	$+\frac{3}{2}g_h\mu_b B$	$-\frac{1}{2}g_h\mu_b B$	0
Triplet	0	-3/2	$-\frac{3}{2}g_h\mu_b B$	$+\frac{1}{2}g_h\mu_b B$	0
Triplet	-1	+3/2	$+\frac{3}{2}g_h\mu_b B$	$-\frac{1}{2}g_h\mu_b B$	$-g_e\mu_b B$
Triplet	-1	-3/2	$-\frac{3}{2}g_h\mu_b B$	$+\frac{1}{2}g_h\mu_b B$	$-g_e\mu_b B$
Triplet	+1	+3/2	$+\frac{3}{2}g_h\mu_b B$	$-\frac{1}{2}g_h\mu_b B$	$+g_e\mu_b B$
Triplet	+1	-3/2	$-\frac{3}{2}g_h\mu_b B$	$+\frac{1}{2}g_h\mu_b B$	$+g_e\mu_b B$

Table 3.4: Overview of Zeeman terms added to the diagonal of eight different Hamiltonian matrices

3.8 Photoluminescence spectra

Evaluated photoluminescence spectra of negative trion under different settings are one of the important results of this thesis. The photoluminiscence associated with trion is the result of annihilation of one of the electrons and the hole. There remains one electron after such annihilation. The transition can thus be illustrated as $|\Psi_{trion}\rangle \rightarrow |e_{1(2)}\rangle$. The energy of such transition is thus the energy difference between the energy of the trion that results from the Hamiltonian diagonalization and the energy of remaining electron. The electron can be generally on any considered Landau level. The remaining electron is assumed not to change neither its Landau level nor its spin (we thus rule out recombination of Auger type).

The spectra are independently computed for σ^+ and σ^- polarizations (equal when zero Zeeman effect assumed). The selection rules are employed so that each σ^+ and σ^- spectrum contains only allowed transitions. Now we use Fermi golden rule to evaluate the probability of transition:

$$P_{i\rightarrow f} \sim |\langle|\Psi_{trion}|H_{int}|e_{1(2)}\rangle|^2 \delta\left(E_{trion} - E_e - E\right) \tag{3.68}$$

We omit the energy of the gap and the quantum well confinement for simplicity.

It can be found in [2] and it also follows from the construction of basis states summarized in table (1.1) that for the light propagating parallel to z-axis, the intensity of light polarized in the x, y direction is three times higher for the heavy hole - electron transitions than for the light hole - electron transitions and thus it is proposed to take:

$$I_{hh} = \langle u^{hh}_{trion}|H_{int}|u_e\rangle = \frac{1}{\sqrt{2}} \tag{3.69}$$

$$I_{lh} = \langle u^{lh}_{trion}|H_{int}|u_e\rangle = \frac{1}{\sqrt{6}} \tag{3.70}$$

The occupancy of the trion states is driven by Boltzmann distribution. The occupancy of given state is thus:

$$f_B(E_i, T) = \frac{exp\left(\frac{-E_i}{k_B T}\right)}{Z}, \tag{3.71}$$

where Z is the state sum given by $Z = \sum_i exp\left(\frac{-E_i}{k_B T}\right)$. Index i may generally run over all trion states, however it is sufficient to include only several lowest states (in our case 100 states). We choose for this thesis $T = 10$ K.

The intensity of the transition is thus simply given by:

$$I_i = \sum_j c_j^2 f_B(E_i, T) I_{hh(lh)}, \tag{3.72}$$

where j runs over the basis states for that at least one of the electrons is allowed to annihilate with the hole and c_j are the appropriate coefficients in the eigenvector associated with E_i. In the case that both electrons can annihilate, the probability of transition is doubled. Note that the excited heavy hole states do not contribute to the spectra in our approximation, since we do not assume any excited electrons and thus all wavefunctions of remaining electron are orthogonal to the excited heavy hole wavefunctions due to the z-dependent part.

We consider that individual transitions appear in the spectrum in the shape of Cauchy-Lorentz distribution with scale parameter Δ (half width at half maximum - HWHM), we set $\Delta = 0.03meV$. The complete spectrum can finally be evaluated as:

$$PL(E) = \sum_i I_i \frac{\Delta}{\pi} \frac{1}{(E - E_i)^2 + \Delta^2} \tag{3.73}$$

4 Results and Discussion

The results of this thesis are presented in the form of charts and figures. The results can be generally divided into three groups:

- The evolution of the ground state energy
- The images of the probability density
- Photoluminescence (PL) spectra

In the first section, we focus on energies and wavefunctions of the negative trion without Zeeman terms. We further proceed by inclusion of Zeeman terms with different g-factors. For chosen combination of g-factors we also investigate the Zeeman splitting. Finally we introduce 'Fixed hole' approximation.

4.1 Evolution of energies without Zeeman terms with magnetic field

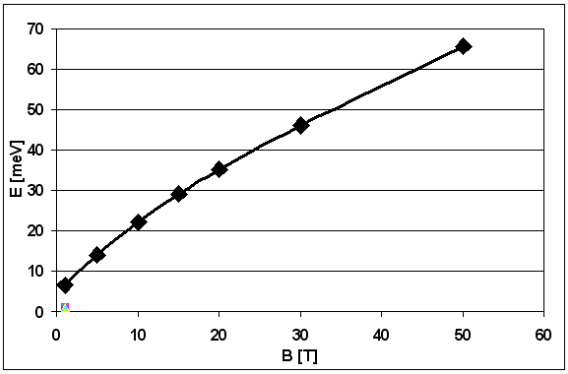

Figure 4.1: Trion dissociation energy - Singlet state

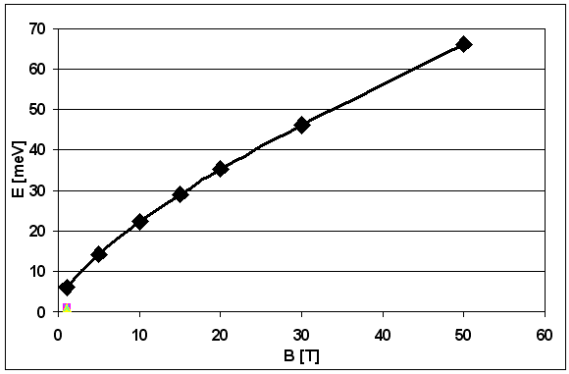

Figure 4.2: Trion dissociation energy - Triplet state

Charts (4.1) and (4.2) show the evolution of dissociation energy of trion in singlet and triplet state with respect to magnetic field. We would have to provide this energy to the trion to dissociate it into free particles on the lowest Landau levels. This energy should not be confused with binding energy that is related to the energy of eciton and thus cannot be evaluated here. Nevertheless, the concave behaviour is common also for binding energies [32].

With rising magnetic field, the particles are becoming squeezed together. As a result the Coulombic interaction becomes larger and thus the dissociation energy rises. We thus get qualitatively correct result. However, very disappointing is that singlet and triplet energies are almost equal and no systematic relation between singlet and triplet energy can be established, which is in contradiction to the literature. Several reasons for such behaviour might be mentioned.

The main reason for that triplet should have higher ground energy is that the lowest basis state (lowest Landau levels and zero wave vectors or other quantum numbers - depending on the basis choice) is never attainable for triplet, because of its unique symmetry. However, under our choice we do not punish triplet for not occupying the lowest state, because with changing the values of the wave vectors we can attain several wave functions with no direct energy lost. However, the Coulombic interaction itself should be weaker for triplet since the electrons are further apart. This effect seems to be negligible and is related to the second explanation.

Under our basis choice, we allow the movement of the hole. Even if one electron is remote from the hole-electron pair, this pair may polarize purely using the movement of the hole. This strengthens the charge-dipole interaction and the triplet attains low energetic state even if the electrons are relatively further apart.

The inconclusive relation between the energy state of singlet and triplet should be verified in detail. However, the cited theoretical papers may have underestimated the possibility of hole movement and the experimental works may only reveal the trion with hole fixed on some impurity as argued by Volkov [16].

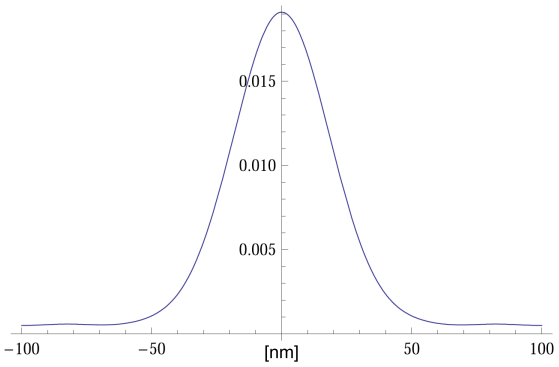

Figure 4.3: $B = 1$ T, Singlet, probability density P(x)

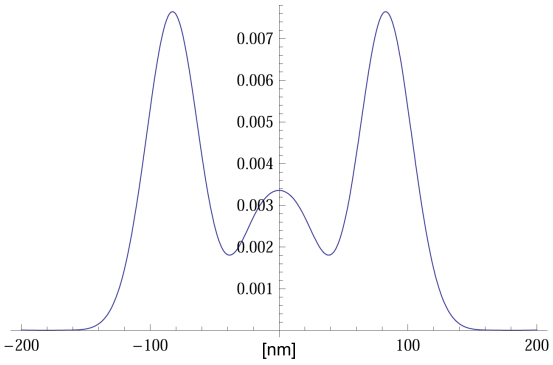

Figure 4.4: $B = 1$ T, Triplet, probability density P(x)

The series of figures (4.3) - (4.20) shows the spatial probabilities of electron(s) for both singlet and triplet states for different magnetic fields. These wavefunctions are associated with the lowest energy states. The line plots show always the probability of one electron occurrence with respect to the direction x. Such probability is calculated by:

$$P(x_1) = \int \Psi^2(x_h, x_1, x_2) dx_h dx_2. \tag{4.1}$$

We formally integrate also over y and z coordinates but this integration results only in the factor 1 since wavefunctions are normalized. From line plots we can establish that the highest probability of the electron occurrence is in the position of the hole for the singlet state. The exception occurs for $B = 15$ T, however the center peak is present though overlapped by surrounding peaks. No center peak might be found for triplet, however two

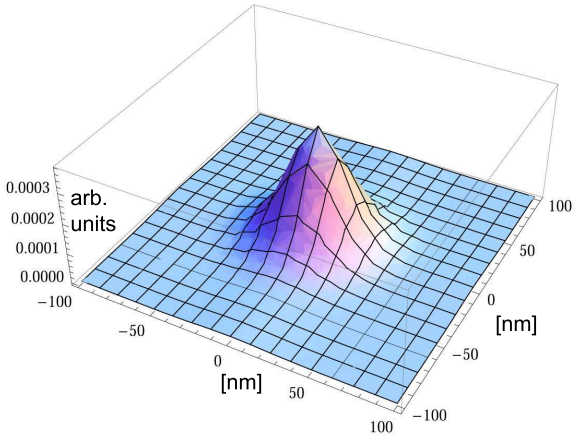

Figure 4.5: $B = 1$ T, Singlet, probability density P(x1,x2)

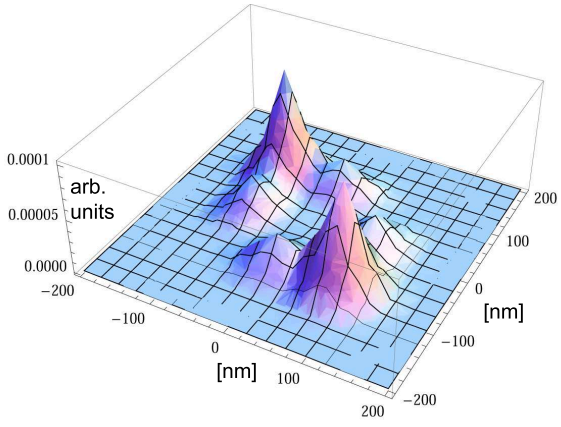

Figure 4.6: $B = 1$ T, Triplet, probability density P(x1,x2)

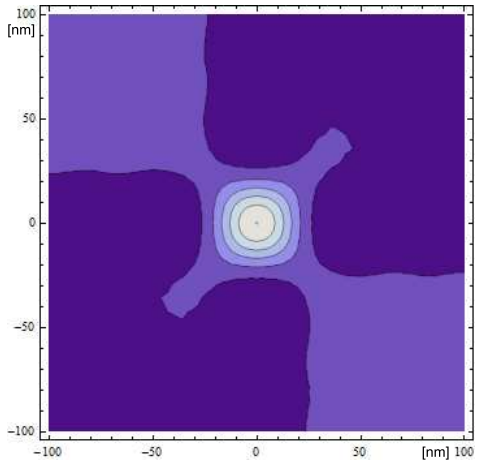

Figure 4.7: $B = 1$ T, Singlet, corr(x1,x2)

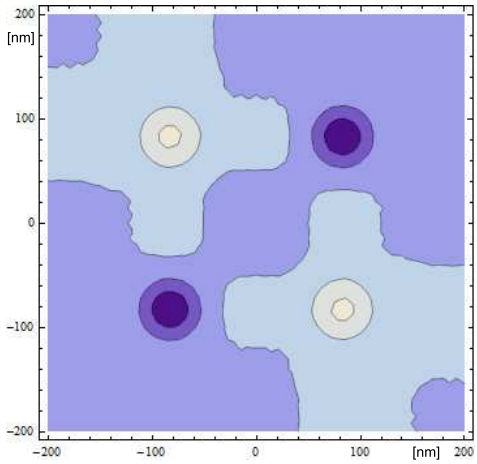

Figure 4.8: $B = 1$ T, Triplet, corr(x1,x2)

symmetric side peaks are present. For high magnetic field, those peaks are squeezed to the vicinity of the hole.

The 3D plots depict the spatial distribution of two electrons with respect to coordinates x_1 and x_2 associated with electron 1 and 2 respectively. If x_1 and x_2 have opposite signs, the electron 1 is situated then on the opposite side of the hole than the electron 2. This joint probability $P(x_1, x_2)$ is evaluated by:

$$P(x_1, x_2) = \int \Psi^2(x_h, x_1, x_2) dx_h. \tag{4.2}$$

Finally, the contour plot shows the correlation of the positions of the two electrons. The correlation is simply calculated as:

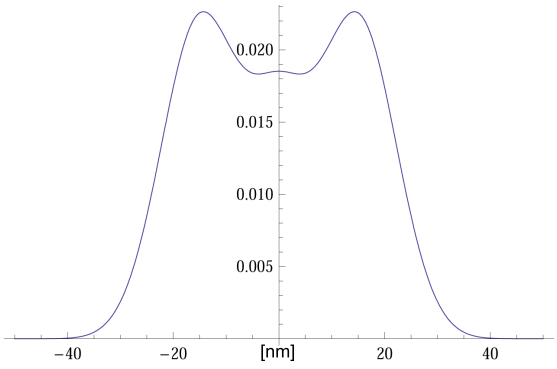

Figure 4.9: $B = 15$ T, Singlet, probability density P(x)

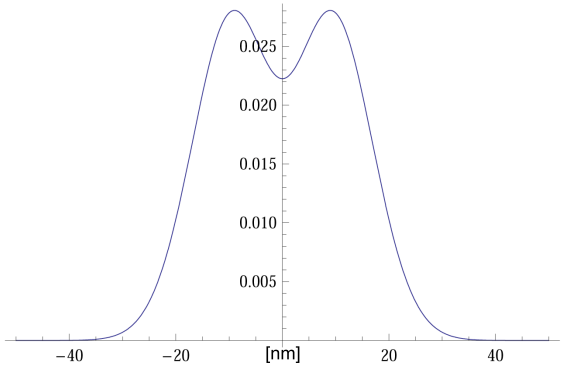

Figure 4.10: $B = 15$ T, Triplet, probability density P(x)

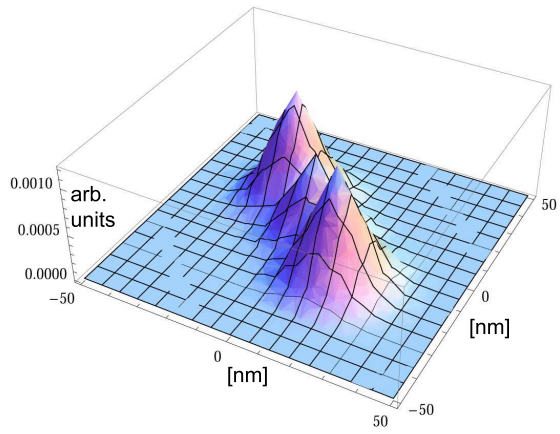

Figure 4.11: $B = 15$ T, Singlet, probability density P(x1,x2)

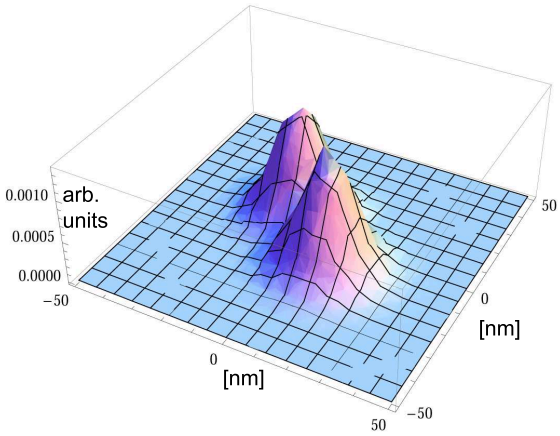

Figure 4.12: $B = 15$ T, Triplet, probability density P(x1,x2)

$$corr(x_1, x_2) = P(x_1, x_2) - P(x_1)P(x_2) \tag{4.3}$$

In the contour plots, the lighter areas express positive correlation, whereas dark areas negative correlation. The colouring of the plots is normalized independently for each plot, thus the comparison can be made only qualitatively. The correlation plots confirm that electrons occupy the opposite sides of the holes, which is not surprising considering that we deal with charge-dipole interaction. Such behaviour might be found also at the 3D plots. However, correlation plots reveal the difference between singlet and triplet. In the case of singlet, both electrons might be in the vicinity of the hole at once, but this is not possible for the trion. Big correlations are also situated for electrons being on the opposte sides of the hole, whereas visible anticorrelation areas disallow electrons to be on the same spot.

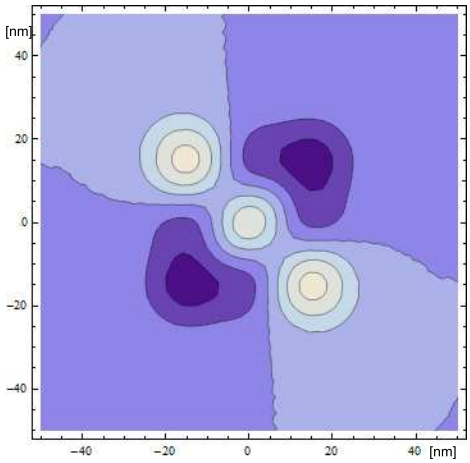

Figure 4.13: $B = 15$ T, Singlet, corr(x1,x2)

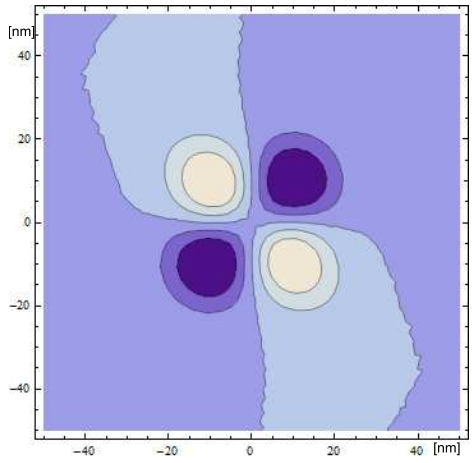

Figure 4.14: $B = 15$ T, Triplet, corr(x1,x2)

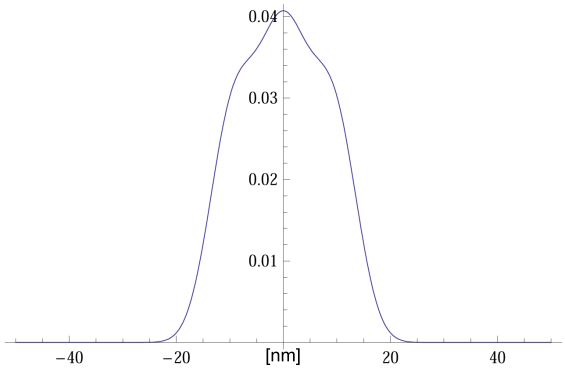

Figure 4.15: $B = 30$ T, Singlet, probability density P(x)

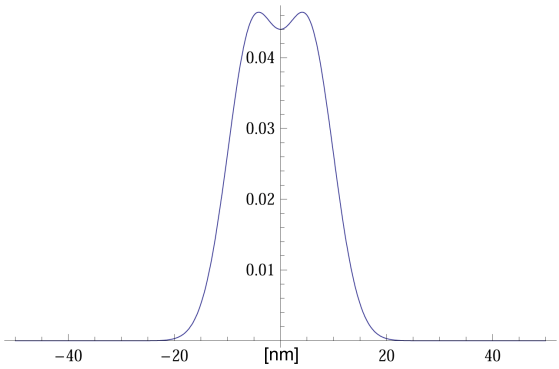

Figure 4.16: $B = 30$ T, Triplet, probability density P(x)

Figures (4.21) - (4.23) show the photoluminescence spectra of the trion without Zeeman terms. Such spectra are experimentally unattainable. Note that horizontal axis varies for different plots. The relative energetic distance of peaks in the spectra can be directly evaluated, but the energy gap and the confinement must be considered in order to get absolute energy of the transition. Without Zeeman terms, the σ^+ and σ^- spectra are equivalent.

4.2 Energies of trion with Zeeman terms

Since the literature is very inconsistent about the g-factor of hole (g_h) and of electron (g_e), we consider several combinations of g_e and g_h. 3D scatter plots (4.24) - (4.28) show the evolution of the ground energy of given triplet state with changing g_e and g_h. Charts (4.24) - (4.26) always compare two triplet states with equal contribution of electron Zeeman term

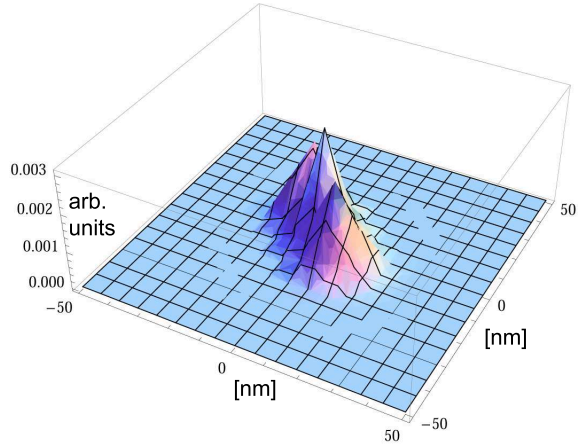

Figure 4.17: $B = 30$ T, Singlet, probability density P(x1,x2)

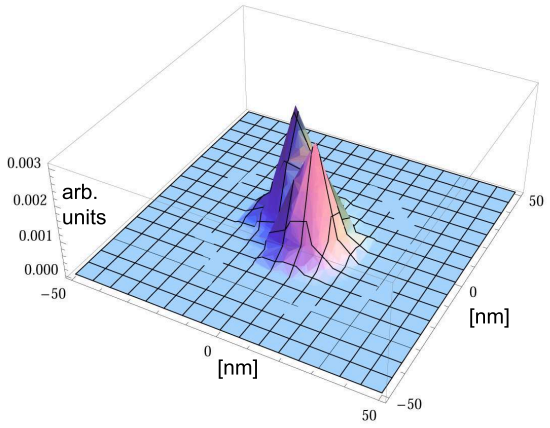

Figure 4.18: $B = 30$ T, Triplet, probability density P(x1,x2)

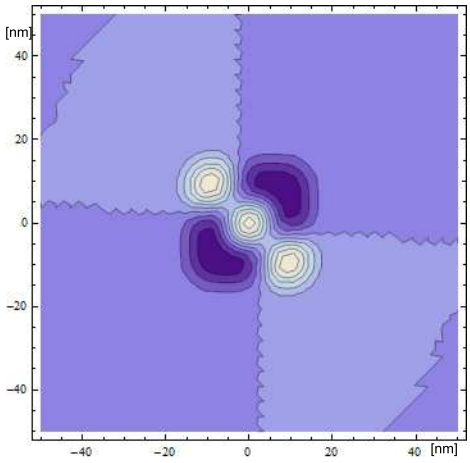

Figure 4.19: $B = 30$ T, Singlet, corr(x1,x2)

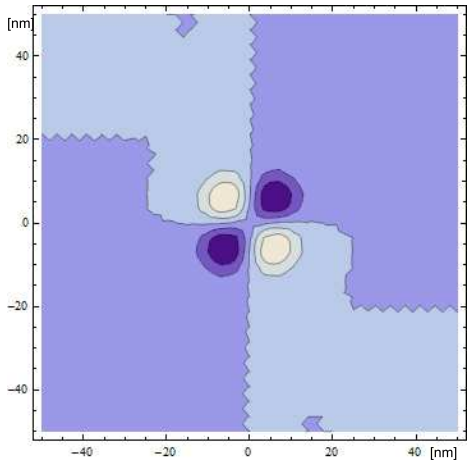

Figure 4.20: $B = 30$ T, Triplet, corr(x1,x2)

but different hole Zeeman effect. Note that for $g_h = 0$ the energies of two compared states coincide. The 'Triplet -3/2 0' and 'Triplet +3/2 0' are independent on g_e (chart 4.25). The charts (4.27) and (4.28) compare the triplets of triplet states with equal contribution of hole Zeeman effect. All three states always coincide for $g_e = 0$. Monotonous behaviour of all states with both g_e and g_h is of no surprise.

4.3 Computed spectra with Zeeman terms

The series of figures (4.29) - (4.34) shows the dependence of the trion PL spectra for both polarizations on the hole g_h-factor with $g_e = 0$. The series of figures (4.41) - (4.40) shows the same but with respect to g_e ($g_h = 0$). Finally, figures (**??**) - (4.46) show the PL spectra

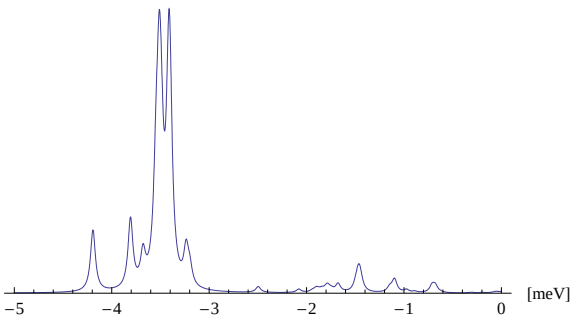

Figure 4.21: PL spectrum; $B = 1$ T; $g_e = 0$, $g_h = 0$

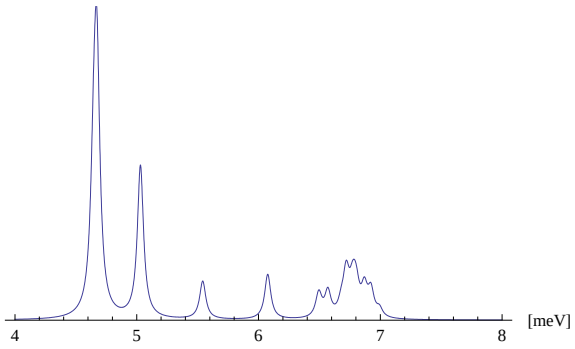

Figure 4.22: PL spectrum; $B = 15$ T; $g_e = 0$, $g_h = 0$

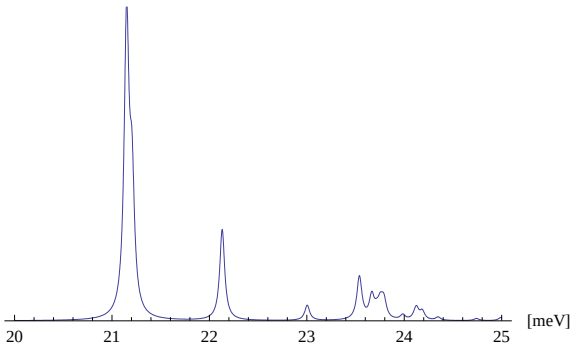

Figure 4.23: PL spectrum; $B = 30$ T; $g_e = 0$, $g_h = 0$

for some non-zero combinations of g_h and g_e. All visible states for given polarization are included in the spectra disregarding whether it is singlet or triplet state. We consider magnetic field $B = 15$ T in all figures.

Main observation is that the peaks for switched polarization do not shift but mainly change their magnitudes. The mixing of heavy and light holes due to Luttinger Hamiltonian approach is the reason for such behaviour. Each of the considered Hamiltonians mixes either heavy hole state $\left|+\frac{3}{2}\right\rangle$ with light hole state $\left|-\frac{1}{2}\right\rangle$ or heavy hole state $\left|-\frac{3}{2}\right\rangle$ with light hole state $\left|+\frac{1}{2}\right\rangle$. One energetic state of the trion thus consists of both heavy hole states and light hole states. It can be found out that the heavy hole states and the light hole states within these combinations are visible in the opposite polarizations according to the selection rules. However, once the states are mixed, one energetic state is then visible in both polarizations.

Usually in given trion state either heavy hole states or light hole states prevail, but peaks are visible in both polarization. This is supported by the thermal occupancy distribution function. Even relatively weak state according to the probability of the transition can be heavily populated if it has sufficiently low energy and thus it is visible in both σ^+ and σ^- polarizations.

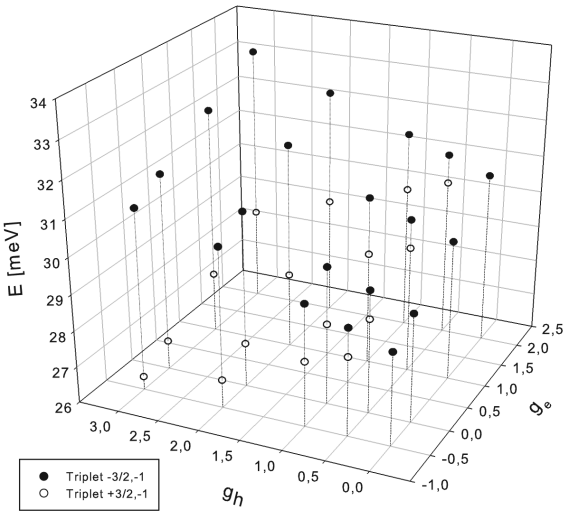

Figure 4.24: Dependence of ground energy on possible choice of g-factors; Triplets $\pm 3/2$; -1; $B = 15$ T

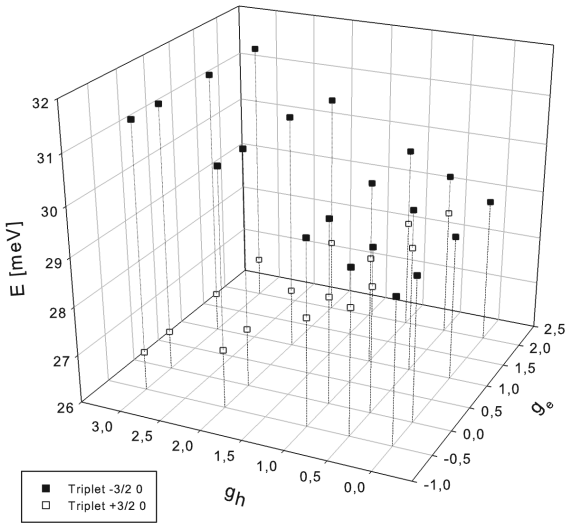

Figure 4.25: Dependence of ground energy on possible choice of g-factors; Triplets $\pm 3/2$; 0; $B = 15$ T

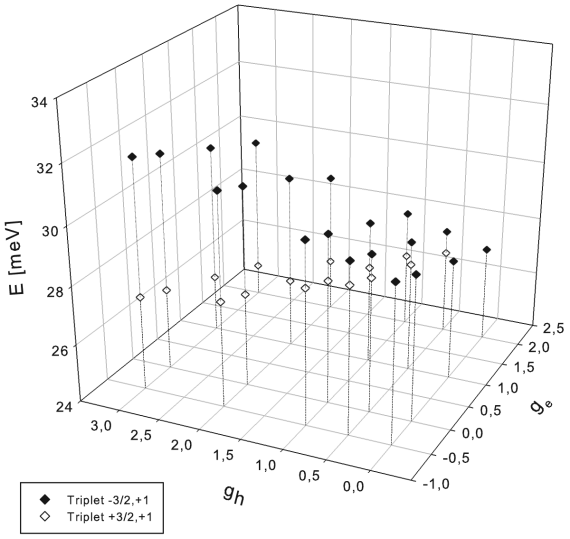

Figure 4.26: Dependence of ground energy on possible choice of g-factors; Triplets $\pm 3/2$; +1; $B = 15$ T

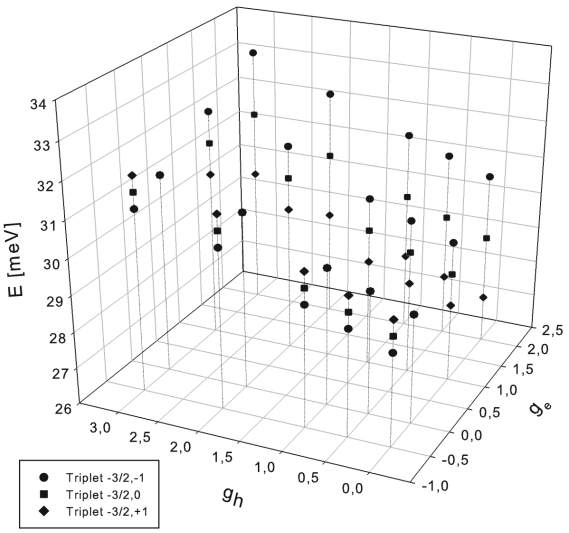

Figure 4.27: Dependence of ground energy on possible choice of g-factors; Triplets $-3/2$; -1,0,+1; $B = 15$ T

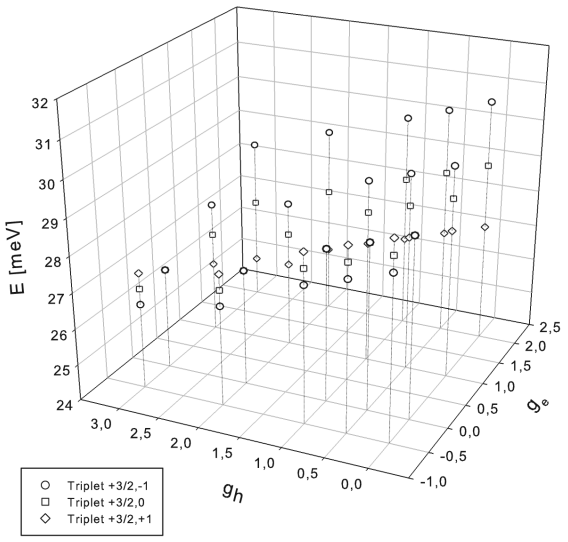

Figure 4.28: Dependence of ground energy on possible choice of g-factors; Triplets $+3/2$, -1,0,+1; $B = 15$ T

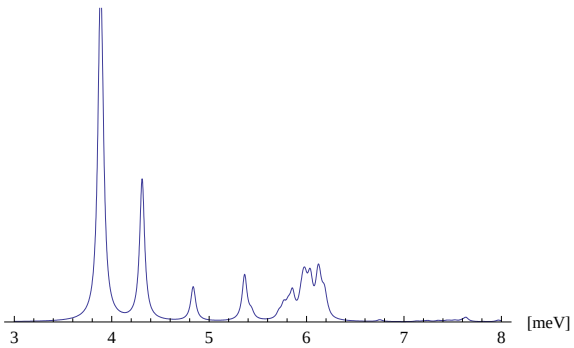

Figure 4.29: PL spectrum σ^+; $B = 15$ T; $g_e = 0$, $g_h = 1$

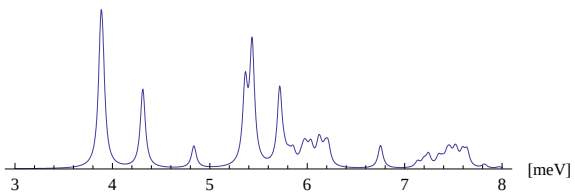

Figure 4.30: PL spectrum σ^-; $B = 15$ T; $g_e = 0$, $g_h = 1$

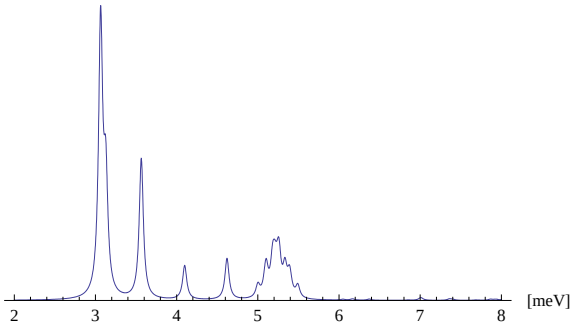

Figure 4.31: PL spectrum σ^+; $B = 15$ T; $g_e = 0$, $g_h = 2$

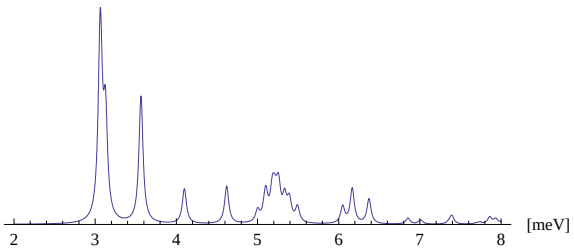

Figure 4.32: PL spectrum σ^-; $B = 15$ T; $g_e = 0$, $g_h = 2$

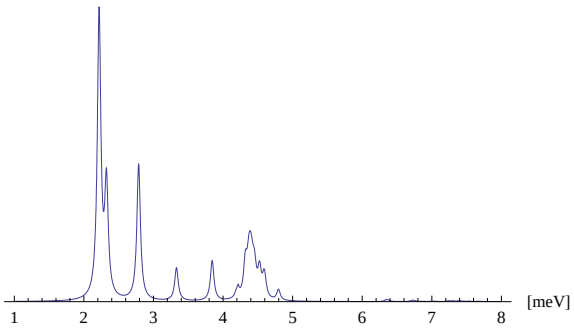

Figure 4.33: PL spectrum σ^+; $B = 15$ T; $g_e = 0$, $g_h = 3$

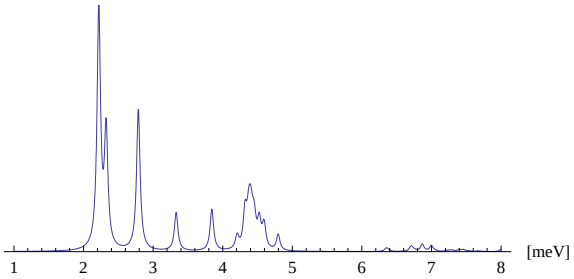

Figure 4.34: PL spectrum σ^-; $B = 15$ T; $g_e = 0$, $g_h = 3$

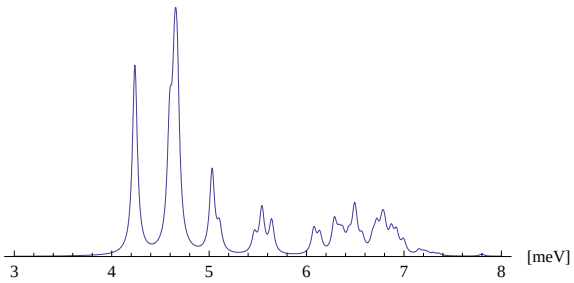

Figure 4.35: PL spectrum σ^+; $B = 15$ T; $g_e = -0.5$, $g_h = 0$

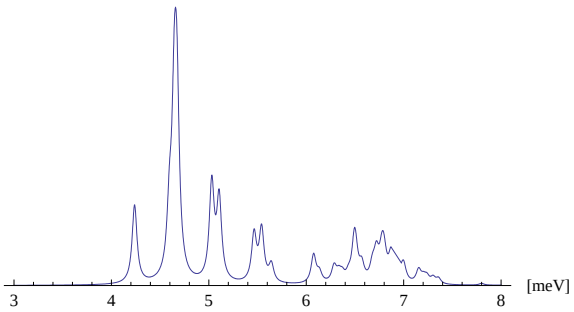

Figure 4.36: PL spectrum σ^-; $B = 15$ T; $g_e = -0.5$, $g_h = 0$

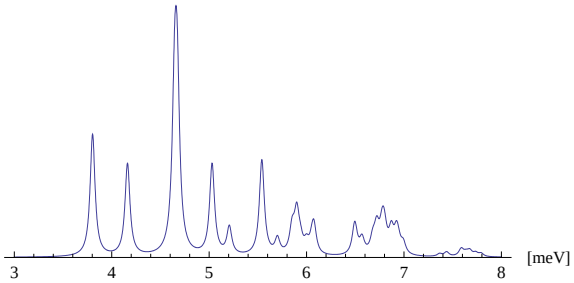

Figure 4.37: PL spectrum σ^+; $B = 15$ T; $g_e = 1$, $g_h = 0$

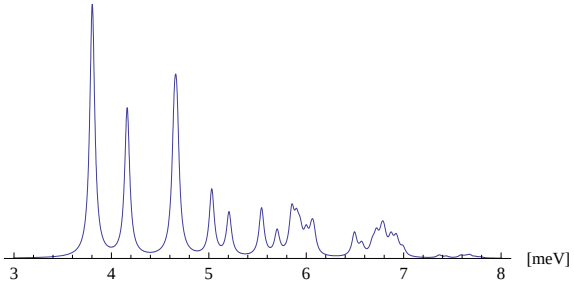

Figure 4.38: PL spectrum σ^-; $B = 15$ T; $g_e = 1$, $g_h = 0$

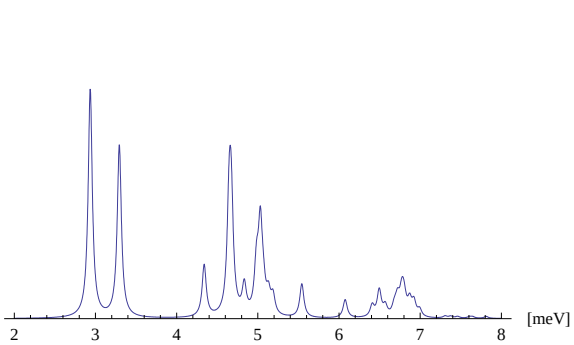

Figure 4.39: PL spectrum σ^+; $B = 15$ T; $g_e = 2$, $g_h = 0$

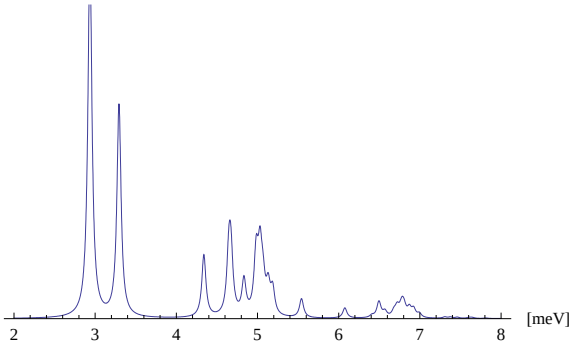

Figure 4.40: PL spectrum σ^-; $B = 15$ T; $g_e = 2$, $g_h = 0$

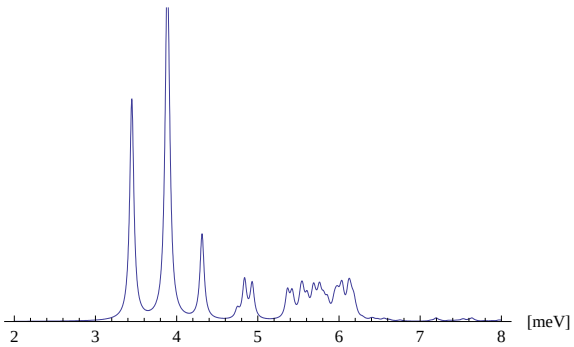

Figure 4.41: PL spectrum σ^+; $B = 15$ T; $g_e = -0.5$, $g_h = 1$

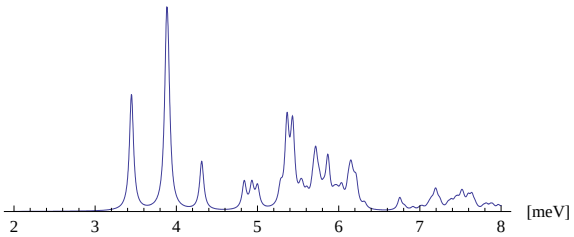

Figure 4.42: PL spectrum σ^-; $B = 15$ T; $g_e = -0.5$, $g_h = 1$

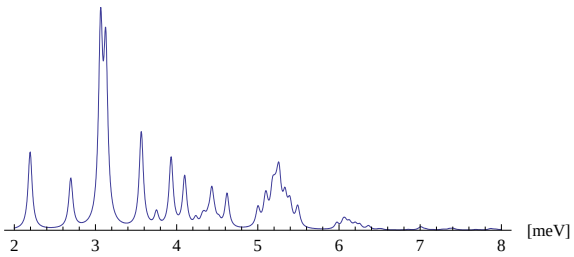

Figure 4.43: PL spectrum σ^+; $B = 15$ T; $g_e = 1$, $g_h = 2$

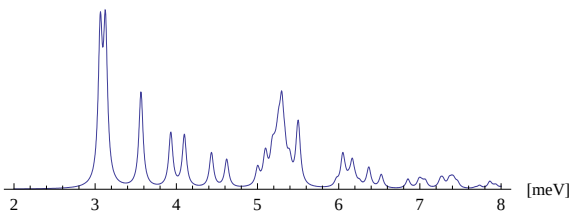

Figure 4.44: PL spectrum σ^-; $B = 15$ T; $g_e = 1$, $g_h = 2$

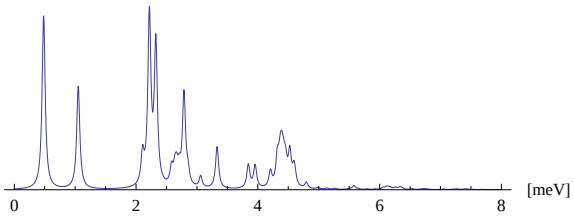

Figure 4.45: PL spectrum σ^+; $B = 15$ T; $g_e = 2$, $g_h = 3$

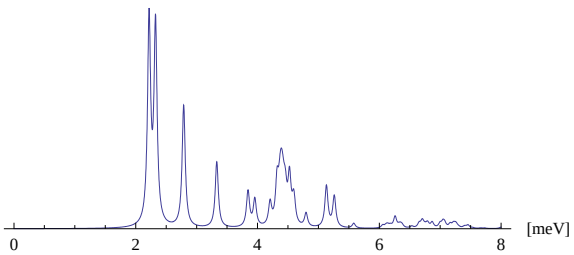

Figure 4.46: PL spectrum σ^-; $B = 15$ T; $g_e = 2$, $g_h = 3$

4.4 Zeeman splitting

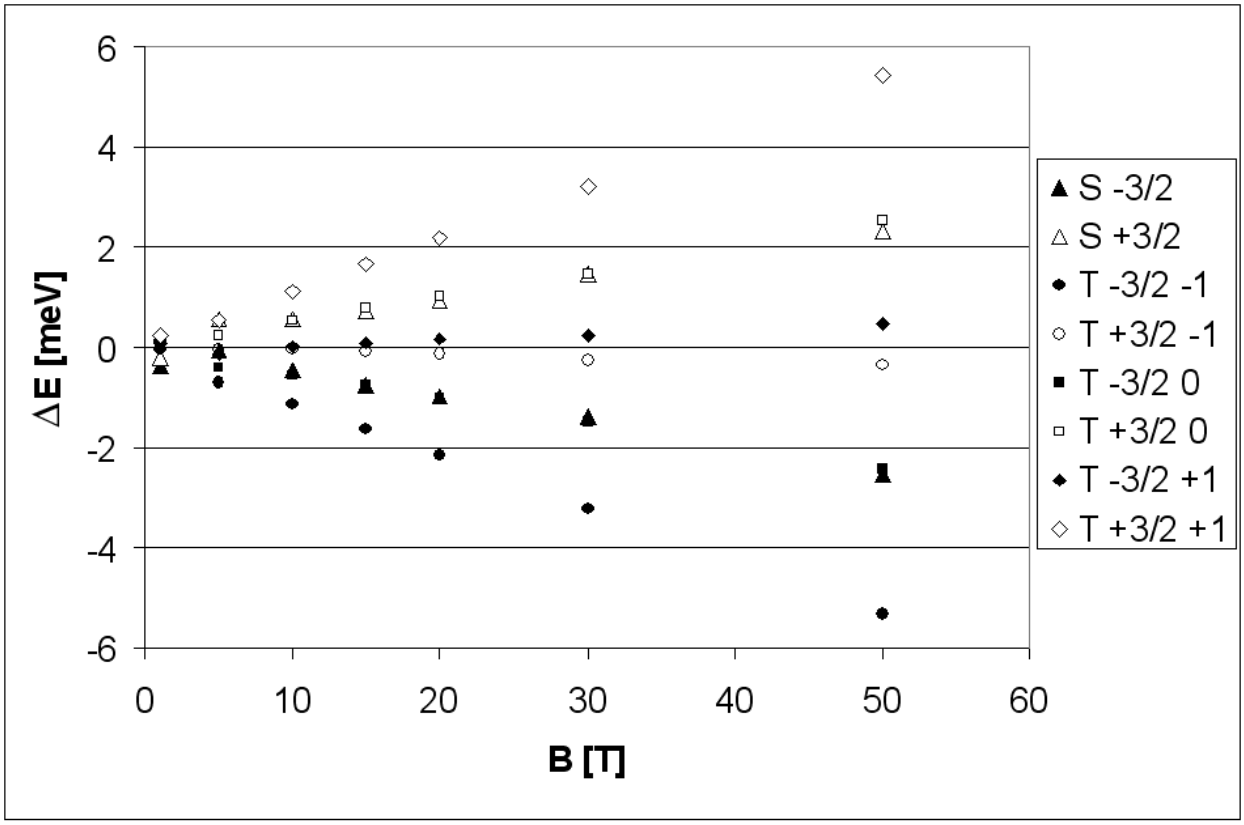

Figure 4.47: Zeeman splitting of ground energies with respect to magnetic field B; $g_e = 1$, $g_h = 1$

Chart (4.47) presents computed Zeeman splitting with respect to the magnetic field. We assume following values of the g-factor: $g_e = 1$ and $g_h = 1$, which implies for the effective Landé g-factor of negative trion $g_{eff} = 2$ as reported by Vanhoucke. This can be well compared to the experimental result by Vanhoucke (lower inset of Figure (2.13), however direct comparison suggests that Vanhoucke measured the photoluminescence of so-called dark trion. This finding is surprising, but it is considered possible in the case of breaking of symmetry or fixing holes, both caused by impurities [16].

Figures (4.48) - (4.53) show the evolution of PL spectra with magnetic field with Zeeman terms included. The change of the polarization is accompanied more by the change of the magnitude of the peaks rather than their shift. However, it must be stressed that the change of the mutual magnitudes of two surrounding peaks with such high theoretical resolution may appear as a shift of one wide peak just because of lower resolution of experiment .

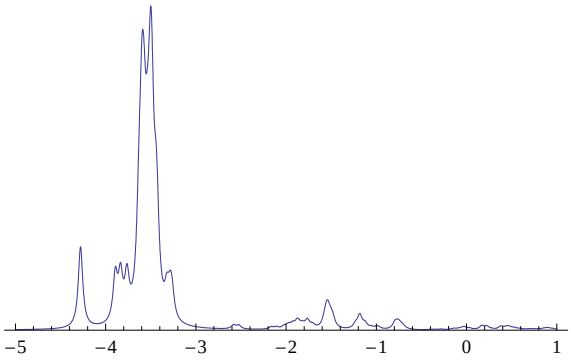

Figure 4.48: PL spectrum σ^+; $B = 1$ T; $g_e = 1$, $g_h = 1$

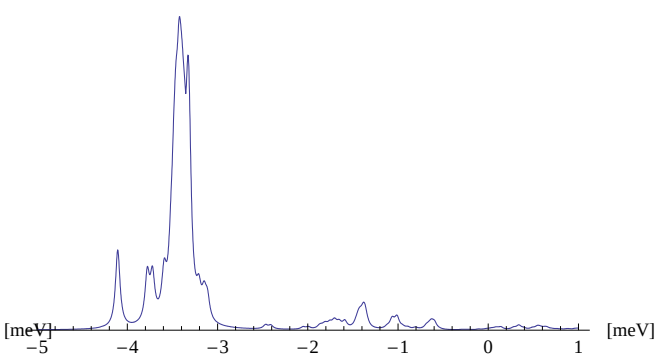

Figure 4.49: PL spectrum σ^-; $B = 1$ T; $g_e = 1$, $g_h = 1$

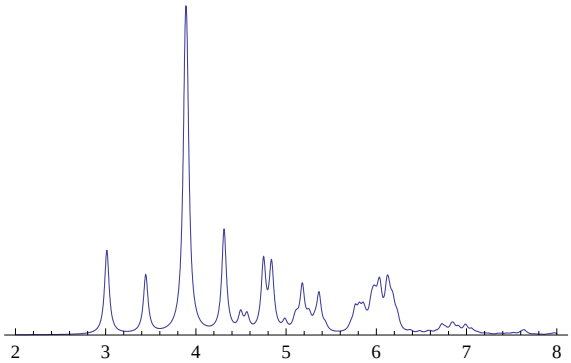

Figure 4.50: PL spectrum σ^+; $B = 15$ T; $g_e = 1$, $g_h = 1$

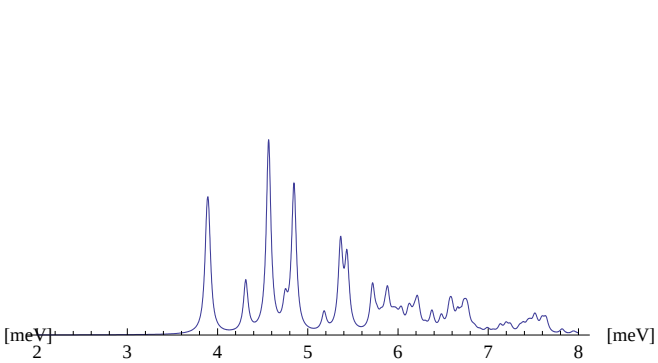

Figure 4.51: PL spectrum σ^-; $B = 15$ T; $g_e = 1$, $g_h = 1$

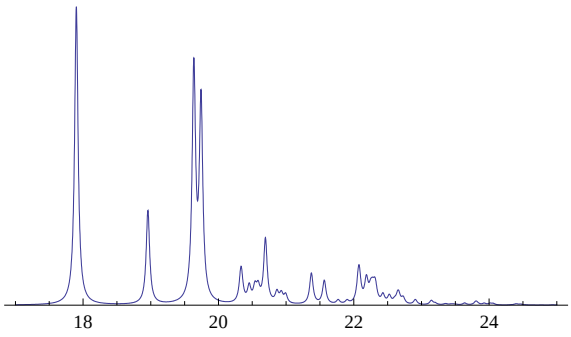

Figure 4.52: PL spectrum σ^+; $B = 30$ T; $g_e = 1$, $g_h = 1$

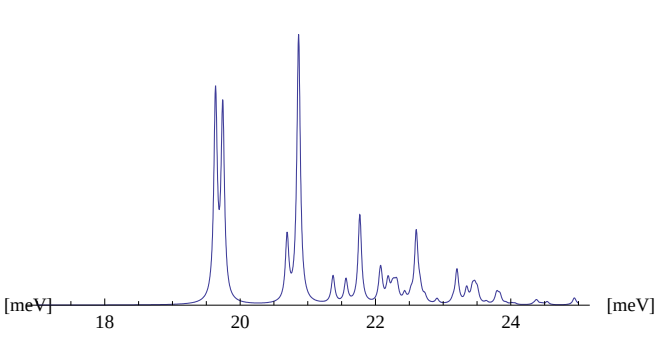

Figure 4.53: PL spectrum σ^-; $B = 30$ T; $g_e = 1$, $g_h = 1$

4.5 Energies of singlet and triplet with fixed hole

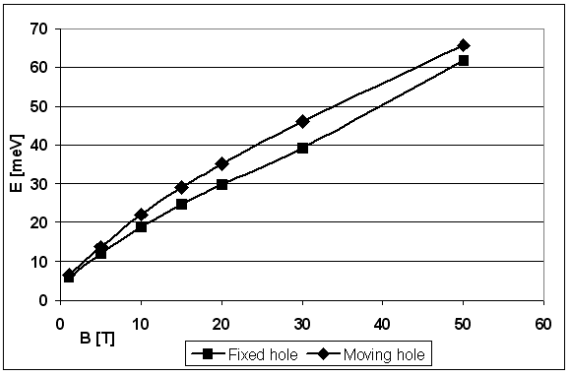

Figure 4.54: Dependence of the ground energies on magnetic field using the bases with fixed and moving hole

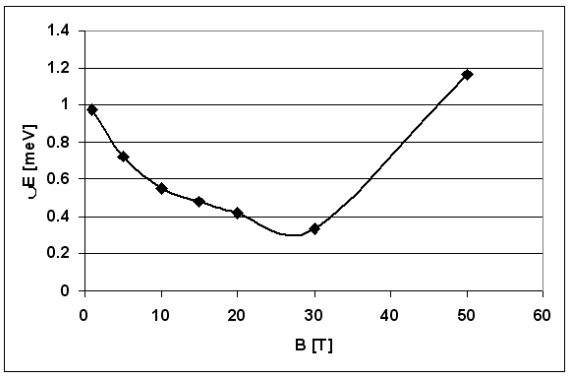

Figure 4.55: Difference in energies of the ground singlet state and the ground triplet state as a function of magnetic field using the basis with fixed hole

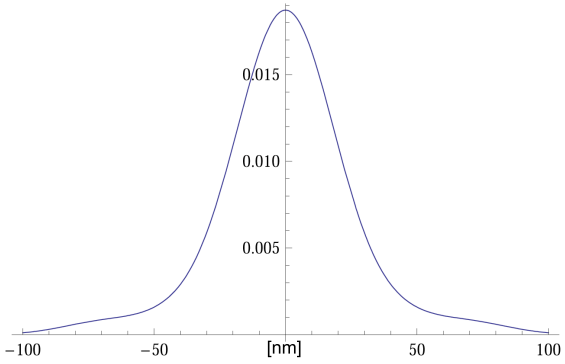

Figure 4.56: $B = 1$ T, Singlet, probability density P(x), Fixed hole

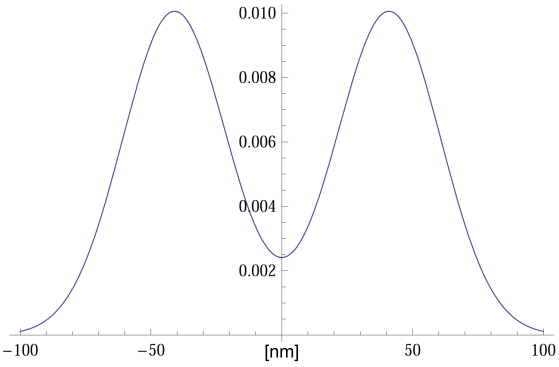

Figure 4.57: $B = 1$ T, Triplet, probability density P(x), Fixed hole

In the beginning of this Results and Discussion chapter, we discussed unsatisfactory results considering offset between singlet and triplet ground energy. Among other possible reasons, it might be attributed to the almost free movement of the hole. We thus undertook following changes. We restrict the wavefunction basis to the states for that $k_h = 0$. The hole is thus fixed in the middle of the assumed 'box'.

We then calculated the ground energies of the lowest triplet and the lowest singlet state for this new settings. Figure (4.54) shows the evolution of dissociation energy with magnetic field for both original ('moving hole') and new ('fixed hole') settings. For the 'fixed hole' the lowest state is always singlet.

Contrary to the full basis settings, we can now observe systematic behaviour of the

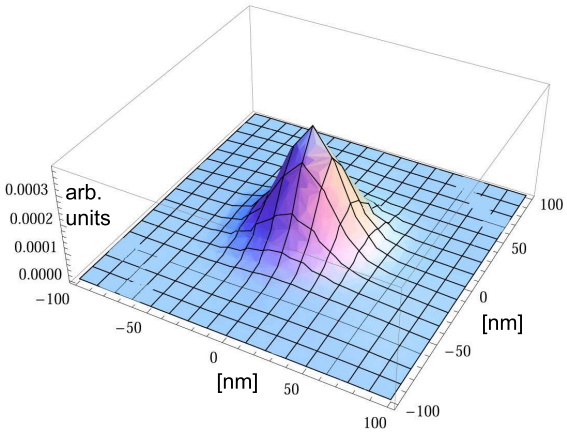

Figure 4.58: $B = 1$ T, Singlet, probability density P(x1,x2), Fixed hole

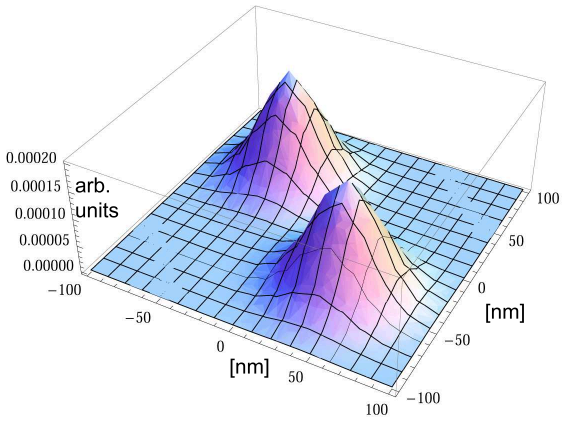

Figure 4.59: $B = 1$ T, Triplet, probability density P(x1,x2), Fixed hole

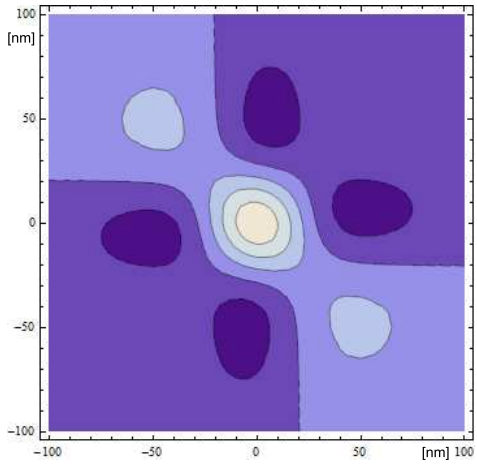

Figure 4.60: $B = 1$ T, Singlet, corr(x1,x2), Fixed hole

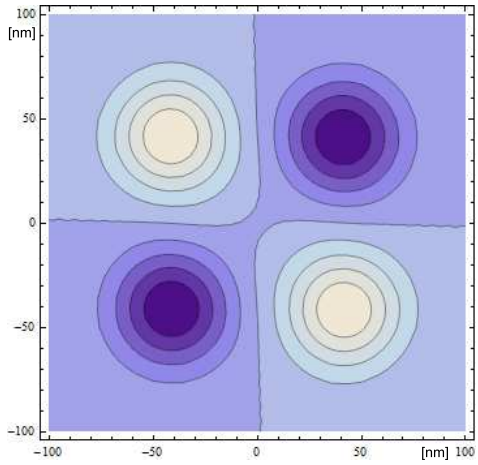

Figure 4.61: $B = 1$ T, Triplet, corr(x1,x2), Fixed hole

energy gap between singlet and triplet ground states as depicted in Fig. (4.55). This systematic behaviour under 'fixed hole' settings supports the reasoning that the energy difference between singlet and triplet is negligible for moving hole basis. The energy gap between singlet and triplet decreases with rising magnetic field up to $B = 30$ T. This can be attributed to the squeezing of the triplet state (actually for both states but having prominent effect on expanded triplet), which results in diminishing difference between singlet and triplet. The last value for $B = 50$T might be only artefact since the reduced basis is very inappropriate for such high fields.

Series of figures (4.60) - (4.73) shows the spatial probability of electron occurrence and the correlations. The squeezing of wavefunctions with rising magnetic field is clearly visible.

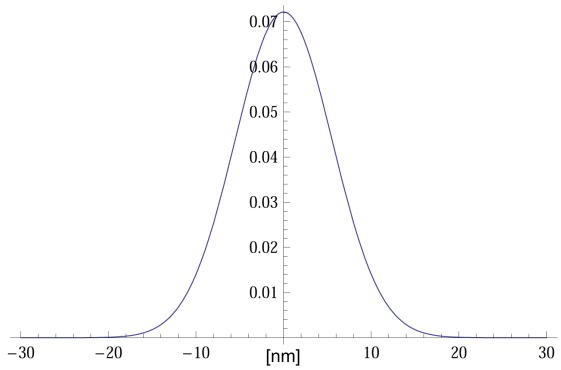

Figure 4.62: $B = 15$ T, Singlet, probability density P(x), Fixed hole

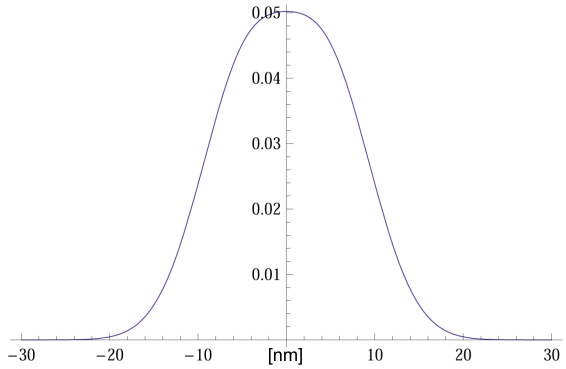

Figure 4.63: $B = 15$ T, Triplet, probability density P(x), Fixed hole

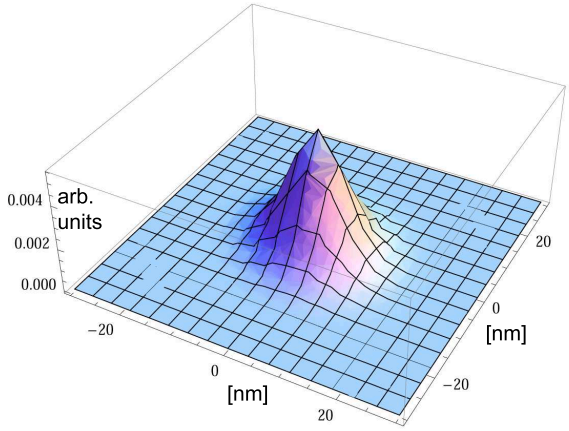

Figure 4.64: $B = 15$ T, Singlet, probability density P(x1,x2), Fixed hole

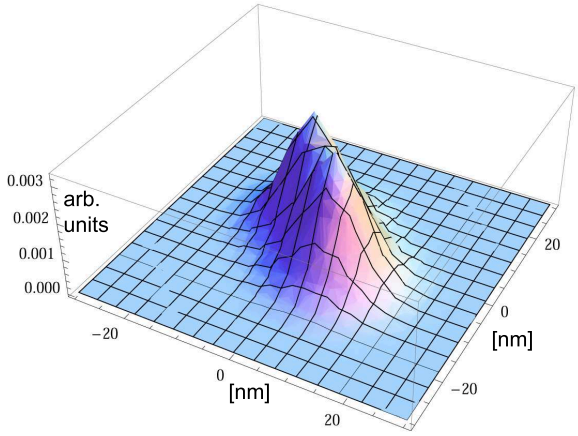

Figure 4.65: $B = 15$ T, Triplet, probability density P(x1,x2), Fixed hole

Such squeezing is more pronounced for the triplet and as a result the wavefunctions of singlet and triplet do not differ much for high magnetic fields. This effect can be best observed on the correlation plots. Completely different correlations are observed in the case of $B = 1$ T where singlet shows typical centered correlation. Correlation plots for triplet and singlet states become almost indistinguishable for $B = 30$ T.

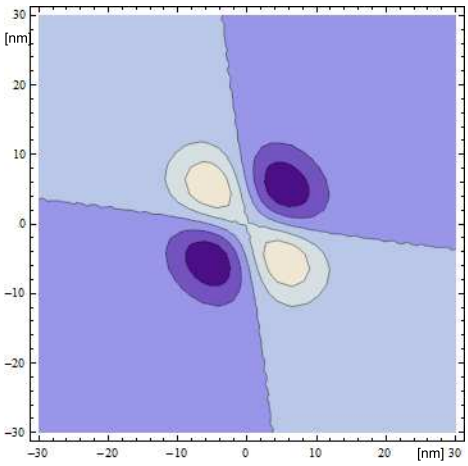

Figure 4.66: $B = 15$ T, Singlet, corr(x1,x2), Fixed hole

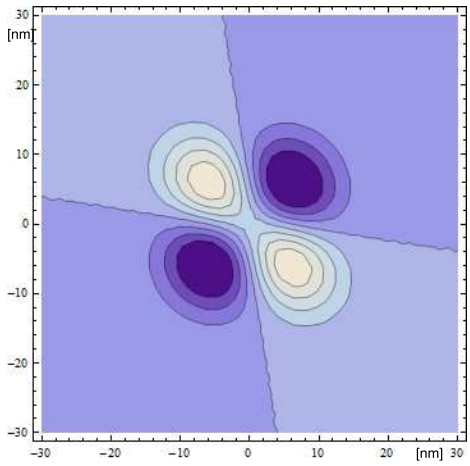

Figure 4.67: $B = 15$ T, Triplet, corr(x1,x2), Fixed hole

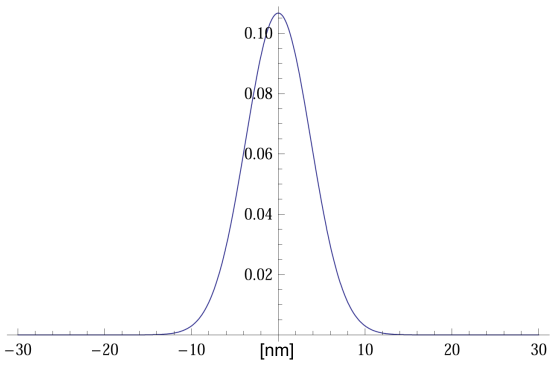

Figure 4.68: $B = 30$ T, Singlet, probability density P(x), Fixed hole

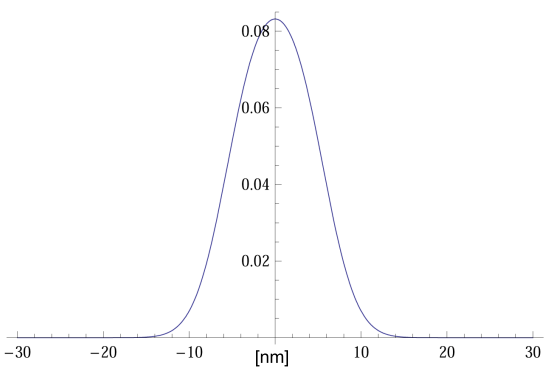

Figure 4.69: $B = 30$ T, Triplet, probability density P(x), Fixed hole

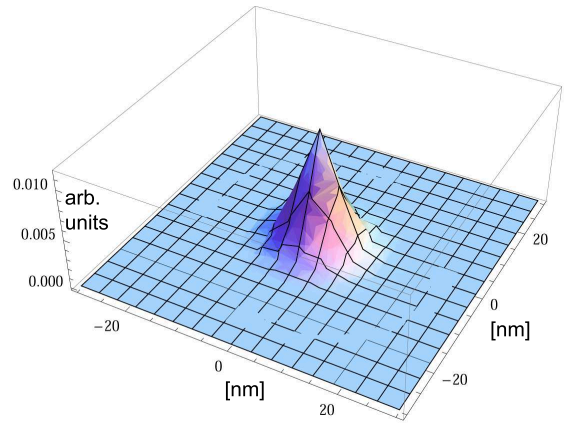

Figure 4.70: $B = 30$ T, Singlet, probability density P(x1,x2), Fixed hole

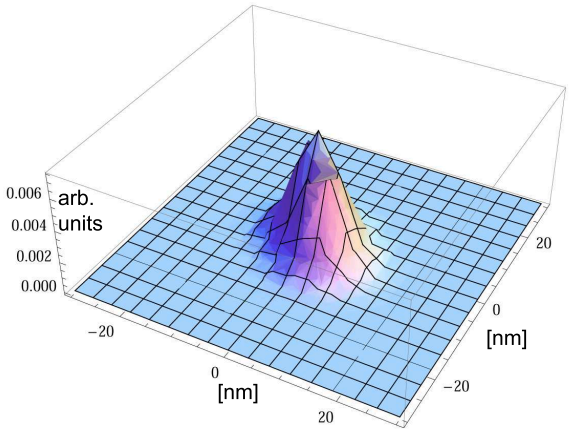

Figure 4.71: $B = 30$ T, Triplet, probability density P(x1,x2), Fixed hole

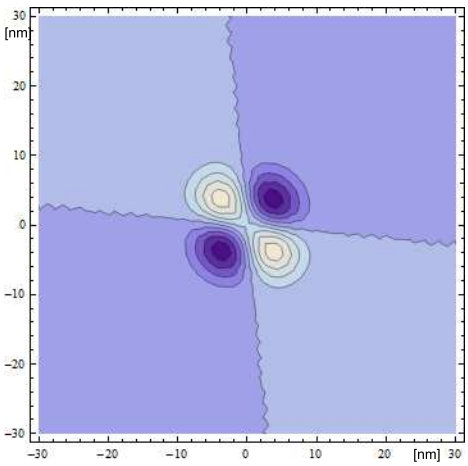

Figure 4.72: $B = 30$ T, Singlet, corr(x1,x2), Fixed hole

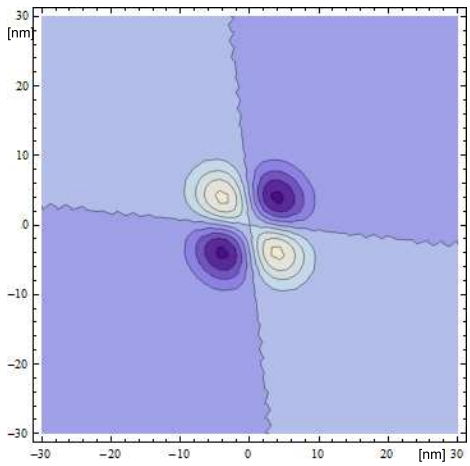

Figure 4.73: $B = 30$ T, Triplet, corr(x1,x2), Fixed hole

5 Conclusion

This theoretical thesis provides theoretical and computational analysis of negative trion quantum system confined in a single quantum well in a presence of perpendicular magnetic field. Main attention is paid to the Zeeman effect of such multi-particle system.

Properties of GaAs-GaAlAs compounds are discussed focusing on the complex valence band structure. Effective mass approximation and Kane model are introduced as a benchmark for the Luttinger Hamiltonian method that is used throughout this thesis. Envelope function approximation for heterostructures is briefly introduced. Luttinger Hamiltonian framework is exploited in a detail and the origin of Zeeman terms is discussed.

Well-known problem of the exciton is solved using the centre-of-mass transform and the description of exciton using Luttinger Hamiltonian and with inclusion of the Zeeman effect is developed. The three-particle problem of charged exciton - trion - is compared to the simple excitonic problem. Mainly, the extreme complications of centre-of-mass transform for trion are discussed. Further development focuses on negative trion that is multi-fermionic system and thus must obey Pauli principle. Singlet and triplet states are introduced along with concepts of binding, dissociation and transition energies. Zeeman terms for singlet and triplet states and for both heavy holes and light holes are discussed in a very detail. The analysis of the Zeeman effect of mixed light and heavy hole states due to Luttinger Hamiltonian in negative trion system goes beyond the considerations in current literature. Comprehensive literature review of related experimental and theoretical works is provided.

Crucial part for subsequent computations is the choice of the wavefunction basis. Unusual basis choice that does not a priori respect the radial symmetry of the problem is based on rarely chosen Landau gauge of magnetic field. The main advantage is inclusion of relatively simple Hermite polynomials. One of the most demanding tasks is the analytical and subsequent numerical evaluation of terms describing Coulomb interaction. The evaluation is based on so-called Ewald summation and several tricky analytical integrations. Time-demanding numerical computations must be finally performed. Numerical analysis of the basis size sufficiency is performed. Special procedure for decomposing singlet and triplet states from complete Hamiltonian has been developed. Such separation allows then for exact treatment of Zeeman effect.

Rising and concave dependence of the dissociation energy of trion on the magnetic field is in accordance with the literature. It is attributed to the squeezing of the trion particles due to the magnetic field, which is accompanied by increasing effect of binding Coulomb interaction. Contrary to the literature, no systematic relation between singlet and triplet ground energies can be established. This contradiction is attributed to the almost free movement of the hole that is allowed by the chosen wavefunction basis. This reasoning is supported by so-called 'fixed hole' approximation. Basis is reduced to the states, such that the hole remains in one place. In this case the ground state of the trion is always singlet state. The difference in energies between singlet and triplet decreases for rising magnetic field from 1 meV to 0.4 meV for $B = 1$ T and $B = 30$ T respectively. Spatial probabilities of occurrence of one or both electrons with respect to the hole positions have

been depicted in 2D and 3D representations. The electrons of the trion in the singlet state are squeezed closer to the hole, whereas trion is more expanded and two side peaks are dominant. Correlation functions images prove qualitative difference between singlet and triplet states. Both electrons in a singlet state may occupy the same lowest state. As a result both electrons at once are with big probability in the position of the hole. The ground state is forbidden for trion states and therefore both electrons never occupy the hole position. Not surprisingly, electrons are usually placed on the mutually opposite side of the hole. The correlation evolves with the rising magnetic field. The trion is being squeezed by the magnetic field and the correlation effects are amplified.

Due to inconclusive results from literature about values of Landé g-factors, several values of electron and hole g-factors have been considered. The evolution of the ground energies with hole and electron g-factors is depicted and demonstrates the intuition behind combining hole and electron Zeeman effects.

Finally, photoluminescence (PL) spectra have been evaluated and depicted for trions without Zeeman effect, with Zeeman effect and different g-factors and for different magnetic fields. The main finding concerning change of magnitude of peaks instead of their shift due to Zeeman effect has never been explicitly discussed in the literature. The considered Luttinger Hamiltonian mixes heavy hole and light hole trion states and thus one trion state includes both light and heavy hole. However, heavy hole and light hole included in one trion state are visible in different light polarizations. As the result the peak on the same energy can be found in the PL spectra for both polarizations. The Zeeman effect thus in this case does not cause the shift of the peaks but significantly changes their magnitude. However, mutual change of the magnitude of two surrounding peaks might appear as a shift of one wide peak in a case of experiment with lower resolution.

High amount of the parameters that enter the computations disable direct comparison to the experimental results, since not all the necessary parameters are provided in the literature. Realization of relevant experiments and direct interrelation to the computations in this thesis would be highly appreciated.

6 Appendix A - Coulombic terms

This Appendix includes evaluation of important analytical integrals of Coulomb terms. The tricky integration over y variables is shown in the main text. Here we focus on possible simplification of integrals over x and z variables.

Integration over x

We deal with following integral:

$$\int_{-\frac{L_z}{2}}^{\frac{L_z}{2}} dz_1 \int_{-\frac{L_z}{2}}^{\frac{L_z}{2}} dz_2 \int_{-\infty}^{\infty} dx_1 \int_{-\infty}^{\infty} dx_h V(|x_2 - x_1|, y, |z_2 - z_1|) \\ \psi_{n_1',k_1'}(x_1)\psi_{n_1,k_1}(x_1)\psi_{n_2',k_2'}(x_2)\psi_{n_2,k_2}(x_2)\varphi_1^2(z_1)\varphi_2^2(z_2) \tag{6.1}$$

We now introduce some useful substitution:

$$x = x_1 - x_2 \tag{6.2}$$
$$x_2 = x_1 - x \tag{6.3}$$
$$\tag{6.4}$$

$$\int_{-\frac{L_z}{2}}^{\frac{L_z}{2}} dz_1 \int_{-\frac{L_z}{2}}^{\frac{L_z}{2}} dz_2 \int_{-\infty}^{\infty} dx V(x, y, |z_2 - z_1|)\varphi_1^2(z_1)\varphi_2^2(z_2) \tag{6.5}$$
$$\int_{-\infty}^{\infty} dx_1 \psi_{n_1',k_1'}(x_1)\psi_{n_1,k_1}(x_1)\psi_{n_2',k_2'}(x_1 - x)\psi_{n_2,k_2}(x_1 - x) \tag{6.6}$$

Integration over x_1 is analytical. In the case that all four interacting states are in the lowest level, the integration is based on the integration of the Gaussian and it is relatively simple:

$$f(x) = \int_{-\infty}^{\infty} dx_1 \psi_{0,k_1'}(x_1)\psi_{0,k_1}(x_1)\psi_{0,k_2'}(x_1 - x)\psi_{0,k_2}(x_1 - x) \tag{6.7}$$
$$= \frac{1}{\lambda\sqrt{2\pi}} e^{\frac{\lambda^2}{8}\left((k_1+k_1'+k_2+k_2'+\frac{2x}{\lambda^2})^2 - 4(k_1^2+k_1'^2+k_2^2+k_2'^2+\frac{2k_2x}{\lambda^2}+\frac{2k_2'x}{\lambda^2}+\frac{2x^2}{\lambda^4})\right)} \tag{6.8}$$

In the particular case when $k_1 = k_1'$, $k_2 = k_2'$:

$$f(x) = \int_{-\infty}^{\infty} dx_1 \psi_{0,k_1}^2(x_1)\psi_{0,k_h}^2(x_1 - x) = \frac{1}{\lambda\sqrt{2\pi}} e^{-\frac{(x-\lambda^2 k_1+\lambda^2 k_2)^2}{2\lambda^2}} \tag{6.9}$$

For higher Landau levels the integration involves integrating Gaussians multiplied by Hermite polynomials. Such analytical integrations must be performed for all combinations

of Landau levels of interacting states. It is straightforward to proceed, however several time-demanding manipulations with the polynomials and lengthy step-by-step integrations must be undertaken. Integrals involving higher Landau levels for more particles are considerably lengthy and cannot be written here explicitly, but those have been pre-computed and stored in order to save computing time of subsequent repetitive calculations.

Integration over z

Now, we would like to integrate over one of the variables in the z-direction. Recall the assumption that the heavy hole can be also in the first excited state. We thus want to perform following two integrations:

$$V_{00} = \frac{4}{L_z^2} \int_{-\frac{L_z}{2}}^{\frac{L_z}{2}} dz_2 \int_{-\frac{L_z}{2}}^{\frac{L_z}{2}} dz_1 \cos^2\left(\frac{\pi}{L_z} z_1\right) \cos^2\left(\frac{\pi}{L_z} z_2\right) V(|z_2 - z_1|) \tag{6.10}$$

$$V_{01} = \frac{4}{L_z^2} \int_{-\frac{L_z}{2}}^{\frac{L_z}{2}} dz_e \int_{-\frac{L_z}{2}}^{\frac{L_z}{2}} dz_h \cos^2\left(\frac{\pi}{L_z} z_1\right) \sin^2\left(\frac{2\pi}{L_z} z_2\right) V(|z_2 - z_1|) \tag{6.11}$$

The first integration corresponds to the interaction between two quantum well ground states, whereas the second one is the interaction between the ground state and the first excited state, in which the heavy hole may occur. The following steps can be performed equivalently for both integrations thus we consider only the first one.

Now we use substitution

$$z = z_1 - z_2 \tag{6.12}$$

$$z_1 = z_2 + z \tag{6.13}$$

$$V_{00} = \frac{4}{L_z^2} \int_{-\frac{L_z}{2}}^{\frac{L_z}{2}} dz_2 \int_{-\frac{L_z}{2} - z_2}^{\frac{L_z}{2} - z_2} dz \cos^2\left[\frac{\pi}{L_z}(z_2 + z)\right] \cos^2\left(\frac{\pi}{L_z} z_2\right) V(|z|) \tag{6.14}$$

For upper bound of the integration holds $z = \frac{L_z}{2} - z_e$ and thus $z_e = \frac{L_z}{2} - z$. Similarly for the lower bound $z = -\frac{L_z}{2} - z_e$ and thus $z_e = -\frac{L_z}{2} - z$. Thus we can write:

$$V_{00} = \frac{4}{L_z^2} \int_{-L_z}^{L_z} dz V(|z|) \int_{max\left(-\frac{L_z}{2}, -\frac{L_z}{2} - z\right)}^{min\left(\frac{L_z}{2}, \frac{L_z}{2} - z\right)} dz_2 \cos^2\left[\frac{\pi}{L_z}(z_2 + z)\right] \cos^2\left(\frac{\pi}{L_z} z_2\right) \tag{6.15}$$

$$V_{00} = \frac{4}{L_z^2} \left[\int_{-L_z}^{0} dz V(|z|) \int_{-\frac{L_z}{2} - z}^{\frac{L_z}{2}} dz_2 + \int_{0}^{L_z} dz V(|z|) \int_{-\frac{L_z}{2}}^{\frac{L_z}{2} - z} dz_2 \right] \cos^2\left[\frac{\pi}{L_z}(z_2 + z)\right] \cos^2\left(\frac{\pi}{L_z} z_2\right) \tag{6.16}$$

In the first term inside the bracket, we now substitute $-z_2$ for z_2.

$$V_{00} = \frac{4}{L_z^2}\int_0^{L_z} dz V(|z|) \tag{6.17}$$

$$\left[\int_{-\frac{L_z}{2}+z}^{\frac{L_z}{2}} dz_2 \cos^2\left[\frac{\pi}{L_z}(z_2 - z)\right]\cos^2\left(\frac{\pi}{L_z}z_2\right) + \int_{-\frac{L_z}{2}}^{\frac{L_z}{2}-z} dz_2 \cos^2\left[\frac{\pi}{L_z}(z_2 + z)\right]\right]\cos^2\left(\frac{\pi}{L_z}z_2\right) \tag{6.18}$$

After substituting z for $-z$ in the first term, we get the final result:

$$V_{00} = \frac{8}{L_z^2}\int_0^{L_z} dz V(|z|)\int_{-\frac{L_z}{2}}^{\frac{L_z}{2}-z} dz_2 \cos^2\left[\frac{\pi}{L_z}(z_2 + z)\right]\cos^2\left(\frac{\pi}{L_z}z_2\right) \tag{6.19}$$

The second cosine function is left unchanged throughout computations, thus we can use the result also for the second integration.

$$V_{01} = \frac{8}{L_z^2}\int_0^{L_z} dz V(|z|)\int_{-\frac{L_z}{2}}^{\frac{L_z}{2}-z} dz_2 \cos^2\left[\frac{\pi}{L_z}(z_2 + z)\right]\sin^2\left(\frac{2\pi}{L_z}z_2\right) \tag{6.20}$$

The integrals over z_2 can now be easily performed. The following functions are the z-dependent parts of Coulombic term that are to be integrated along with the Coulomb potential with respect to z over interval $(0, L_z)$.

$$g_{00}(z) = \frac{8}{L_z^2}\int_{-\frac{L_z}{2}}^{\frac{L_z}{2}-z} dz_e cos^2\left[\frac{\pi}{L_z}(z_e + z)\right] cos^2\left(\frac{\pi}{L_z}z_e\right) \tag{6.21}$$

$$= \frac{(Lz - z)[2 + sin(\frac{2\pi}{L_z}z)]}{L_z^2} + \frac{sin(\frac{2\pi}{L_z}z)]}{2\pi L_z} \tag{6.22}$$

$$g_{01}(z) = \frac{8}{L_z^2}\int_{-\frac{L_z}{2}}^{\frac{L_z}{2}-z} dz_e cos^2\left[\frac{\pi}{L_z}(z_e + z)\right] sin^2\left(\frac{2\pi}{L_z}z_e\right) \tag{6.23}$$

$$= \frac{12\pi(Lz - z) + 8L_z sin\left(\frac{2\pi}{L_z}z\right) - L_z sin\left(\frac{4\pi}{L_z}z\right)}{6\pi L_z^2} \tag{6.24}$$

7 Appendix B - List of functions

Development of processes that lead to all the results in this thesis has not been straightforward. Following lists of functions and files (Mathematica notebooks) include functions that are sufficient for repeating all the results in the presented thesis. These files are available on the enclosed CD. However, at least ten times more functions and their variants and hundred times more testing Mathematica notebooks have been created on the way.

Parameters

$Lz = 10$ nm - size of the quantum well $Ly = 100$ nm - size of the box in y-direction
$m0 = 511\ 000$ eV - mass of the electron
$me = 0.067 * m0$ - effective mass of the electron
$mhh = 0.112 * m0$- effective mass of the heavy hole in-plane
$mlh = 0.211 * m0$ - effective mass of the light hole in-plane
$c = 2.998 * 10^{17}$ nm/s - speed of light
$eps = 12.9 * 8.853 * 10^{-12}$ - permitivity
$q = 1.60218 * 10^{-19}$ C - elementary charge
$h = 6.582 * 10^{-16}$ eV.s - Planck constant
$Bm = 0.05788$ mev/T - Bohr magneton
$gam1 = 6.85$, $gam1 = 2.1$, $gam3 = 2.9$ - Luttinger parameters
$Splith1 = 16$ meV - excited heavy hole states offset
$Splitl = 10$ meV - light hole states offset

Principle variables

B - magnetic field
lam - associated magnetic length $nmax$ - size of the basis
$Landaumax = 0, 1, 2$ - maximal included Landau level
$Landau$ - boolean type, if true - Landau levels energies included
$Heavyhole$ - boolean type, true denotes heavy hole, false denotes light hole
$Hlevel = 0, 1$ - describes either ground or first excited heavy hole states
ghh - hole g-factor ge - electron g-factor $shh = \pm 3/2$ - total angular momentum projection for heavy hole $slh = \pm 1/2$ - total angular momentum projection for light hole

Functions

Intz = INTz[Hlevel, Lz]
- stores two analytical integrals over z-variable

Intx = INTx[Landau1, Landau2, Landau1a, Landau2a, c1, c1a, c2, c2a]
- stores all 81 analytical integrals over x-variable
- inputs Landau1 - Landau2a describes the combination of Landau levels of four interacting particle states
- inputs c1 - c2a denote wavevectors of interacting particle states

Vnondiag = Coulombnondiag[c1, c1a, c2, c2a, lam, Lz, Ly, Prec, q, eps, Hlevel, Landau1, Landau2, Landau1a, Landau2a]

- computes single non-diagonal Coulom term with precision Prec

Vdiag = Coulombdiag[c1, c1a, c2, c2a, lam, Lz, Ly, Prec, q, eps, Hlevel, Landau1, Landau2, Landau1a, Landau2a]
- computes single non-diagonal Coulom term with precision Prec

Bigmat = BIGMAT[Landaumax, nmax, Ly, lam, Lz, Prec, q, eps, Hlevel]
- returns list of all Coulombic terms that are involved in the Hamitonian

kmatc, kmatcl = Kmatc[nmax]
- constructs all allowed combinations of wavevectors

Lmat = LMAT[Landaumax]
- constructs all combinations of Landau levels

LVtri = Vblock[Bigmat, kmatc, kmatcl, Landauh, Landaue1, Landaue2, Landauha, Landaue1a, Landaue2a, Heavyhole, me, mhh, mlh, Landau, Hlevel, Splith1, Splitl]
- construct the matrix of all Coulomb term involved for one combination of Landau levels

Mathhtri = MATHEAVY[Bigmat, kmatc, kmatcl, Heavyhole, me, mhh, mlh, Landau, Lmat, Hlevel, Splith1, Splitl]
- construct the Hamiltonian matrix for either all the heavy hole ground states or all the first excited states or all the light hole states

LutC, LutCcc, LutB, LutBcc = Lutmat[kmatcl, Lmat, Luttinger]
- construct the off diagonal matrices with Luttinger terms

Completetrihalf = COMPLETETRIHALF[Lmat, kmatcl, Mathh1tri, Mathhtri, Matlhtri, LutC, LutB, LutBcc, LutCcc];
- constructs complete Hamiltonian matrix for trion (based on 3×3 Hamiltonian)

Etri = ECOMPLETE[Completetrihalf, eigprec]
- Hamitonian matrix diagonalization with precision eigprec

Mathhtri2 = AddLandau[Mathhtri, Heavyhole, Hlevel, me, mhh, mlh, Splith1, Splitl, Lmat]
- allows separate addition of Landau levels energies

kmatsing, kmatsingl = Kmatsing[nmax]
- constructs all allowed combinations of wavevectors for singlet

kmattripl, kmattripll = Kmattripl[nmax]
- constructs all allowed combinations of wavevectors for triplet

Mathhsing, Describesing = MatSing[kmatsing, kmatsingl, kmattripl, kmattripll, kmatc, kmatcl, Lmat, Mathhtri]
- performs the rearranging procedure so that final Hamiltonian includes only singlet states
- matrix Describesing includes quantum numbers description of each state

Mathhtripl, Describetripl = MatTripl[kmatsing, kmatsingl, kmattripl, kmattripll, kmatc, kmatcl, Lmat, Mathhtri]
- performs the rearranging procedure so that final Hamiltonian includes only triplet states

LutCsing, LutCccsing, LutBsing, LutBccsing = Lutmatsing[Describesing, Luttinger]
LutCtripl, LutCcctripl, LutBtripl, LutBcctripl = Lutmattripl[Describetripl, Luttinger]

- compute Luttinger matrices for singlet and triplet states respectively

Completetrising = COMPLETETRIsing[Describesing, Mathh1sing, Mathhsing, Matlhsing, LutCsing, LutBsing, LutBccsing, LutCccsing]
Completetritripl = COMPLETETRItripl[Describetripl, Mathh1tripl, Mathhtripl, Matlhtripl, LutCtripl, LutBtripl, LutBcctripl, LutCcctripl]
- construct complete Hamitonian matrices for singlet and triplet states, respectively

Etriz = Zeeman2[Completetrising, ghh, glh, shh, slh, B, eigprec]
- adds hole Zeeman terms and provides diagonalization of Hamiltonian matrix

EtrizsM32, EtriztM32, EtrizsP32, EtriztP32 = Eigspin2[Completetrising, Completetritripl, ghh, glh, ge, B, eigprec]
- adds electron Zeeman terms

kmatc, kmatcl = Kmatc2[nmax]
- constructs all allowed combinations of wavevectors for 'fixed hole' approximation

A0 = Amat1[delka, Etriz, Describetripl, Eg, lam, me, c, h]
- computes the transition probabilities for low energy states

ProbINT[Landauh, Landaue1, Landaue2, kh, k1, k2, X]
- contains the analytical integration over x for plotting the probability densities and correlation of electrons

Files

functions1.mnb
functions2.mnb
AS_fun.mnb
intx_fun.mnb
- contain all previously described functions

putmat.mnb
putmat_0h.mnb
- evaluate the complete Hamiltonian matrix for trion for moving hole and fixed hole cases and save them

get4.mnb
- loads previously saved Hamiltonian matrix and separates it to singlet and triplet states
- allows also for investigation of energies and eigenvectors

matice3_wavfun2.mnb
- performs testing of wavefunctions basis size, creates appropriate plots and computes eccentricity

prob_final.mnb
prob_final_0h.mnb
- evaluate and plot the probability densities and correlations of electrons for both moving hole and fixed hole cases

AS5.mnb
- evaluates and plots photoluminescence spectra for different settings

8 Bibliography

[1] Uxa Š.; Magnetooptical Propecties of Semiconductor Quantum Structures, Master's thesis, 2009

[2] Bastard G.; Wave Mechanics Applied to Semiconductor Heterostructures, Les éditions de physique, 1992, ISBN 2-86883-092-7

[3] Kane E.O.; Band Structure of Indium Antimonide, Journal of Physics and Chemistry of Solids, **1**, 249 - 261 (1957)

[4] Luttinger J.M., Kohn W.; Motion of Electrons and Holes in Perturbed Periodic Fields, Physical Review, **97**, 869 - 883 (1955)

[5] Luttinger J.M., Kohn W.; Quantum Theory of Cyclotron Resonance in Semiconductors: General Theory, Physical Review, **102**, 1030 - 1041 (1956)

[6] Whittaker D.M., Shields A.J.; Theory of X^- at high magnetic fields, Physical Review B, **56**, 185-194 (1997)

[7] Formánek J., Úvod do kvantové teorie, Academia, 2004, ISBN 80-200-1176-5

[8] Kesteren H.W. van, Cosman E.C., Poel W. A. J. van der; Fine structure of excitons in type-II GaAs/AlAs quantum wells, Physical Review B, **41**, 5283 - 5292 (1990)

[9] Vanhoucke T., Hayne M., Henini M., Moshchalkov V.V.; Magnetophotoluminiscence of negatively charged excitons in narrow quantum wells, Physical Review B, **63**, 125331-1 - 125331-8 (2001)

[10] Vanhoucke T., Hayne M., Henini M., Moshchalkov V.V.; High field Zeeman contribution to the trion binding energy, Physical Review B, **65**, 041307-1 - 041307-4 (2001)

[11] Bauer G.E.W., Ando T., Exciton mixing in quantum wells, Physical Review B, **38**, 6015 - 6030 (1988)

[12] Winkler R., Culcer D., Papadakis S.J., Habib B., Shayegan M., Spin orientation of holes in quantum wells, Semiconductor science and technology, **23** 114017-1 - 114017-13 (2008)

[13] Bradley R.R., MOCVD growth and characterization of GaAlAs/GaAs double heterostructures for opto-electronic devices, Journal of Crystal Growth, **55** 223-228 (1981)

[14] Pan J.L., Clifton G., Fontad Jr., Theory, fabrication and characterization of quantum well infrared photodetectors, Materials Science and Engineering, **28** 65-147 (2000)

[15] Andre J.P., Briére A., Rocchi M., Riet M., Growth of (Al,Ga)As/GaAs heterostructures for HEMT devices, Journal of Crystal Growth, **68** 445-449 (1984)

[16] Volkov O.V., Tovstong S.V., Kukushkin I.V., Klitzing K. von, Eberl K., Localization of negatively charged excitons in GaAs/AlGaAs quantum wells, JETP Letters, **70**, 595 - 601 (1999)

[17] Schmitt-Rink S., Stark J.B., Knox W.H., Chemla D.S., Schäfer W., Optical Properties of Quasi-Zero-Dimensional Magneto-Excitons, Appl. Phys. A **53**, 491-502 (1991)

[18] Dohler, G.H., private communication

[19] Wikipedia, Ewald summation

[20] Kheng K., Cox R.T., Merle d´Aubigné Y., Bassani F., Saminadayar K., Tatarenko S., Observation of Negatively Charged Excitons X^- in Semiconductor Quantum Wells, Phys Rev Let **71**, 1752-1755 (1993)

[21] Finkelstein G., Shtrikman H., Bar-Joseph I., Optical Spectroscopy of a Two-Dimensional Electron Gas near the Metal-Insulator Transition, Phys Rev Let **74** 976-979 (1995)

[22] Glasberg S., Finkelstein G., Shtrikman H., Bar-Joseph I., Comparative study of the negatively and positively charged excitons in GaAs quantum wells, Phys Rev B **59** 425 - 428 (1998)

[23] Groholová A., Luminiscence spectroscopy of two-dimensional quantum structures in the system GaAs/AlGaAs, Master's thesis, 2006

[24] Snelling M.J., Flinn G.P., Plaut A.S., Harley R.T., Tropper A.C., Eccleston R., Phillips C.C., Magnetic g-factor in GaAs/$Al_xGa_1 - x$As quantum wells, Phys Rev B **44** 345 - 352 (1991)

[25] Snelling M.J., Blackwood E., McDonagh, C.J., Harley R.T., Foxon C.T.B., Exciton, heavy-hole, and electron g factors in type-I GaAs/$Al_xGa_1 - x$As quantum wells, Phys Rev B **45** 3922 - 3925 (1992)

[26] Tutuc E., Melinte S., Shayegan M., Spin Polarization and g Factor of a Dilute GaAs Two-Dimensional Electron System, Phys Rev Let, **88** 036805-1 - 036805-4 (2002)

[27] Proskuryakov Y.Y., Savchenko A.K., Safonov S.S., Pepper M., Simmons M.Y., Ritchie D.A., Hole-Hole Interaction Effect in the Conductance of the Two-Dimensional Hole Gas in the Ballistic Regime, Phys Rev Let **89** 076406-1 - 076406-4

[28] Riva C., Peeters F. M., Varga K., Magnetic field dependence of the energy of negatively charged excitons in semiconductor quantum wells, Phys Rev B **63** 115302-1 - 115302-9 (2001)

[29] Riva C., Peeters F. M., Varga K., Positively and negatively charged excitons in a semiconductor quantum well, Phys Stat Sol(b) **227** 397-404 (2001)

[30] Riva C., Peeters F. M., Varga K., Theory of trions in quantum wells, Physica E **12** 543-545 (2002)

[31] Shields A.J., Osborne J.L., Whittaker D.M., Simmonds M.Y., Bolton F.M., Ritchie D.A., Pepper M., Charged excitons under applied electric and magnetic fields, Physica B **249 - 251** 584 - 588 (1998)

[32] Yusa G., Shtrikman H., Bar-Joseph I., Photoluminiscence in the fractional quantum Hall regime, Physica E **12** 49 - 54 (2002)

[33] Redliński P., Kossut J., Negative trions in CdTe quantum wells in the presence of a magnetic field - a numerical study, Semicond. Sci. Technol. **17** 237 - 242 (2002)

[34] Wójs A., Quinn J. J., Exact-diagonalization of trion energy spectra in high magnetic fields, Phys Rev B **75** 085318-1 - 085318-14 (2007)